The Thesis Committee for Ssu-Chi Yang
Certifies that this is the approved version of the following Thesis:

Assessing the CO_2 Sequestration Potential of the Frio Formation in South Texas, USA

APPROVED BY
SUPERVISING COMMITTEE:

Carlos A. Uroza, Co-Supervisor
Susan D. Hovorka, Co-Supervisor
Charles Kerans, Reader

Assessing the CO_2 Sequestration Potential of the Frio Formation in South Texas, USA

by

Ssu-Chi Yang

Thesis

Presented to the Faculty of the Graduate School of

The University of Texas at Austin

in Partial Fulfillment

of the Requirements

for the Degree of

Master of Science in Energy and Earth Resources

The University of Texas at Austin

May 2026

Dedication

I am dedicating this thesis to my family and friends. Thank you all for your constant encouragement and emotional support; I would not have it without you.

For those in Taiwan, thank you for the late-night and early-morning phone calls across time zones. I miss you very much. For my friends here in Austin, I am deeply grateful for your wonderful friendship. You have enriched my life during this Master's degree, and I have already started missing you.

Finally, special thanks to my parents, I would not be here without your support in education. Thank you so much for answering my phone call every night and sharing every moment of this journey with me from afar.

Acknowledgements

I would like to express my sincere gratitude to my supervisors, Dr. Carlos A. Uroza and Dr. Susan D. Hovorka, for their guidance, support and countless encouragement. I have learned a lot from them, not only knowledge about Carbon Capture and Storage, but also about a way of thinking that has reshape how I approach research. I am also grateful to my reader, Charles Kerans, for taking time to review my thesis and provide valuable feedback. Lastly, I would like to thank my workmates in Gulf Coast Carbon Center for your support throughout my study at Gulf Coast Carbon Center.

In addition, I would like to acknowledge the support from these projects and institutions. This material is based in part upon work supported by 1. Regional CO_2 Utilization and Storage Acceleration Partnership (SECARB-USA), DOE Award Number DE-FE0031830. 2. Partnership for Offshore Carbon Storage Resources and Technology Development in the Gulf of Mexico (GoMCarb), DOE Award Number DE-FE0031558. 3. Texas Louisiana Carbon Management Community, Award Number DE-FE-0032361. 4. The Energy and Earth Resources Graduate Program**.** 4. Gulf Coast Carbon Center, Bureau of Economic Geology.

Abstract

Assessing the CO_2 Sequestration Potential of the Frio Formation in South Texas, USA

Ssu-Chi Yang, MSEER

The University of Texas at Austin, 2026

Co-Supervisor: Carlos A. Uroza

Co-Supervisor: Susan D. Hovorka

The Frio sandstones in South Texas present geological challenges for CO_2 storage capacity and injectivity as they contain abundant volcanic and carbonate material, which undermine their reservoir quality through diagenetic processes. As research on their potential for geological carbon sequestration remains limited, this thesis provides some insights into the impact of reservoir quality on CO_2 storage capacity and injectivity by conducting a geological characterization of the South Texas Frio Formation and evaluating the storage capacity of its saline reservoirs. The study area includes Nueces, Kleberg, Kenedy, Brooks, Willacy, Hidalgo, and Cameron Counties. Well log correlation and porosity-permeability evaluation were used to characterize sandstone presence and continuity as well as their rock quality distribution. Storage capacity estimation was performed on five selected injection sites to quantify storage resources.

Results indicate that porosity generally deteriorates towards the south and with depth, while spatial variation in permeability was not linked to a specific trend. Although laterally continuous sand-rich facies are found in southern Corpus Christi, the Baffin Bay, and the coastal area of Kenedy County, the overall injectivity is limited by the suboptimal permeability. Nevertheless, the storage capacity estimates suggest that a large reservoir area can effectively compensate for the limitation on storage capacity due to the unfavorable reservoir quality in the Frio sandstones of South Texas. The proposed sites have a combined estimated storage capacity of 797 million metric tons (MMT) under closed-boundary conditions. Although this value is inferior to analogs with high reservoir quality, it is sufficient to provide CO_2 storage for more than 40 years of local CO_2 emissions. The Frio Formation in South Texas is considered a viable target for commercial-scale geological CO_2 sequestration.

Table of Contents

List of Tables

List of Figures

Chapter 1: Introduction

Climate change and global temperature rise are not only affecting human daily life but also impacting ecosystems around the world. According to the United Nations (UN) website (2025), scientific evidence has shown that limiting the increase in global average temperature to within 1.5°C above pre-industrial levels is essential to avoid more severe climate-related catastrophes. In line with this objective, world leaders reached a consensus under the Paris Agreement that the global greenhouse gases should reach net zero emission by 2050 (UN, 2025).

As the Earth has already warmed up 1.2°C from pre-industrial level (UN, 2025), achieving net zero emissions has become a top priority for international community and the environmentally responsible global corporations. One of the effective methods to reach this goal is carbon capture and geological CO_2 sequestration, which involves capturing the carbon dioxide directly from atmosphere or from point sources and injecting it into the subsurface pore spaces for long-term and secure storage.

1.1 Statement of the Problem

Carbon sequestration interest in the Frio Formation, onshore Texas, has increased over the years. However, the formation presents geological challenges for storage capacity and injectivity in the South Texas region. Compared to the Frio in the east Texas, where good reservoir quality has been preserved, the South Texas Frio may contain important amounts of volcanic and carbonate material, which can degrade porosity and permeability if submitted to significant diagenesis. However, diagenesis may not be widespread and may show variations among structural compartments. This poses a significant challenge when evaluating the CO_2 sequestration potential within the Frio Formation in the South Texas region.

Loucks et al. (1984) subdivided the Texas Gulf Coast into Upper, Middle, and Lower Texas regions (Figure 1) and concluded that the Frio Formation in the middle and upper Texas Gulf Coast showed higher reservoir quality than the Frio in the lower Texas region, which includes the area of interest of this research. The Frio Formation along the lower Texas Gulf Coast is low in quartz, rich in carbonate material and contains significant amounts of volcanic lithic fragments. The volcanic material came from volcanic terrains of the Sierra Madre Oriental and was deposited into the Norias Delta System by the antient Rio Grande River system (Loucks et al. 1984; Snedden et al., 2019).

Since reservoir compartmentalization caused by growth faulting is a main structural feature in the south Texas Gulf Coast (Hammes et al., 2007), the variation of reservoir properties between the compartments could be attributed to parameters such as facies changes, differences in clay content, or sandstone diagenesis processes. Reservoir compartmentalization also poses difficulties in tracing the sandstone continuity.

While previous studies of the Frio Formation in South Texas have primarily focused on its hydrocarbon viability, investigations into its potential for geological carbon sequestration remain limited. Given the circumstances, the purpose of this study is to address this gap by understanding the distribution of sandstone reservoirs of the Frio Formation within several counties in South Texas and addressing the impact of the rock quality on CO_2 injectivity. Through this assessment, this study aims to obtain an estimation of the feasible CO_2 storage capacity of the Frio saline reservoirs within several counties in South Texas, including Nueces, Kleberg, Kenedy, Brooks, Willacy, Hidalgo, and Cameron.

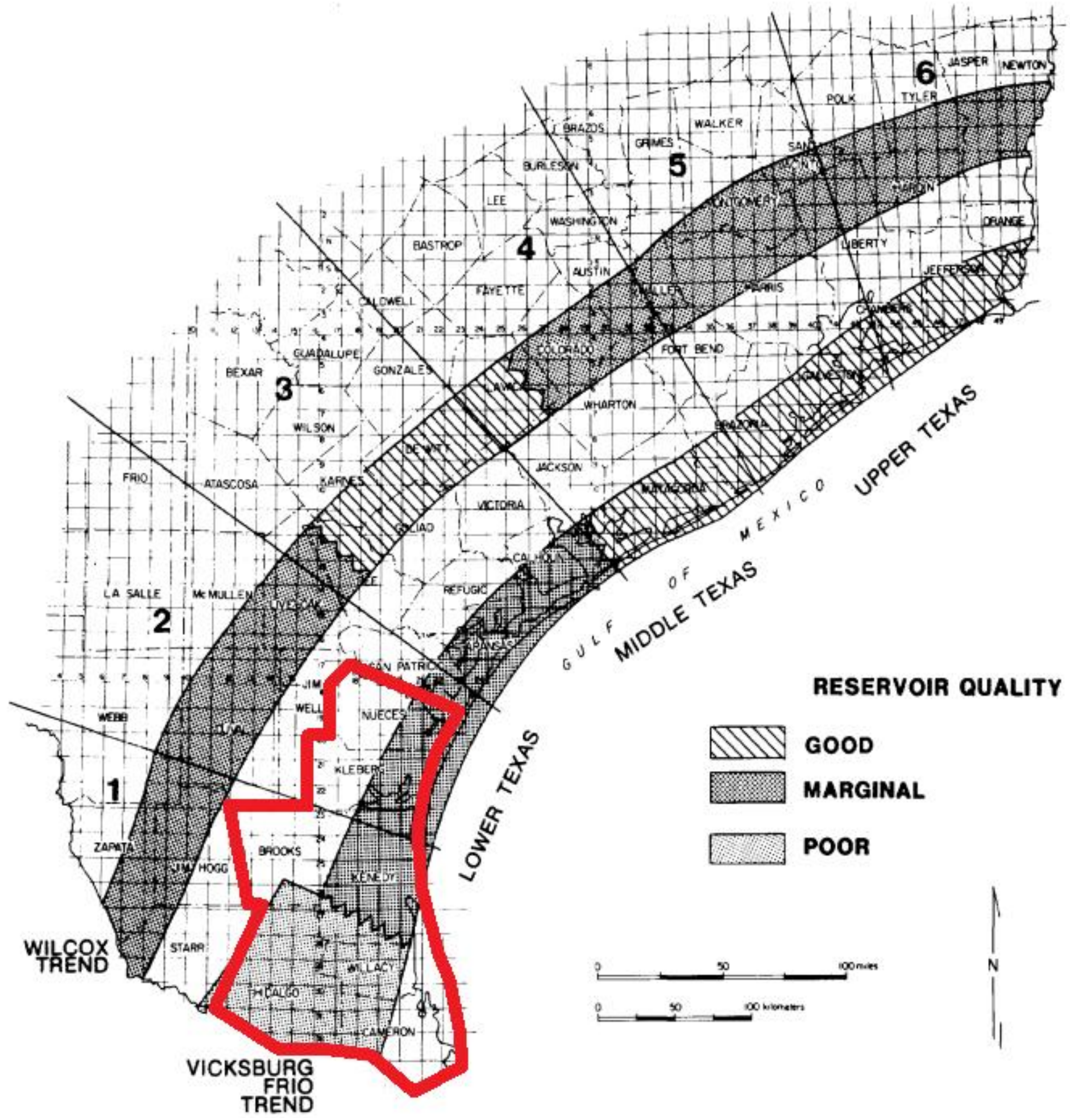

Figure 1. Location map showing the regional subdivisions and exhibiting the potential for high-quality, deep reservoirs (>3350 m, 11,000 ft) in Lower Tertiary strata along the Texas Gulf Coast (Loucks et al., 1984).
Good represents permeability values typically greater than 20 millidarcys. Marginal means permeability values generally less than a few millidarcies, but some reaching 20 millidarcies. Poor indicates permeability values are commonly less than a millidarcy. The AOI of this research is located within the lower Texas area in this figure, outlined in red polygon. The reservoir quality of the Frio Formation is marginal in Nueces, Kleberg, and Kenedy Counties, and is poor in Hidalgo, Willacy, and Cameron Counties.

1.2 Relevance of the Problem

According to United States Energy Information Administration (EIA, 2025a), Texas' total carbon dioxide emissions in 2023 significantly exceeded all the other states – nearly twice that of the second highest state, California, and three times that of the third highest state, Florida. As shown in Figure 2 from the United States Environmental Protection Agency (EPA, 2025b), these tremendous emissions are mainly driven by the state's extensive oil and gas and petrochemical industrial infrastructure.

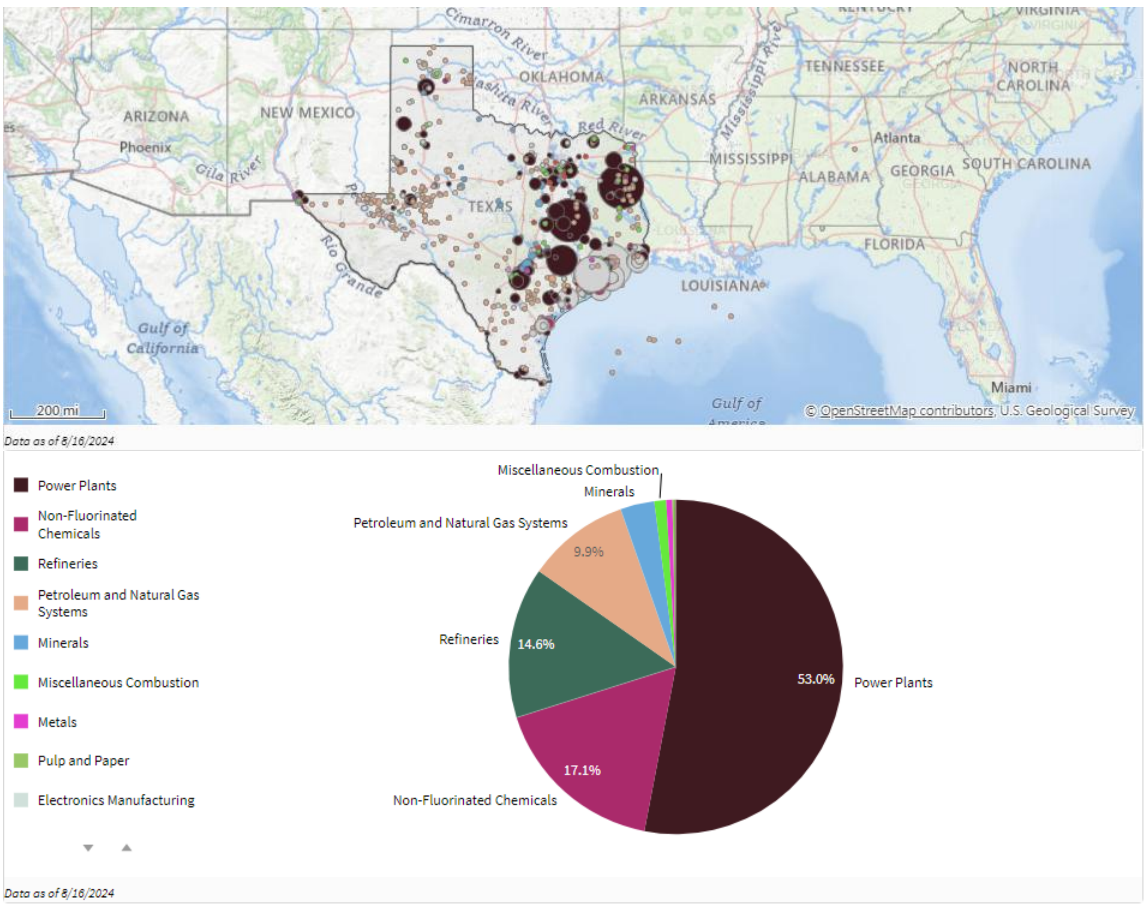

Figure 2. Map of GHGRP facilities reporting emissions in 2023, color-coded by sectors and a pie chart showing the proportion of emissions by sector (GHGRP State and Tribal Fact Sheet of EPA, 2025b).

A similar pattern is observed in state-wide energy consumption as well. EIA's analysis (2025b) indicates that Texas consumed roughly twice as much energy as California and three times as much as Florida in 2023. It is also mentioned in the analysis, industrial sectors— including chemical manufacturing, oil and gas extraction, and petroleum refineries— accounted for nearly half of Texas' total energy use. Additionally, coal and natural gas together made up nearly third fourths of the state's electric power generation. EIA (2025c) further reports that the electricity demand within the Electric Reliability Council of Texas (ERCOT) is expected to increase by 14% in 2026 as the large data centers and cryptocurrency mining facilities are going into operation.

Since the carbon dioxide emissions in Texas are expected to continue increasing in the near future, demand for carbon capture and storage (CCS) in Texas is not only substantial but also persistently increasing as seeking to reduce net emissions. Geological carbon sequestration is one of the means to achieve this goal. Given the context, it is crucial to investigate potential storage locations and evaluate the geological and petrophysical properties of these reservoirs as part of the initial regional screening.

Previous research of the Frio Formation has primarily focused on its hydrocarbon potential, and the reservoir quality assessments are mostly focused within the specific depth intervals that contain hydrocarbon. However, there is limited research on Frio Formation in southern Texas regarding its suitability for geological carbon sequestration. This research aims to bridge part of this gap by examining the characteristics of the reservoir rock within the CO_2 storage window, that is, the intermediate subsurface depth range of 4000 to 11000 ft, in a number of wells within the area of interest. By expanding research objectives outside the framework of hydrocarbon exploration/production, this study would make contributions to academic knowledge and provide practical recommendations in accessing CO_2 storage capacity and reservoir injectivity in South Texas.

Based on the information summarized from the Facility Level Information on Green House gases Tool (FLIGHT) of EPA (2025a), the CO_2 emitters in the AOI of this study are concentrated around Corpus Cristi of Nueces County and Edinburg of Hidalgo County (Figure 3). In 2023, the total amount of approximately 2.87 MMT of CO_2 from the power plants are the main source of emissions near Edinberg. Around Corpus Christi, power plants along with the refineries and chemical plants together emitted 13.2 MMT of CO_2. Although few significant emitters are present in the remaining counties within the study area, this study identifies potential injection sites in these counties for future CCS projects, such as Direct Air Capture (DAC), or for emission sources associated with the growth in natural gas infrastructure, including Texas LNG and Rio Grande LNG projects under development in Brownsville in South Texas (Texas LNG Brownsville LLC, 2026; NextDecade, 2026).

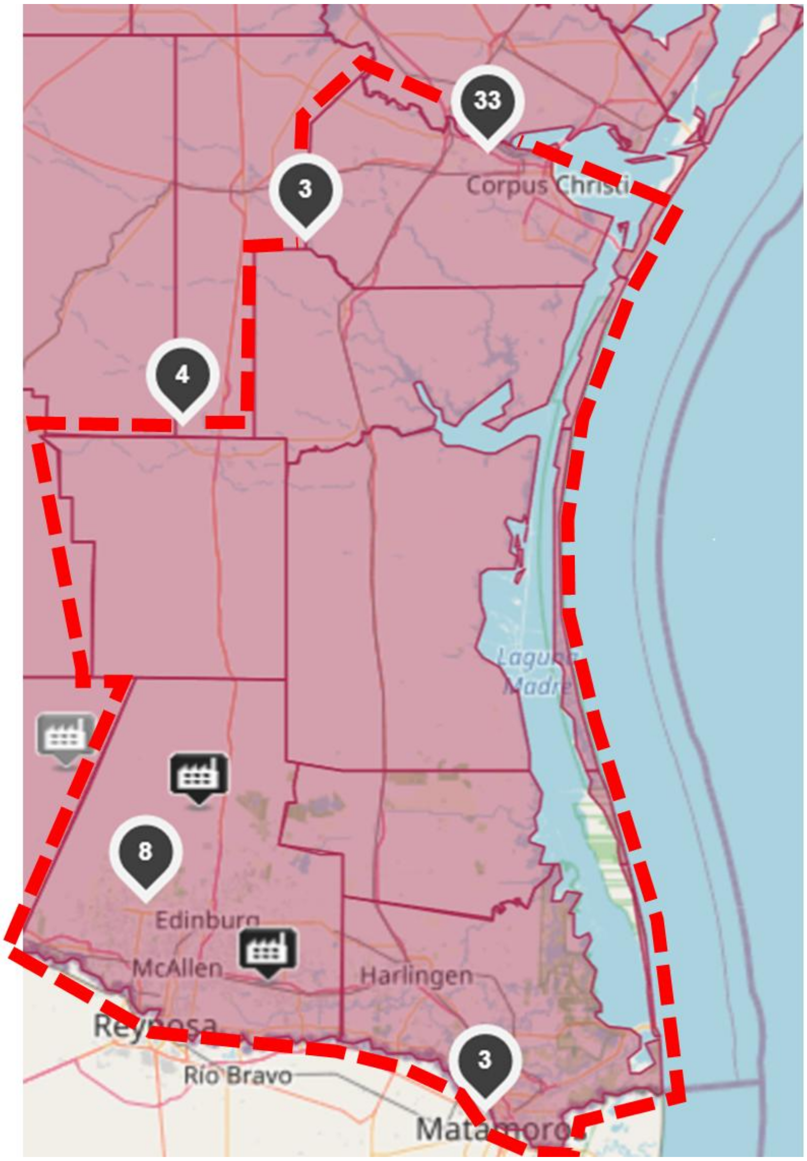

Figure 3. Location map of point-source emissions from large facilities reported in 2023. The study area is outlined in red polygon. Numbers indicate total emitting large facilities within each cluster. Image obtained and modified from Facility Level Information on Greenhouse Gases Tool (FLIGHT) of the U.S. EPA (2026a).

1.3 KEY CHALLENGES

Based on the previous research regarding the hydrocarbon potential in South Texas, this study will further elaborate on the following challenges for CO_2 storage capacity estimation.

(1) Reservoir continuity: The complex depositional environment, including wave reworked deltas, distributary channels, fluvial features, and the compartmentalization caused by growth faults makes it harder to trace the continuity of the sandstone reservoirs when conducting stratigraphic analysis.

(2) Reservoir quality: Variability in rock composition and diagenesis, burial, compaction, and lack of petrographic data, make it difficult to assess the reservoir quality in the AOI. It will be addressed partially in this research.

(3) Source and sink matching: According to EPA FLIGHT website (2026a), there are not many emitters within the AOI, especially not around the areas that have the highest sand content such as Kleberg and Kenedy counties. Given this situation, direct air capture would be considered in the future financial analysis.

Chapter 2: Background

2.1 Study Area

The study area covers parts of South Texas, including Nueces, Kleberg, Kenedy, Brooks, Willacy, Hidalgo, and Cameron counties as outlined in Figure 4.

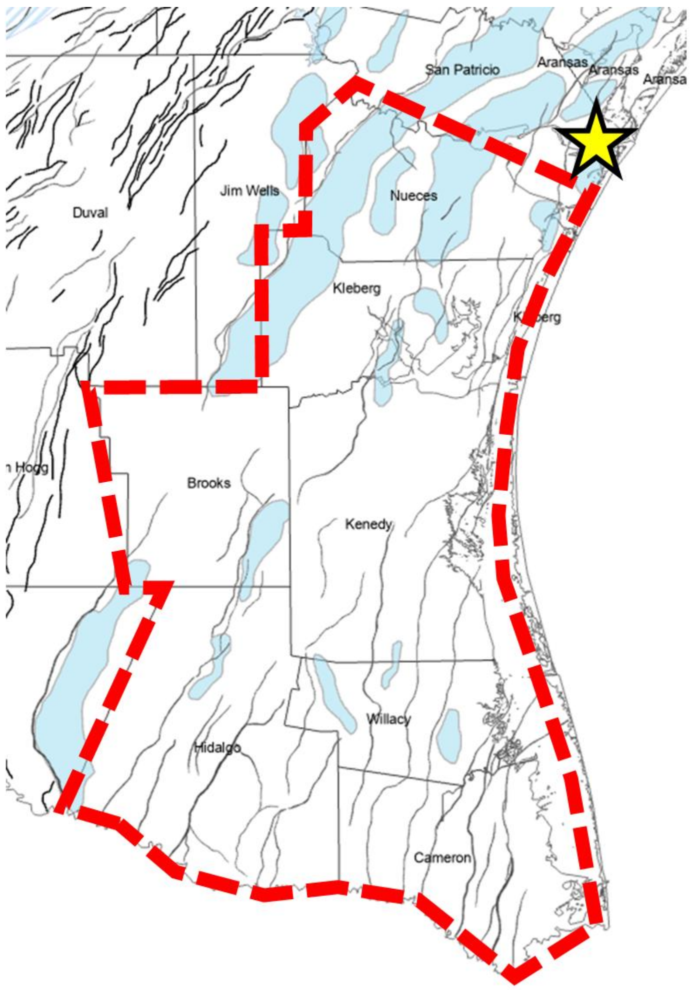

Figure 4. Location map of the study area within South Texas, outlined by a red polygon. Gray lines are the main faults that affect the Frio Formation. Blue areas indicate location of Frio's hydrocarbon production. Map courtesy of GCCC-BEG (unpublished). The star marks Red Fish Bay, where the composite log used in Figure 7, the S^5-benchmark chart from Hammes et al. (2007), is located.

2.2 Geologic Setting

2.2.1 Depositional History of Oligocene Frio Deposode in the South Texas

The Oligocene Frio Deposode lasted over 10 million years, which included Catahoula, Vicksburg, Frio, and Anahuac stratigraphic units (Galloway et al., 1982a), and the schematic diagram showing their stratigraphic correlations is illustrated in Figure 5. The deposode was dominated by the significant volume of sediment influx (Figure 6), contributed mainly by volcanism and tectonic uplift and erosion along the Sierra Madre Oriental (Snedden & Galloway, 2019).

The south Texas Gulf Coast basin-fill is directly impacted by the tectonism in the early Oligocene (Snedden and Galloway, 2019). The Vicksburg succession was unsettled by tilting, which caused a detachment at the upper Eocene level, and consequently resulting in the extensional faulting and displaced both deltaic and upper slope facies basinward along the detachment (Langford and Combes, 1994; Snedden and Galloway, 2019). The tectonic uplift is also recorded in the updip Frio and its equivalent units, such as Catahoula Formation (Snedden and Galloway, 2019).

Including the regional explosion and caldera formation, the volcanism across southwestern USA and Mexico provided sediment supply for the drainage basin of Rio Grande River System with two source– volcanic airfall ashes and the fragments from the erosion of volcanic edifices and ejecta (Galloway et al., 1977; Snedden and Galloway, 2019). In particular, the airfall ash had been rapidly weathered and been altered during pedogenesis, resulting in smectite-rich clay.

According to Galloway et al. (1982a), in the Oligocene, Frio Formation is the main progradational deposode, overlying the Vicksburg Formation and regionally underlying the maximum flooding surface of Anahuac Shale. The progradation started around a major sea level fall. The sea level continued to rise slowly for an extended period and then followed by the Anahuac Shale transgression that lasted for about 2 million years. The thickness of Frio Formation exceeds 12,000 ft (3,600 m) in South Texas (Galloway et al., 1982a).

Stratigraphically, the Frio Formation is subdivided into Shallow Frio, Middle Frio and Deep Frio in S5 -benchmark chart of Red Fish Bay area (Figure 7) created by Hammes et al. (2007). Deep Frio predominantly represents low stand system tracts, whereas the Shallow and Middle Frio are generally transgressive.

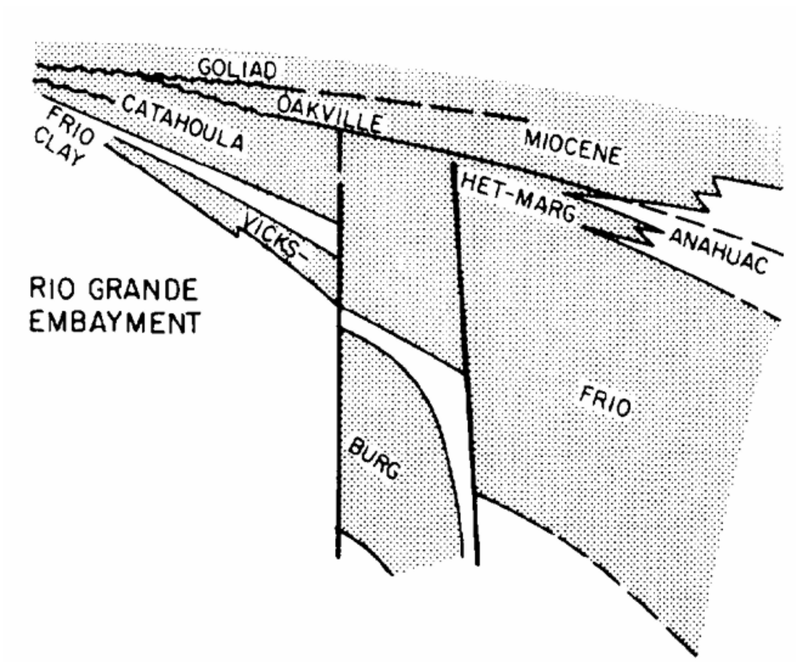

Figure 5. Conceptual diagram of stratigraphic correlation sections for Rio Grande embayments. (Galloway et al., 1982a).

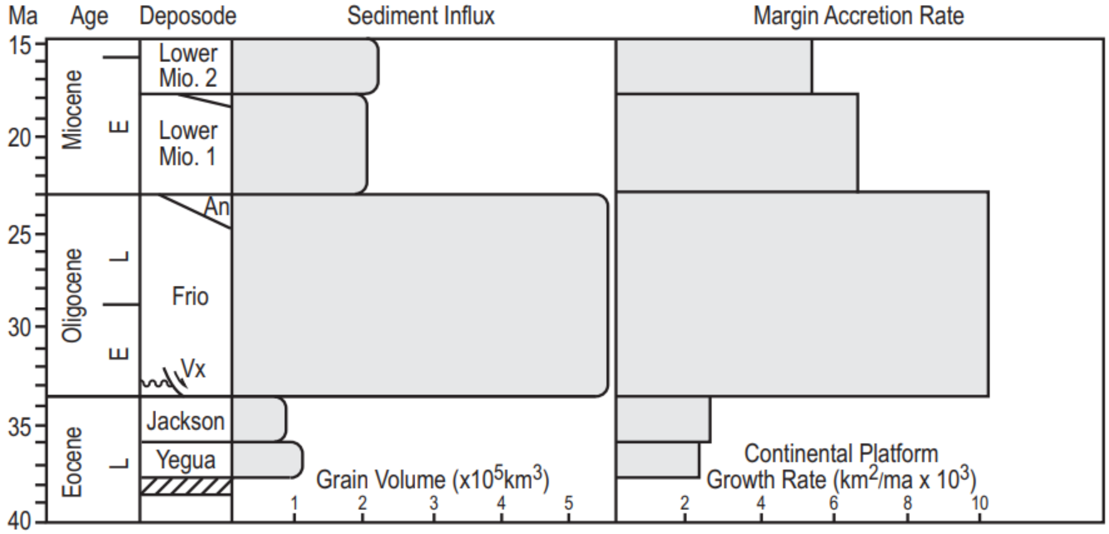

Figure 6. Depositional episodes and chronology of the Middle Cenozoic Geothermal Phase (Snedden & Galloway, 2019).
Image shows the sediment influx, calculated as total grain volume, and continental margin accretion rates of each deposodes along the Northern Gulf of Mexico margin.

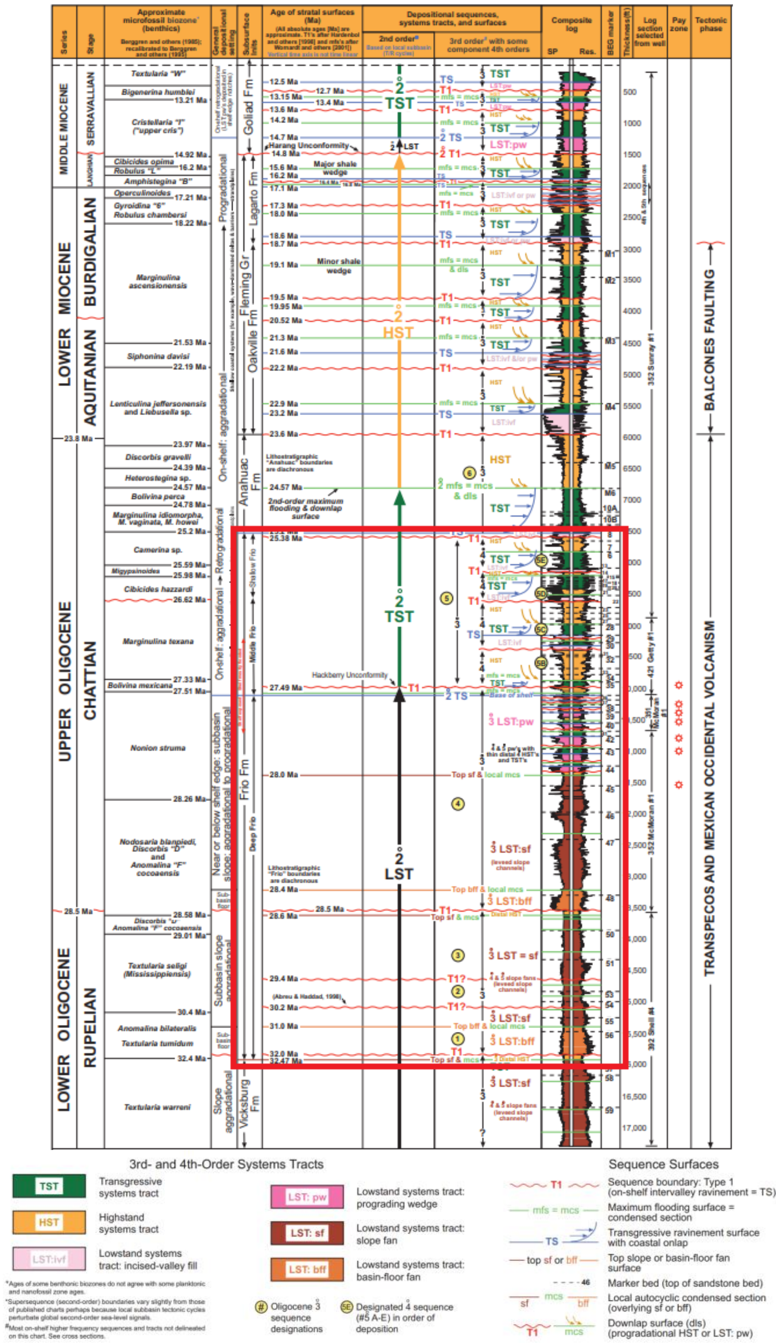

Figure 7. S_5 benchmark chart with composite log and sequence stratigraphy of the Red Fish Bay area (Hammes et al., 2007); Oligocene Frio section outlined in red. Location of this composite log is marked with a yellow star on Figure 4.

The main depocenter of the Frio Formation on the south Texas Gulf Coast is the Norias Delta system, which is investigated by Galloway et al., (1982a) and summarized in the following paragraphs: Converged from the Rio Grande and Rio Bravo fluvial systems (Figure 8) (Snedden & Galloway, 2019), the Norias Delta system is the major wave-dominant progradational complex. Its thickness in the Frio section is more than 12000ft (3700m), containing 20-40% of sand content, and there is abundant carbonate debris in its deltaic facies. The maximum width of the delta system is over 125 miles (200 km), in which its sand- rich facies extend more than 10 miles (16 km) offshore from Kenedy County. The delta system grades into the Greta Barrier/ Strandplain northward at Nueces County, which presents about 4000ft (2500m) thick massive, blocky, stacked barrier and strandplain sands interbedded with shaly interbeds (Galloway et al., 1982a).

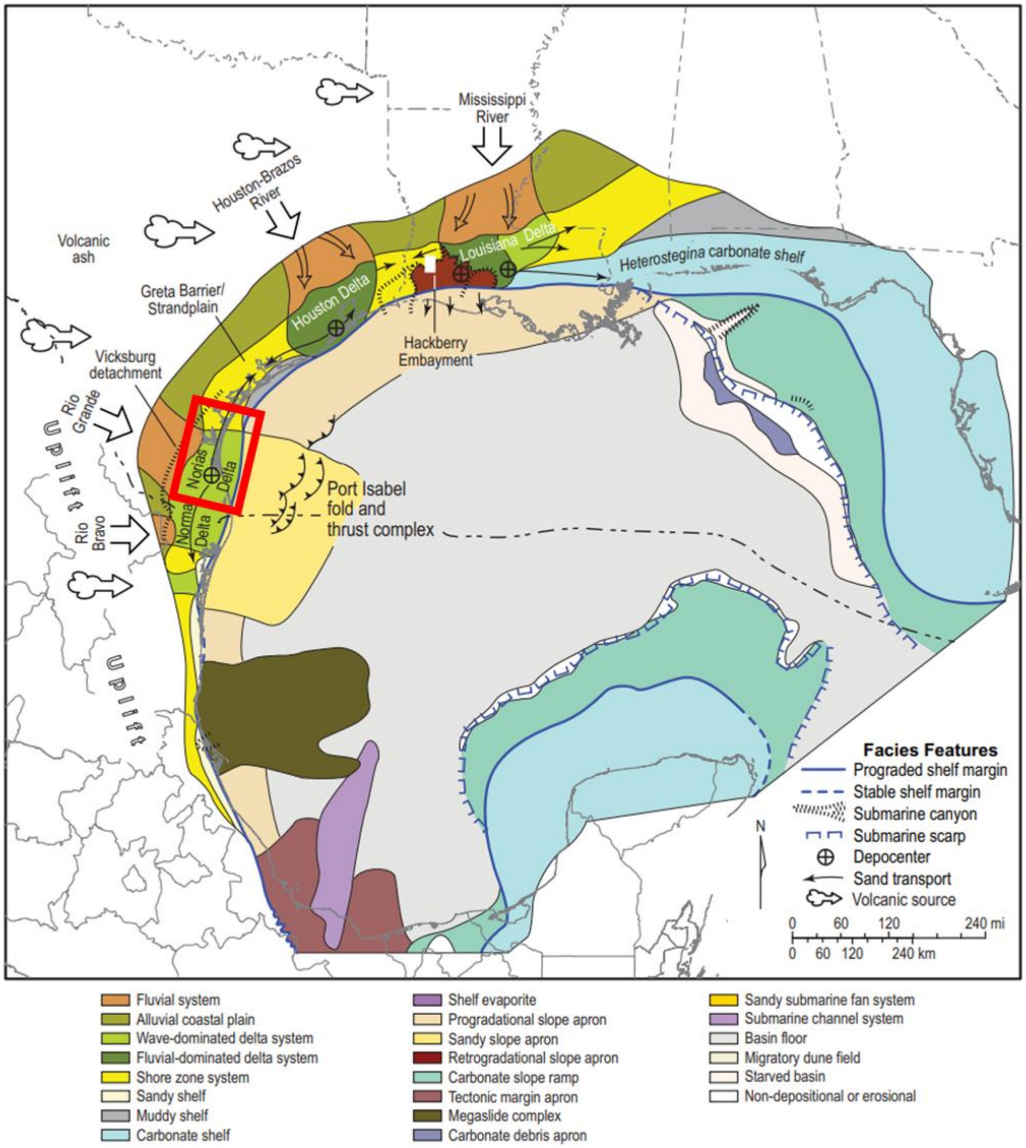

Figure 8. Paleogeographic map of the Oligocene Frio deposode (Snedden & Galloway, 2019) with the study area outlined with a red rectangle.
The outline of the depositional system and the shelf edge at the maximum progradation is shown on the map.

2.2.2 Rock Quality

The diagenetic processes and their influence in the Frio sandstones were comprehensively analyzed by Loucks et al. (1984, 1986). The information from these studies specifically related to South Texas Frio is summarized here in this subsection.

The mineral composition varies largely within Frio sandstones (Loucks et al. 1986), and the abundance of volcanic fragments and plagioclase feldspar decrease eastward (Snedden & Galloway, 2019). As illustrated in Figure 1, Loucks et al. (1984) subdivided the Texas Gulf Coast into lower Texas, middle Texas, and upper Texas. In the lower Texas, temperature and composition of sediments are the most critical controls of diagenesis process within the Frio Formation, which greatly affects the events of compaction, cementation, and dissolution.

Temperature is the primary control of diagenesis. Compared to middle and upper Texas Gulf Coast, Frio Formation in lower Texas has the highest geothermal gradient (Figure 9) which allows the thermally controlled diagenetic events occurring in a shallower depth (Loucks et al., 1984). Additionally, due to the arid climate of post-Eocene in the South Texas, volcanic rock fragments were well-preserved into sandstones, remained both mechanically and chemically unstable and vulnerable to cementation in the subsurface (Figure 10) (Loucks et al., 1984).

GEOTHERMAL GRADIENT INCREASES ←

TREND \ AREA	LOWER TEXAS 1 & 2	MIDDLE TEXAS 3 & 4	UPPER TEXAS 5 & 6
WILCOX	2.25° F/100 Ft.	2.11° F/100 Ft.	1.88° F/100 Ft.
VICKSBURG / FRIO	2.05° F/100 Ft.	1.76° F/100 Ft.	1.79° F/100 Ft.

↑ GEOTHERMAL GRADIENT INCREASES

Figure 9. Average geothermal gradient of lower, middle and upper Texas for updip Wilcox trend and downdip Vicksburg/Frio trend. (Loucks et al., 1984)

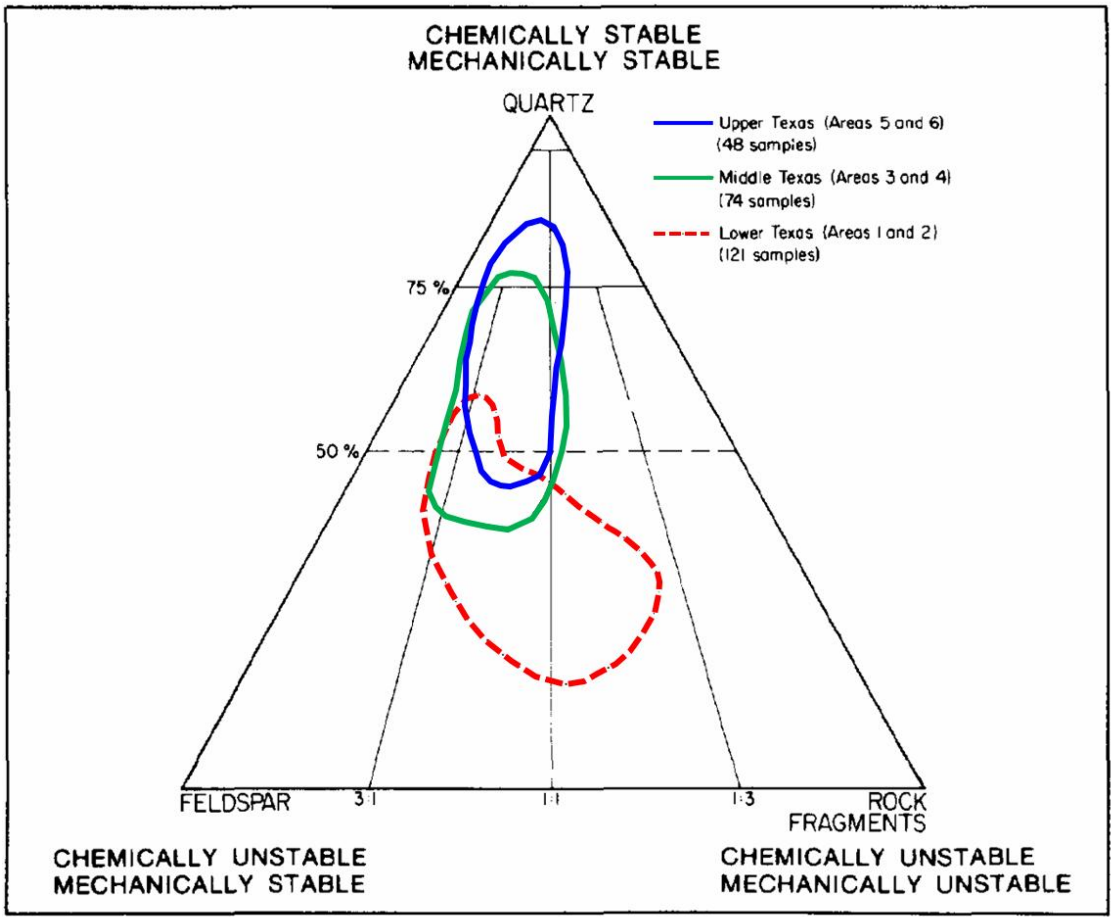

Figure 10. Frio sandstone ternary composition of quartz, feldspar, and rock fragments. Modified from Loucks et al. (1984).

Following the classification proposed by Loucks et al. (1984), most of the Frio Formation in the AOI of this study lies within the intermediate subsurface diagenesis zone (1200 to 3400 m ±; 4000 to 11,000 ft ±). According to Loucks et al., (1984), within this zone cementation and dissolution are the major controls depending on depth, and compaction is ended by strong cementation. Quartz overgrowth cementation and Fe-poor carbonate cementation are the critical events that typically reduces the porosity to about 10%. Nevertheless, the secondary dissolution porosity is created at the bottom of this diagenesis zone (Figure 11). Constituents such as feldspar, volcanic rock fragments, and carbonate cements were dissolved, resulting in restoration of porosity by more than 30%, but only occurs in 20-30% of the sandstones.

To conclude from Loucks et al. (1984, 1986), sandstones from the Frio Formation in lower Texas Gulf Coast are poorly sorted, fine-grained, and represent feldspathic litharenites to lithic arkoses. They are low in quartz, rich in carbonate rocks and contain great amount of volcanic lithic fragments, and they have relatively high subsurface temperatures. Also, rapid subsidence in Rio Grande embayment contributed to high compaction rate. These features are conductive to diagenesis and lead to poor reservoir quality in the region (Loucks et al., 1984).

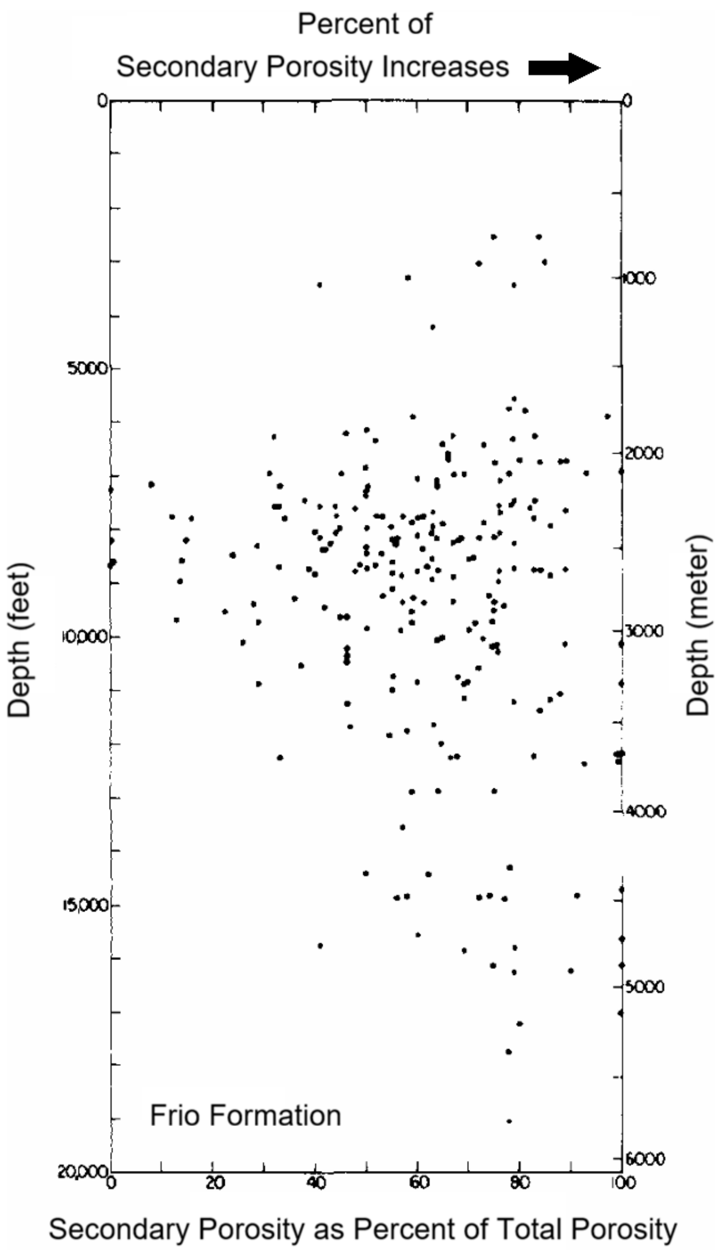

Figure 11. Cross-plot of secondary porosity (expressed as a percentage of total porosity) versus depth for Frio sandstones. Modified from Loucks et al. (1984).

2.2.3 Structural Style

Growth faults and shale ridges are the notable structural features in the South Texas Gulf Coast. Major structural traps are formed by shale-cored rollover anticlines and faulted anticlines (Galloway et al., 1982a). Loaded by the slope-fan facies, which are associated with third-order relative sea level fall, fluid-saturated, undercompacted deepwater muddy sediments were mobilized along the detachment surface, initiating syndepositional growth faults (Figure 12) (Brown et al., 2004; Hammes et al., 2007). The overburden mud masses were displaced basinward and formed shale ridges. The growth faults and their orthogonal normal faults between them control the reservoir compartmentalization in the South Texas Gulf Coast (Hammes et al., 2007). In the Rio Grande Embayment, as the depositional units thickened across growth faults, the thickening is notably significant in its outermost subbasin (Galloway et al., 1982a).

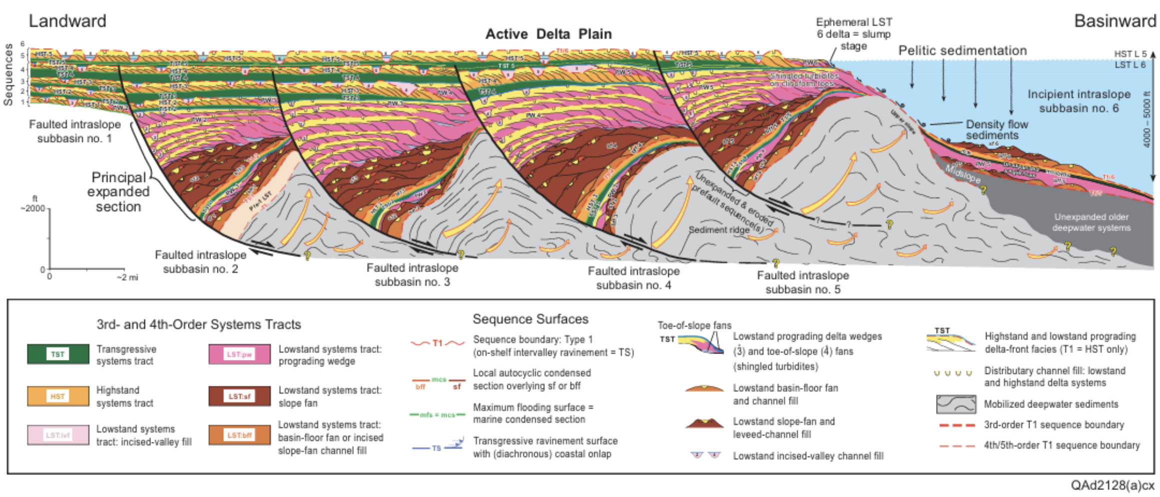

Figure 12. Schematic dip-oriented profile illustrates the structure of growth-faulted subbasins along the South Texas Gulf Coast. Adapted from Hammes et al. (2007), originally modified from Brown et al. (2004).
The Red Fish Bay subbasin is located in basin 4.

2.2.4 The Gulf Coast Aquifer

The Gulf Coast Aquifer is the major aquifer in Texas that covers the area of interest of this study. The information of this aquifer from the website of Texas Water Development Board and the Conceptual Model Report: Central and Southern Portions of Gulf Coast Aquifer System in Texas by Shi et al. (2022) is summarized in this section.

According to Texas Water Development Board, the study area of this research is located within the Groundwater Management Area 16, coinciding with the southern portion of the Gulf Coast Aquifer System, outlined in red polygon in the location map of Figure 13. According to Shi et al. (2022), the Gulf Coast Aquifer System included 4 hydrogeologic units, which are the Chicot Aquifer and the overlying alluvium deposits, the Evangeline Aquifer, the Burkeville Units, and the Jasper Aquifer as shown in Figure 14. The four units all dip toward the Gulf Coast and increase in thickness as shown in the hydrostratigraphic cross-sections in Figure 15, 16, and 17.

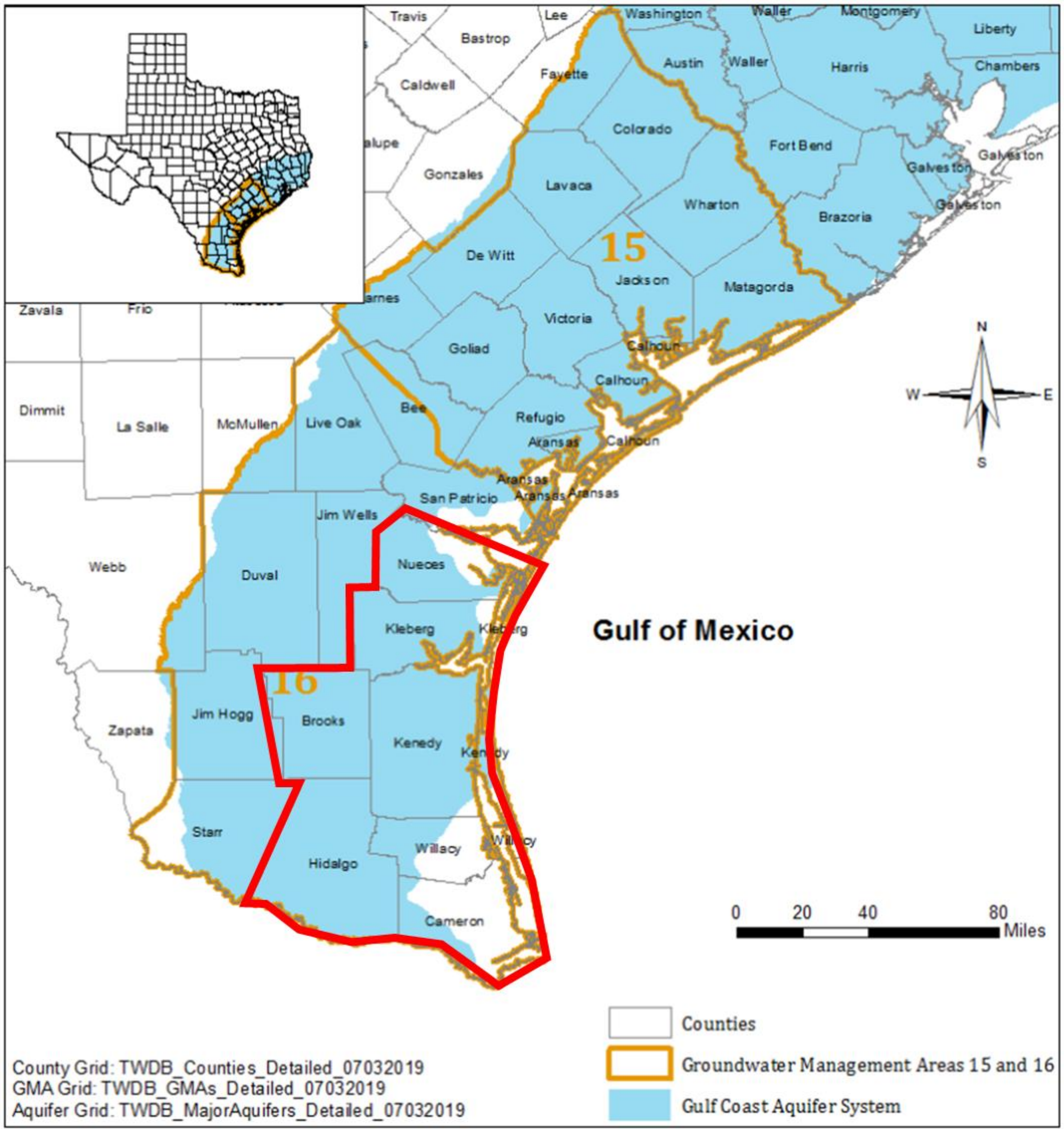

Figure 13. Location map of Groundwater Management Area 15 and 16 (Shi et al., 2022). These management areas represent the central and southern portions of the Gulf Coast Aquifer System in Texas, respectively,

<table>
<tr><th>ERA</th><th colspan="2">Period</th><th>Epoch</th><th>Stratigraphic Unit</th><th colspan="3">Hydrogeologic Unit</th></tr>
<tr><td rowspan="10">Cenozoic</td><td rowspan="4">Quaternary</td><td rowspan="4"></td><td>Holocene</td><td>Alluvium and Eolian Sand</td><td>Alluvium /Eolian Aquifer</td><td rowspan="4">Model Layer 1</td><td rowspan="10">Gulf Coast Aquifer System</td></tr>
<tr><td rowspan="3">Pleistocene</td><td>Beaumont Formation</td><td rowspan="3">Chicot Aquifer</td></tr>
<tr><td>Lissie Formation</td></tr>
<tr><td>Willis Formation</td></tr>
<tr><td rowspan="6">Tertiary</td><td rowspan="5">Neogene</td><td>Pliocene</td><td>Goliad Formation</td><td rowspan="2">Evangeline Aquifer</td><td rowspan="2">Model Layer 2</td></tr>
<tr><td rowspan="4">Miocene</td><td>Upper Fleming Formation</td></tr>
<tr><td>Middle Fleming Formation</td><td>Burkeville Unit</td><td>Model Layer 3</td></tr>
<tr><td>Lower Fleming Formation</td><td rowspan="3">Jasper Aquifer</td><td rowspan="3">Model Layer 4</td></tr>
<tr><td>Oakville Formation</td></tr>
<tr><td>Paleogene</td><td>Oligocene</td><td>Catahoula Formation (sand)</td></tr>
</table>

Figure 14. Correlation table for Stratigraphic and Hydrogeologic units. Adapted from Shi et al. (2022), originally modified from Baker (1995).

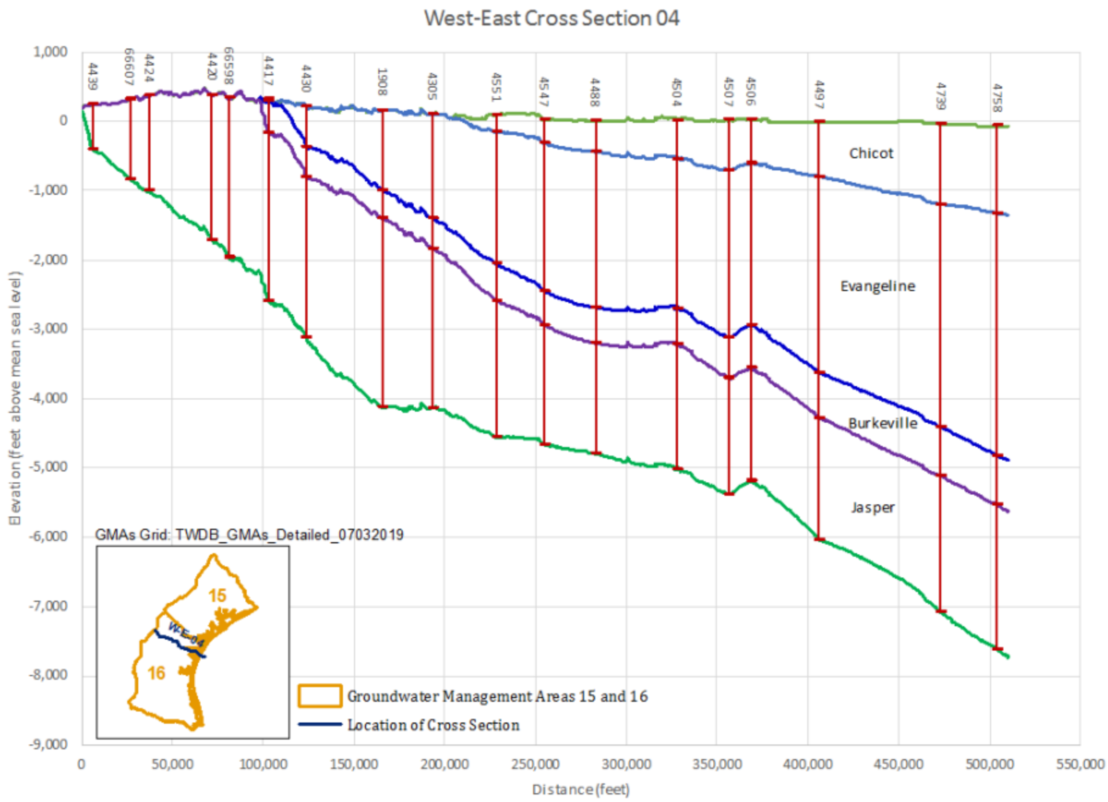

Figure 15. West-East Hydrostratigraphic Cross Section 04 from Shi et al. (2022). Vertical lines are the well log locations, and the horizontal bars represent hydrostratigraphic picks.

Figure 16. West-East Hydrostratigraphic Cross Section 05 from Shi et al. (2022). Vertical lines are the well log locations, and the horizontal bars are hydrostratigraphic picks.

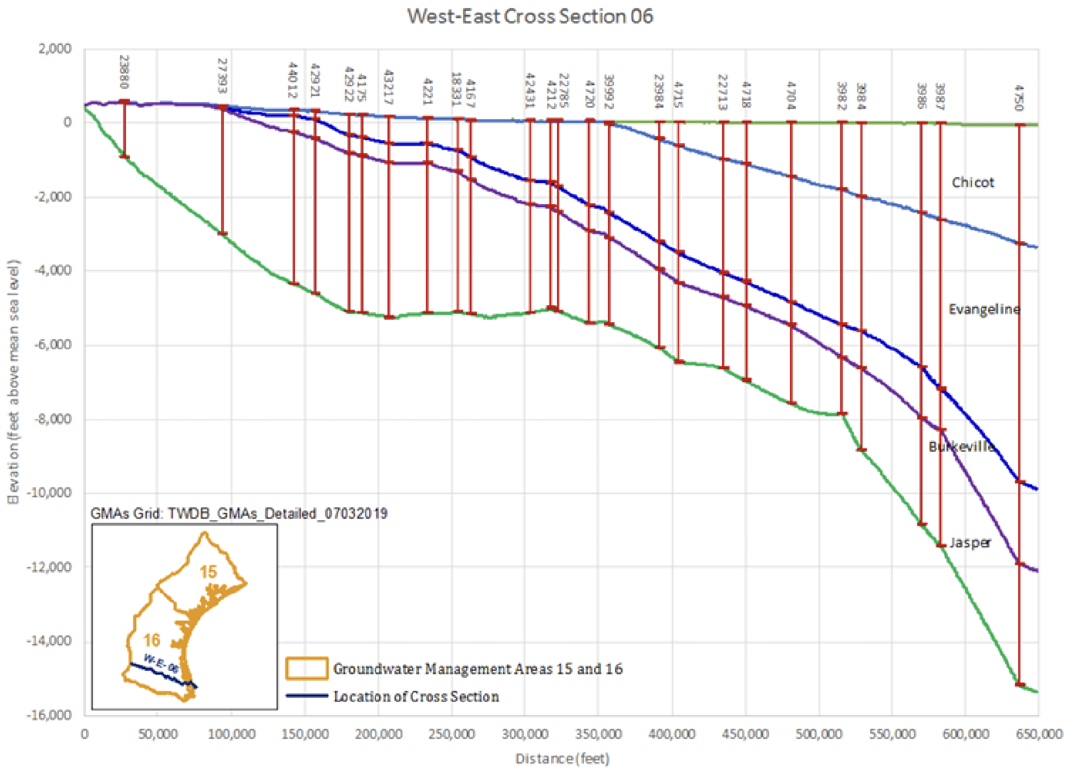

Figure 17. West-East Hydrostratigraphic Cross Section 06 from Shi et al. (2022). Vertical lines are the well log locations, and the horizontal bars are hydrostratigraphic picks.

In particular, the Jasper Aquifer is the deepest hydrogeologic unit in the system and is the closest aquifer to the Frio Formation. It comprises the lower Fleming Formation and Oakville Formation of Miocene and the upper sandy part of the Oligocene Catahoula Formation. At the updip area of the Jasper Aquifer where the Catahoula Formation contains mostly sand, it contacts and connects directly with the underlying Yequa-Jackson Aquifer. As for the downdip area, the clayey part of Catahoula Formation and Anahuac Formation separates the Jasper Aquifer and the Yequa-Jackson Aquifer. Therefore, it is assumed in the report by Shi et al. (2022) that there is no flow through the bottom of the Jasper Aquifer. In conclusion, carbon dioxide injections within the Frio Formation should not be affecting underground water in the Gulf Coast Aquifer System.

In this report (Shi et al., 2022), the groundwater is classified into the following categories based on the content of the total dissolved solids:

- Fresh – less than 1000 milligrams per liter.
- Brackish, further classified into:
- Slightly Saline – 1000 to less than 3000 milligrams per liter,
- Moderately Saline – 3000 to less than 10000 milligrams per liter.
- Very Saline – 10000 to less than 35000 milligrams per liter.
- Brine – greater than 35000 milligrams per liter.

The salinity maps of the groundwater samples in each hydrogeologic unit are shown in Figure 21 – 24 (Shi et al., 2022). A summary of groundwater salinity of each hydrogeologic unit within Groundwater Management Area 16 is provided below:

- Chicot aquifer: The groundwater is mostly brackish and is very saline only in Kenedy and Willacy counties.
- Evangeline Aquifer: The groundwater is fresh or slightly saline in the outcrop area. As the TDS increases down dip, it becomes very saline along the coastal line, such as Cameron, Hidalgo, and Willacy counties.
- Burkeville Unit: Brackish groundwater is in the outcrop area and the adjacent subcrop area. Like Evangeline Aquifer, the TDS increases rapidly and becomes very saline at the coastline counties. Brine groundwater is predominant in Cameron, Hidalgo, and Willacy counties.
- Jasper Aquifer: The trend is similar to the Burkeville Unit. The outcrop area in Groundwater management Area 15 is mostly fresh but rapidly become brackish in the subcrop area. It further turns into very saline groundwater in the coastal counties.

Brine groundwater was found in Brooks, southern Hidalgo and possibly in Cameron and Willacy counties.

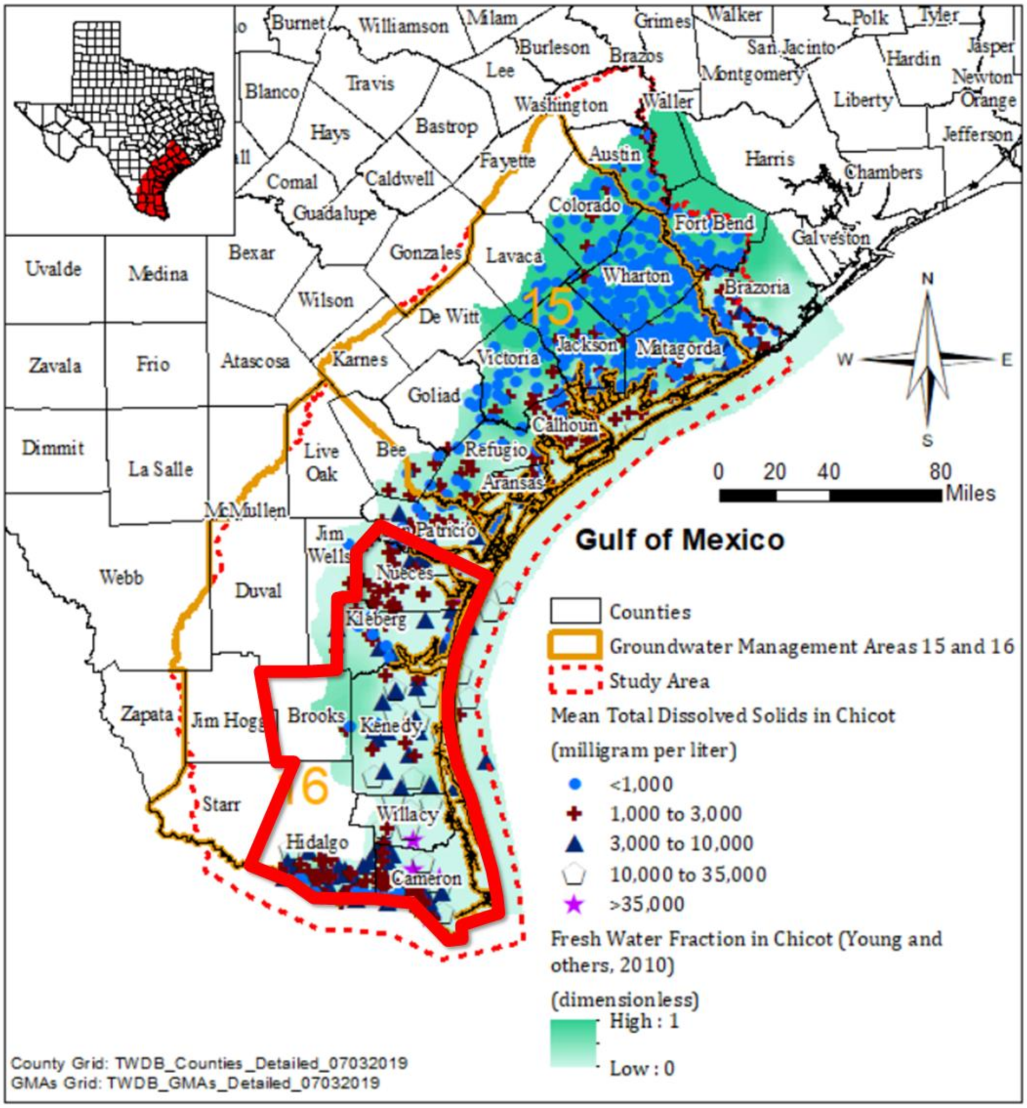

Figure 18. Total dissolved solids average concentration in groundwater samples collected from water wells in Chicot aquifer unit between 1980 and 2015 (Shi et al., 2022). Study area is outlined with the red polygon.

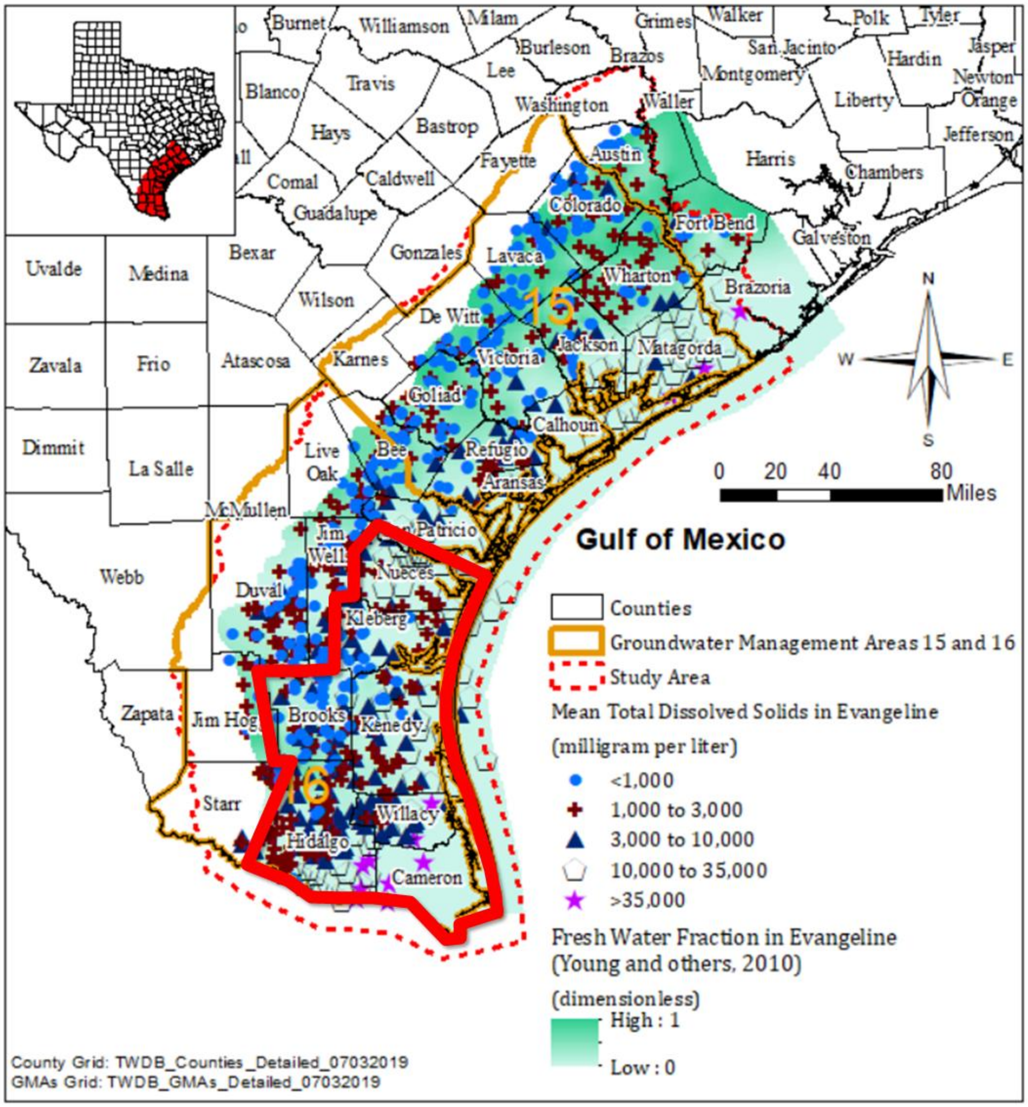

Figure 19. Total dissolved solids average concentration in groundwater samples collected from water wells in Evangeline aquifer unit between 1980 and 2015 (Shi et al., 2022). Study area is outlined with the red polygon.

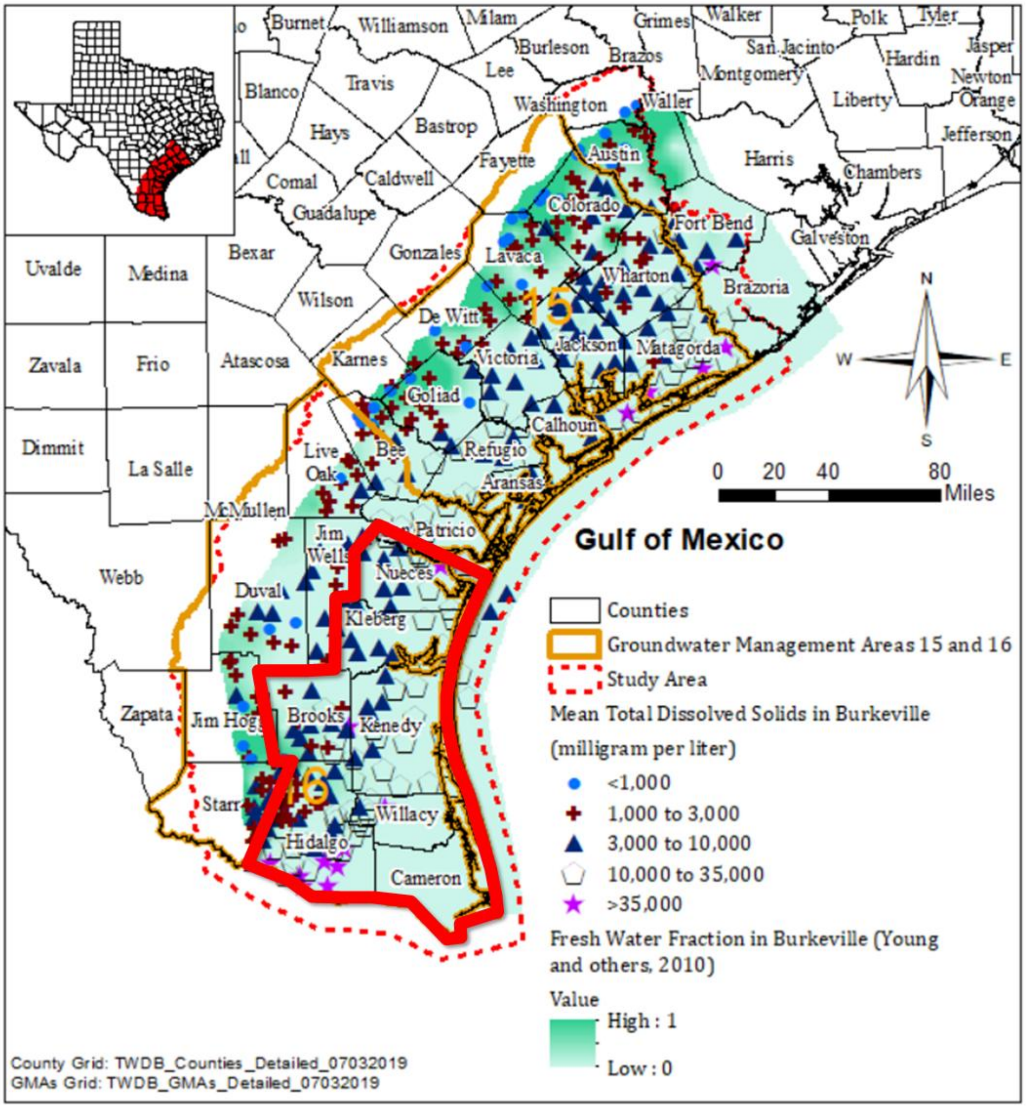

Figure 20. Total dissolved solids average concentration in groundwater samples collected from water wells in Burkeville aquifer unit between 1980 and 2015 (Shi et al., 2022). Study area is outlined with the red polygon.

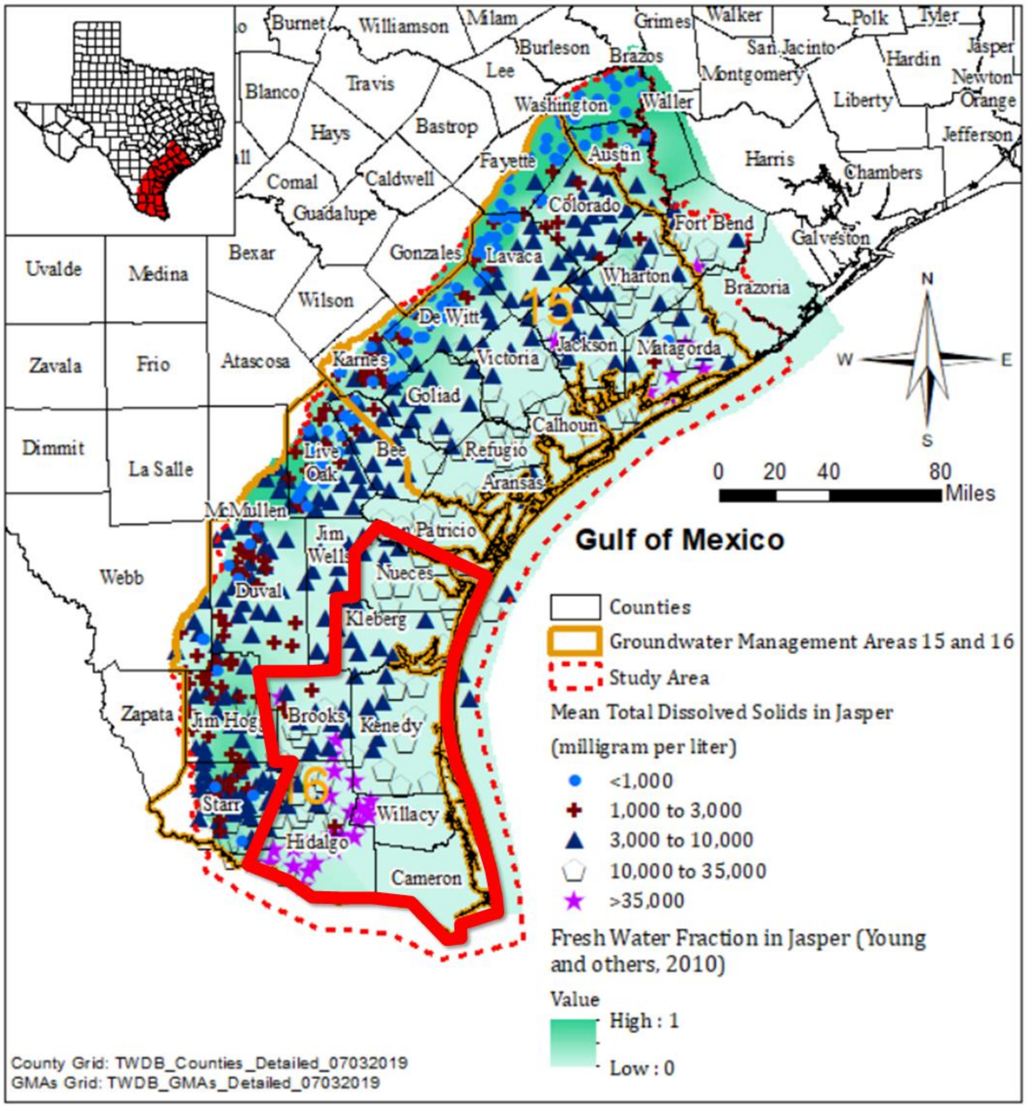

Figure 21. Total dissolved solids average concentration in groundwater samples collected from water wells in Jasper aquifer unit between 1980 and 2015 (Shi et al., 2022). Study area is outlined with the red polygon.

2.3 CO_2 SEQUESTRATION AND RELATED REGULATIONS

2.3.1 Protection for USDW

USDW is the underground source of drinking water, defined in the Code of Federal Regulations (40 C.F.R. §144.3) (2026) as:

> *An aquifer or its portion: (a)(1) Which supplies any public water system; or (2) Which contains a sufficient quantity of ground water to supply a public water system; and (i) Currently supplies drinking water for human consumption; or (ii) Contains fewer than 10,000 mg/l total dissolved solids; and (b) Which is not an exempted aquifer.*

Meanwhile, the Underground Injection Control (UIC) Program regulates the Class VI well, as known as injection wells for geologic CO_2 sequestration, to protect public health and USDWs (EPA, 2026c). Hence, the depth of the USDW base is a critical information for CO_2 injection. It is not only used for defining the upper bound of the CO_2 storage window but also for determining the area of review in which the USDW may be endangered by injection activities (EPA, 2013a).

The upper bound of a storage window is either 800m/ 2600ft or the base of USDW, whichever is lower. Carbon dioxide has to be injected into and preserved below 800m, where it maintains a dense supercritical state under the subsurface pressure and temperature (Benson et al., 2005), allowing CO_2 to be stored rather than to escape in gas form.

The base of the USDW is also used in the calculation for the critical pressure increase. It is a minimum value of pressure increase when the injection zone fluid could lift up to top of the borehole and would flow into the USDW, assuming hydrostatic conditions (EPA, 2013a). This value is used to define the edge of the front of pressure buildup, that is, the area of review (AoR), in which legacy wells should be examined and mitigated for USDW protection.

2.3.2 Injectivity

Injectivity index is a straightforward and widely used metric for evaluating the potential of a site for CO_2 injection. Valluri et al. (2021) demonstrates a linear relationship exists between injectivity index and the product of reservoir permeability and thickness (kh). Additionally, Hoffman et al. (2015) proposed a classification system to categorize reservoir types based on kh, as shown in the crossplot of Figure 22. Type 1 reservoir is where injectivity exceeds 100 darcy-meters, representing high commerciality and few technical difficulties in injection process. Type 2 reservoir is viable for onshore commercial projects but may require extra efforts in addressing plume imaging and pressure control. Type 3 reservoirs have injectivity lower than 10 darcy-meters. It is only viable for small amounts of injections and is identified to be unsuitable for developing CO_2 storage for large volumes, which might be difficult for pressure management (Hoffman et al., 2015).

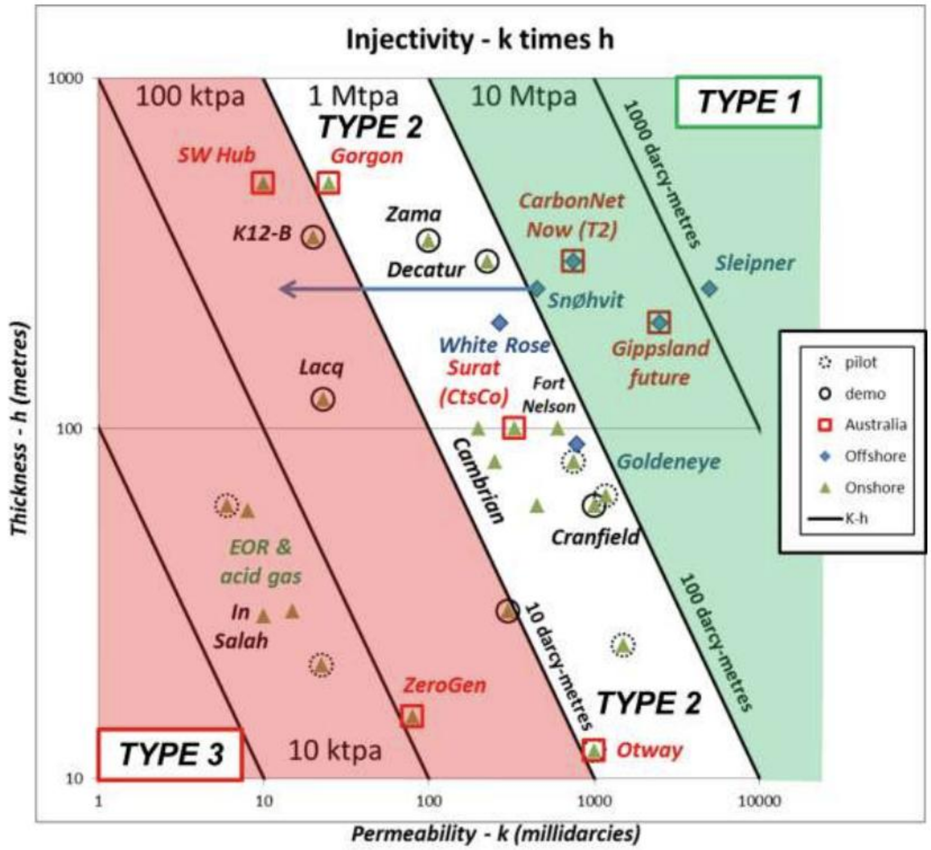

Figure 22. Thickness-permeability crossplot for injectivity from Hoffman et al. (2015).

Chapter 3: Dataset and Methodology

3.1 Datasets

3.1.1 Well logs

The database available for this project consists of more than 20000 well logs provided by Bureau of Economic Geology, including digital logs and raster logs. From the database, 766 wells with sufficient depth into the Frio Formation were selected to conduct well log correlation to identify the formation tops and to subdivide the Frio section into correlatable reservoir units (Figure 23). The SP logs were mainly used for well log correlations, assisted with resistivity logs and few available gamma ray logs. Sonic logs are used for identifying the overpressure zone. Notably, the selected wells are sparser in the southeast of the AOI. This is because the wells in that area are not deep enough to reach the Frio Formation. The IHS Petra software is used for managing the well logs, creating cross-sections and mapping, and reservoir properties analysis.

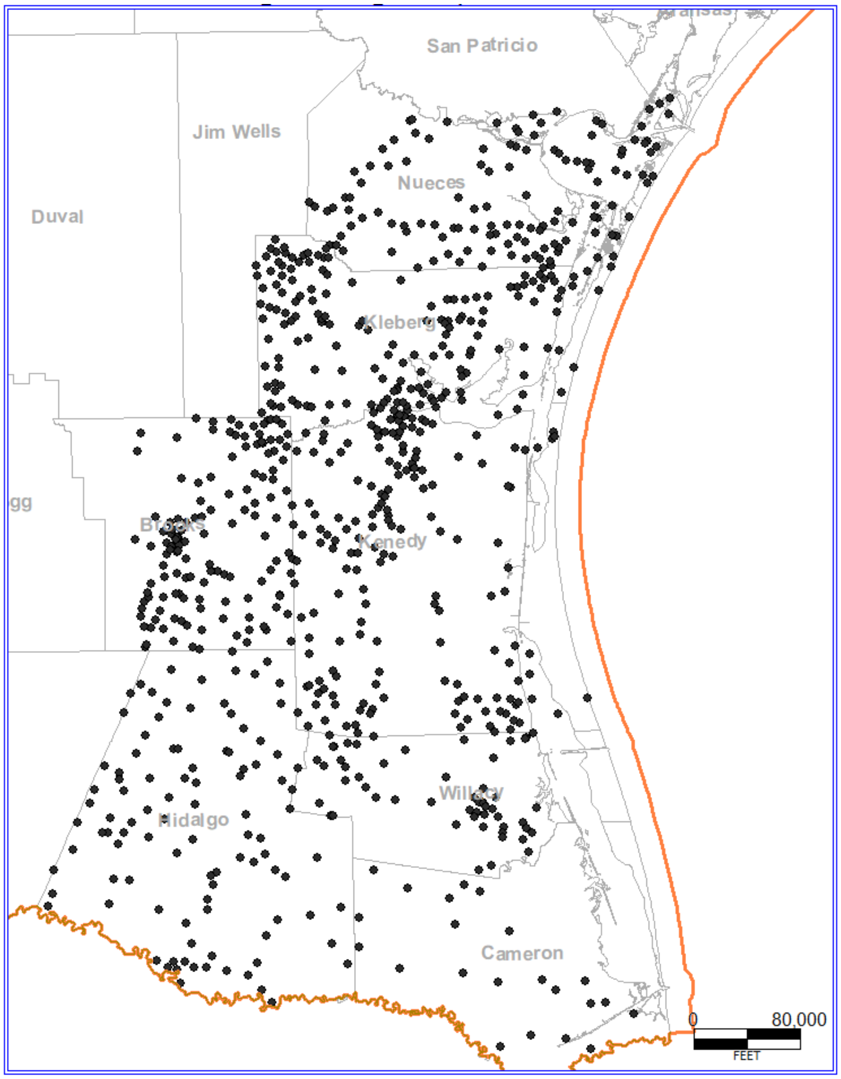

Figure 23. Location map of well log data used in this study (n = 766), indicated with black dots.

3.1.2 Core Data

Available at Austin Core Research Center of Bureau of Economic Geology, the Union Pacific No.36 Elliff, King Ranch Alazan North 183, and CW-1 were used to understand the depositional facies. Among these core data, Union Pacific No.36 Elliff and King Ranch Alazan North 183 (also named as Humble No. 183 Alazan) were published by Rogers and Ambrose (2024) (Figure 24), and CW-1 was published by Uroza et al. (2025).

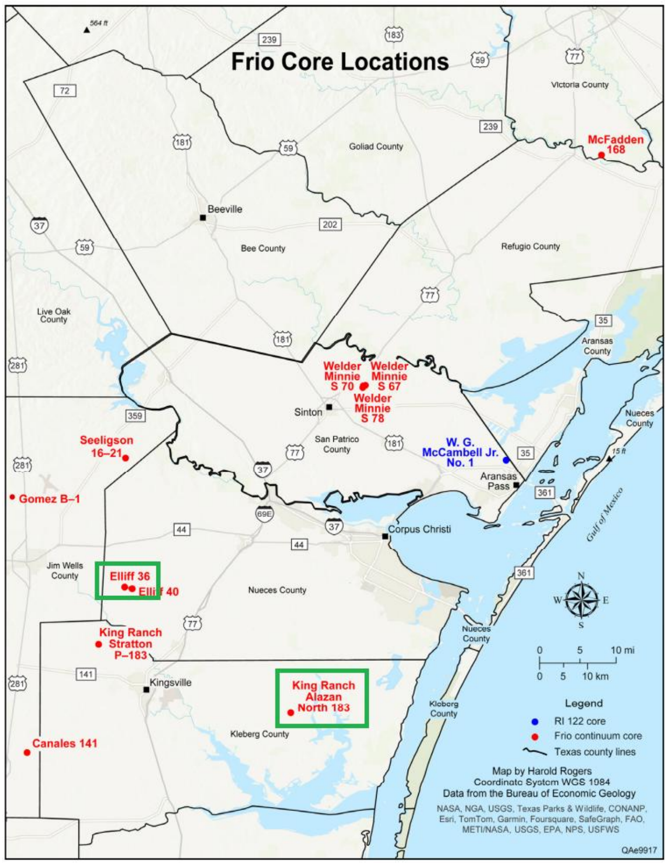

Figure 24. Location map of cored wells in the lower and middle Frio Formation from Bureau of Economic Geology's Continuum Database (Rogers and Ambrose, 2024).
Elliff 36 is located in the eastern Nueces County, and King Ranch Alazan North 183 is located in Kleberg County. They are marked up with green rectangles. CW-1 is not on this map.

3.1.3 Petrophysical Core Measurements

Obtained confidentially from Bureau of Economic Geology, core measurements from 50 cored wells were used to conduct permeability-porosity evaluation, and their location is indicated in Figure 25. The reservoir properties for site-specific storage capacity estimation were also derived from this dataset.

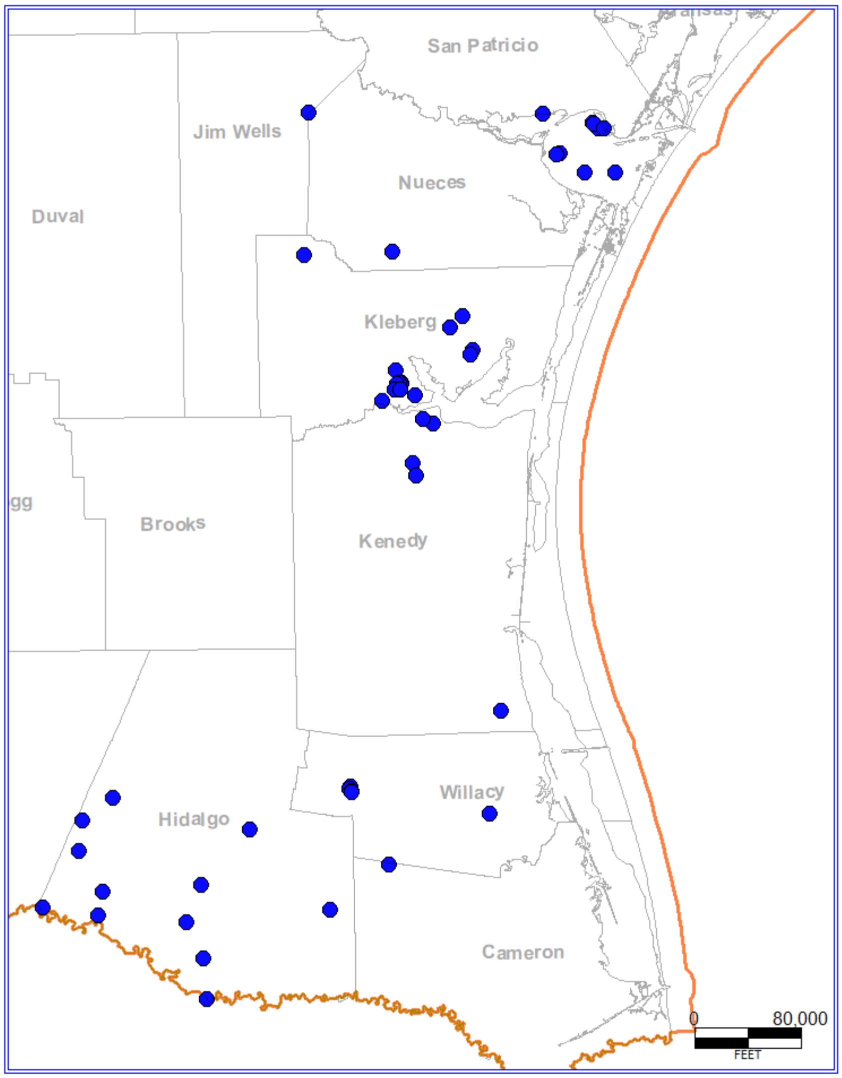

Figure 25. Location map of wells with core petrophysical measurements from the Frio Formation (dark blue dots).
The orange line represents the international boundary.

3.2 METHODOLOGY

3.2.1 Geological Characterization

The geologic characterization involves conducting extensive well log correlation to track the continuity of Frio reservoir units within the study area, which provided the framework for creating structural maps, cross-sections and net-sand distribution maps, as well as reservoir properties analysis. All of these tasks are performed with the IHS Petra software.

The well-log correlation and net sand thickness summation largely relied on the Spontaneous Potential (SP) log data, because it is the most densely distributed available log data for this study. Therefore, SP logs were normalized with the Percentage Range Method to minimize the negative effects caused by abnormal log values and to assure the quality of subsequent analysis. In this method, the low and high percentiles were set to 5 and 95, respectively, and the SP log curves were normalized to a scale low value of -120 mV and a scale high value of 20 mV. A threshold value of -35 mV was applied as a sand cutoff. This threshold is decided from the identification of shale baselines on the SP log curves. SP log values below -35 mV were interpreted as sandstone, whereas values above the baseline were interpreted as shale. In all SP logs presented in this study are displayed with a scale range of -120 to 20 mV, sandy intervals are highlighted in yellow and shaly intervals are in gray.

After being normalized, SP logs are mainly used to trace flooding surfaces across the study area to identify stratigraphic reservoir units and subunits, with support from few resistivity logs and gamma ray logs. Based on previous stratigraphic work supported with paleo data, the base of the Anahuac Shale is identified as the marker to trace the top of the Frio Formation. Subsequently, the Frio Formation was subdivided into three reservoir intervals named Zone 1, Zone 2, and Zone 3 following the regional correlatable shale-prone surfaces. The subdivision picks are developed independently by this study. Cross-sections were created for displaying the variation and continuity of reservoir units along depositional strike and depositional dip.

In what follows, the log footage summation tool in the IHS Petra software was used to sum up the thickness of the sandy sections with SP log values between -120 and -35 MV to calculate the net sand content for each subdivision. Net sand content maps were created to visualize the spatial distribution of sandstone in the area of study and served as a screening for potential CO_2 sequestration sites.

Additionally, in order to define the upper and lower bound of the storage window, the base of USDW and the overpressure zone is required. Thorough investigation regarding aquifer system in South Texas is done by Shi et al. (2022). The hydrostratigraphic unit that contains the base of USDW at a given location can be identified with the maps of groundwater samples expressed in the amount of total dissolve solid for each aquifer unit (figure 20s) from the report. As for the specific depth of the USDW base, it can be obtained by reading the depth from the hydrostratigraphic cross-sections provided in Shi et al. (2022).

Sonic (DT) logs were used to identify the overpressure zone. According to SLB Energy Glossary website (2025), an overpressure zone is a depth interval where the pressure of the fluid in the pores is higher than the hydrostatic pressure at that depth, indicating that this zone does not have available pressure space to accommodate the injected carbon dioxide. Overpressure can be recognized on sonic logs at the depth where the transit time (Δt) starts to rapidly increase due to the overpressured fluid. The sonic logs presented in this study are displayed in blue log curves with a left scale of 150 μs/ft and a right scale of 50 μs/ft. Depths of overpressure zone together with information of USDWs define a CO_2 storage window.

Finally, permeability-porosity analysis of the core measurements was conducted. A permeability-porosity transform was obtained by zone to zone for several locations to assess how these reservoir parameters vary spatially. Also, statistical analysis is done to decide the representative values for later capacity estimations.

3.2.2 Storage Capacity Estimation with EASiTool

The maximum storage module of EASiTool was used for calculating the capacity estimation in this study. Developed by the Gulf Coast Carbon Center, Bureau of Economic Geology, University of Texas at Austin (Ganjdanesh and Hosseini, 2017; 2018), the software is a CO_2 storage capacity calculation tool that assumes the reservoir is a homogeneous formation with consistent properties. Therefore, one of the major tasks of this study is to obtain and calculate the representative values of the reservoir properties as EASiTool inputs. Most of the reservoir properties are available in the core measurement datasets. The methods for obtaining each parameter for estimation are as follows:

- Boundary Conditions – All estimations were made assuming open boundary conditions. Although fault lines from Ewing (1991) were used to assist with deciding the reservoir area, every reservoir of the proposed sites is not completely closed by faults. Additionally, whether sandstones beds are connected to the adjacent compartments remains unknown without seismic data and further investigations into the faults.

- Representative depth of the reservoir – Determined as the depth of the mid-point of a zone, calculated by adding half of the average zone thickness to the average depth of the zone top in a reservoir area.
- Net sand thickness – Obtained with the log footage summarization tools built in Petra software, which calculated the average net sand thickness of each zone in the reservoir areas.
- Porosity – Determined by the average of all porosity data available in the zone.
- Permeability – Determined the geomean of all permeability data available in the zone, instead of arithmetic means because permeability data is log-normal distributed.
- Initial pressure at the representative depth – Derived from local pressure gradient calculated from core measurement data, if core data is available in the reservoir wish to be assessed. Else, a hydrostatic pressure gradient of 10.5 MPa/ km (0.465 psi/ft) for saline reservoirs obtained from Tiab and Donaldson (2016) is used since the measured pressure from core data is not reliable when it is not in the same pressure compartment as the storage site.
- Reservoir temperature – Obtained in the same way as initial pressure. According to Loucks et al., (1984), a geothermal gradient of 37 C/km (0.0205 F/ft) specified for the Frio Formation in lower Texas is used when local temperature data is unavailable.
- Salinity – obtained from the concentration profile of total dissolved solids (TDS) along depth within the Frio formation in Portland field and Corpus Christi field (Nueces County) or in Candelaria field (Kenedy County), as reported on the page 42 and 50 of the Annual Report of salinity variations and chemical compositions of waters in the Frio Formation, Texas Gulf Coast by Morton et al. (1981). The

salinity data were originally provided in TDS (milligram per liter, mg/ L) and were then converted to moles per kilogram for use in EASiTool calculations. Salinity values were selected from the concentration profile of the field closets to the candidate site. If the depth of a targeted zone lies above the range of the concentration profile, the salinity of that zone is assigned using the uppermost available data point in the profile.

- Maximum allowable injection pressure – Calculated using Eaton's method (Zhang and Yin, 2017) as 85% of a thumbnail of fracture pressure gradient of 17 MPa/km (0.75 psi/ft) for the Frio Formation, obtained from Uroza (2026, personal communication).
- Critical pressure increase – Determined by the injection-zone fluid density, the fluid density of the USDW, the representative depth of the injection zone, and the representative depth of the USDW. The information related to USDW in this study was obtained from Shi et al. (2022). This study adopted the method developed by Nicot et al. (2008) and Bandilla et al. (2012). Assuming under hydrostatic conditions, and when density varies linearly in boreholes initially and becomes a constant once the injection fluid is lifted up to the top of the borehole, the critical pressure increase (ΔPc) can be calculated as (EPA, 2013a):

$$\Delta P_c = \frac{1}{2} \cdot g \cdot \xi \cdot (z_u - z_i)^2$$

as ξ represents a linear coefficient that is defined by:

$$\xi = \frac{\rho_i - \rho_u}{z_u - z_i}$$

Where ρ_u = fluid density of the USDW; ρ_i = fluid density of injection zone fluid; z_u = representative depth of USDW; z_i = representative depth of injection zone.

- Injection duration – Set to 20 years.
- Rock compressibility – set as default values of $5 \times 10^{(-10)}\ Pa^{(-1)}$
- Relative permeability properties – Use 3 for Water Corey Exponent, 3 for Gas Corey Exponent, 1 for Endpoint Water Relative Permeability, 0.3 for Endpoint Gas Relative Permeability, 0.2 for Residual Water Saturation, and 0.1 for Critical Gas Saturation.
- Inputs for the sensitivity simulations – The minimum and maximum values of porosity, permeability, and net sandstone thickness were set to ±1 standard deviation from the base-case values. The maximum allowable injection pressure was varied by applying multipliers of 1.15 and 0.85 to the base case. All other input parameters were adjusted by applying multipliers of 1.02 and 0.98 to their base-case values.

Chapter 4: Geological Characterization

4.1 STRATIGRAPHIC ANALYSIS

Anahuac Shale, one of the most continuous flooding surfaces/ shales in South Texas, serves as an index formation to trace top of Frio Formation and also serves as the major seals across the AOI.

Three subdivision markers are placed where continuous flooding surfaces/ shale are present, and three sandstone reservoir units are identified from the Frio Formation. The three markers are named FRIO_MKR1, FRIO_MKR2, FRIO_MKR3, and Zone 1, Zone 2, Zone 3 are defined by the top of Frio Formation and these markers as shown in example logs in Figure 26. It should be noted that the last subdivision marker, FRIO_MKR3, is not the base of the Frio Formation.

The thickness of both Zone 1 and Zone 2 is about 1000 ft to 1500 ft. Zone 3 is remarkably thicker than Zone 1 and 2, due to a continuously prograding stacking pattern identified in the Nueces County, where the type-log is located (Figure 27, 28, and 29). The thickness of Zone 3 varies from 2000 ft to 3000 ft.

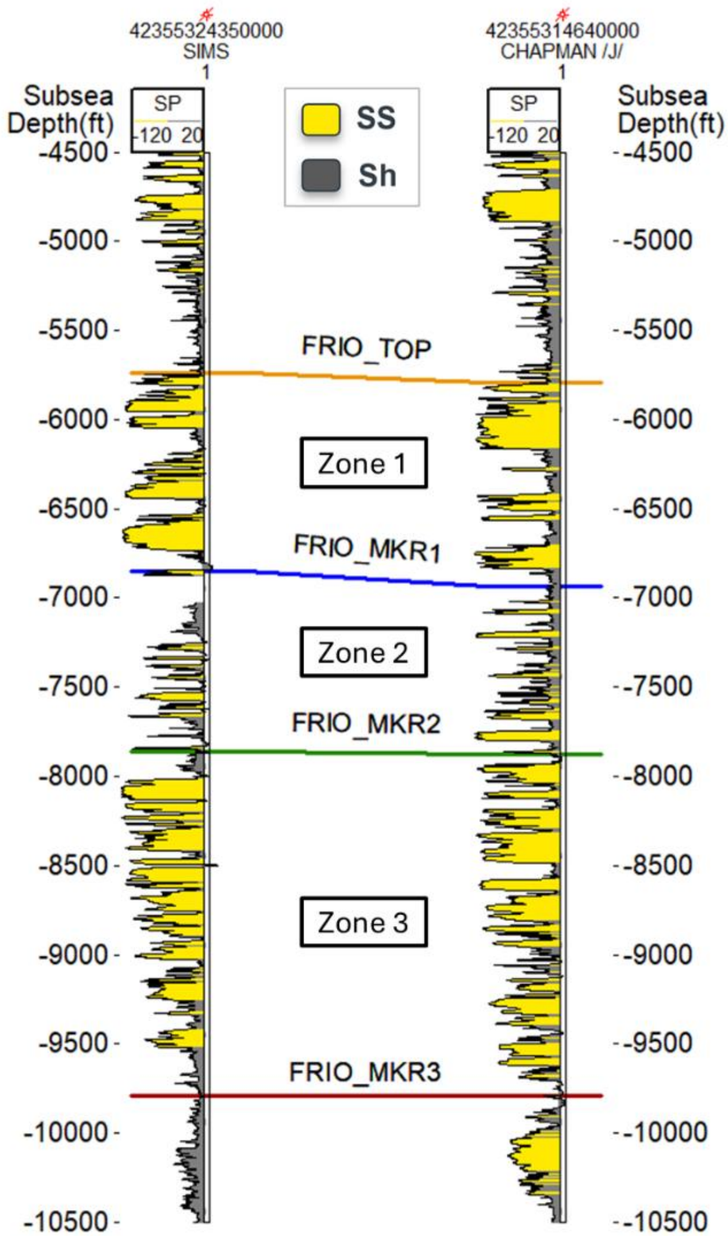

Figure 26. Example SP logs in the southern Nueces for identifying stratigraphic markers. A cutoff of -35 mV on the SP logs was applied to distinguish sandy intervals (marked in yellow) from shaly intervals (marked in gray). Their API number, well name, and number are indicated at the well symbol. The location of these logs is indicated with the star sign in the following sand maps (Figure 27, 28, and 29).

4.1.1 Confinement Assurance - Anahuac Shale

According to the results of well log correlation in this study, the average thickness of Anahuac shale is about 140 m (460 ft) thick, with a minimum around 50 m in the updip and a maximum up to 450 m in the downdip. Anahuac Shale is a useful shale marker not only acts as a regional seal to constrain the injection fluids within the Frio Formation, but it is also a shale layer that effectively separates the USDWs and brine in Frio saline reservoirs (Shi et al., 2022).

4.1.2 Net Sandstone Maps

Based on the flooding surfaces defined in the example logs (Figure 26), the markers are correlated to the whole AOI mainly by the SP logs with few gamma ray logs and resistivity logs. The net sand maps are subsequently created for each reservoir zone to visualize the aerial distribution of reservoir sandstone. They are used to determine the location of depocenters, and they also indicate the net sandstone thickness of a zone at a given location, which assists with selecting candidate storage sites and provides numerical inputs for storage capacity estimation.

Correlated along the strike orientation, the strike-oriented cross-section AA' and BB' (Figure 30 and 31) illustrates the continuity of reservoir units beginning with the example logs (Figure 26) in the Nueces County.

4.1.2.1 Zone 1

Zone 1 is at depths of approximately 5500 ft to 7000 ft. The main depocenter was developed below the present-day Baffin Bay and the northern area of Kenedy County (Figure 27). High sandstone content along the coastal area of Kleberg, Kenedy, Willacy are likely to be delta front sandstones. Blocky sandstones are also found in the north bound of Nueces County, interpreted as the Greta Barrier/ Strandplain system according to Galloway et al. (1982a).

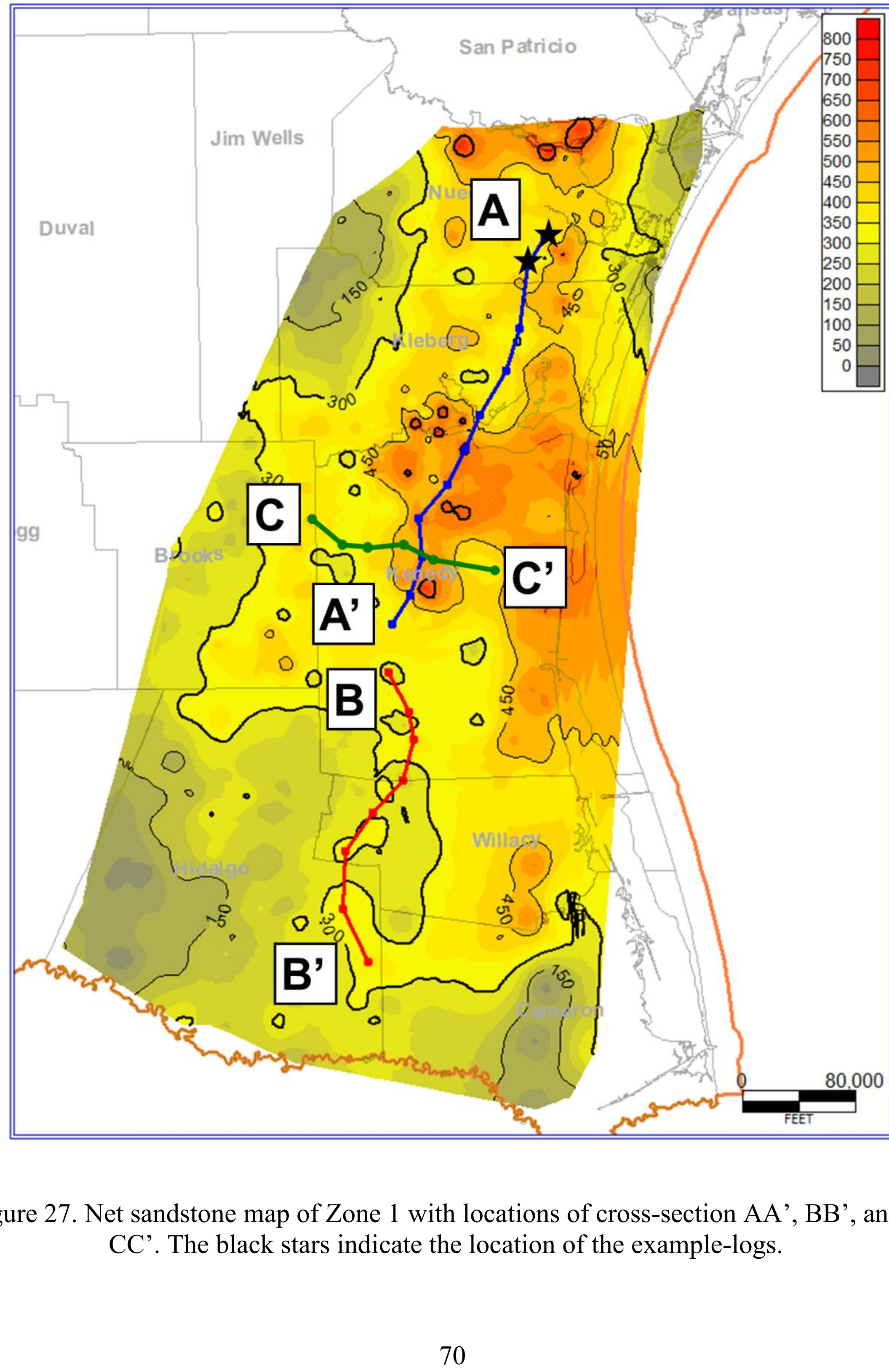

Figure 27. Net sandstone map of Zone 1 with locations of cross-section AA', BB', and CC'. The black stars indicate the location of the example-logs.

4.1.2.2 Zone 2

Zone 2 is at depths of approximately 7000 ft to 8000 ft. In Figure 28, the high sand content with thickness of more than 500 ft beneath the Baffin Bay area and the modern coastal area of Kenedy, and Willacy County may be interpreted as delta front facies according to Rogers and Ambroses (2024). Fluvial sandy facies are also clearly observed along the boundary of the Brooks and Kenedy counties.

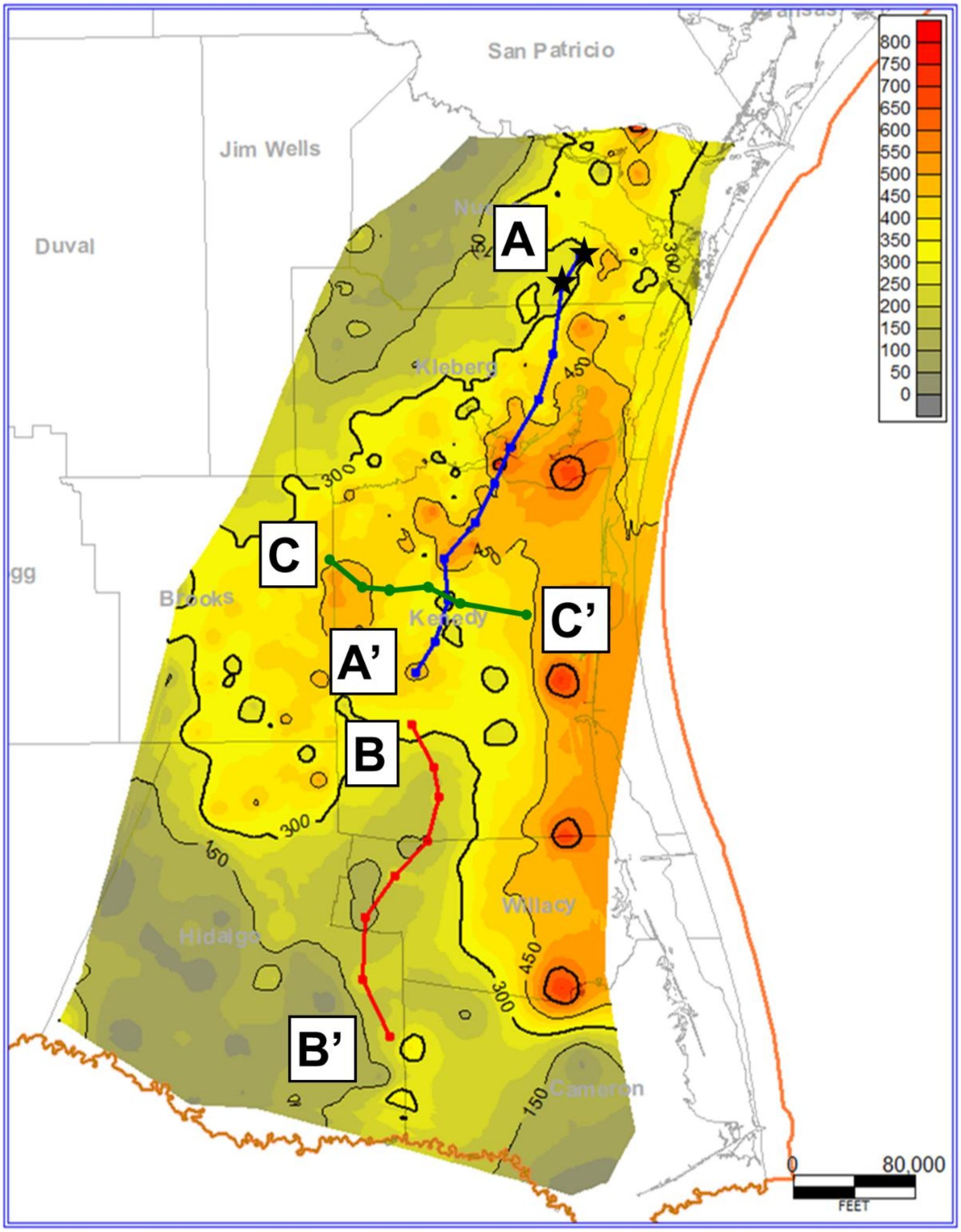

Figure 28. Net sandstone map of Zone 2 with locations of cross-section AA', BB', and CC'. The black stars indicate the location of the example logs.

4.1.2.3 Zone 3

Zone 3 is at depth of approximately 8000 ft to 10000 ft. In Figure 29, a higher net sandstone content appears on the northeastern Nueces County, could be associated with development of the Greta Barrier/ Strandplain system (Galloway et al., 1982a). The delta front facies are observed across the Kenedy and Willacy County. The most significant difference between Zone 1 and Zone 2 is that Zone 3 has thicker sandstone in the southeastern part of the AOI.

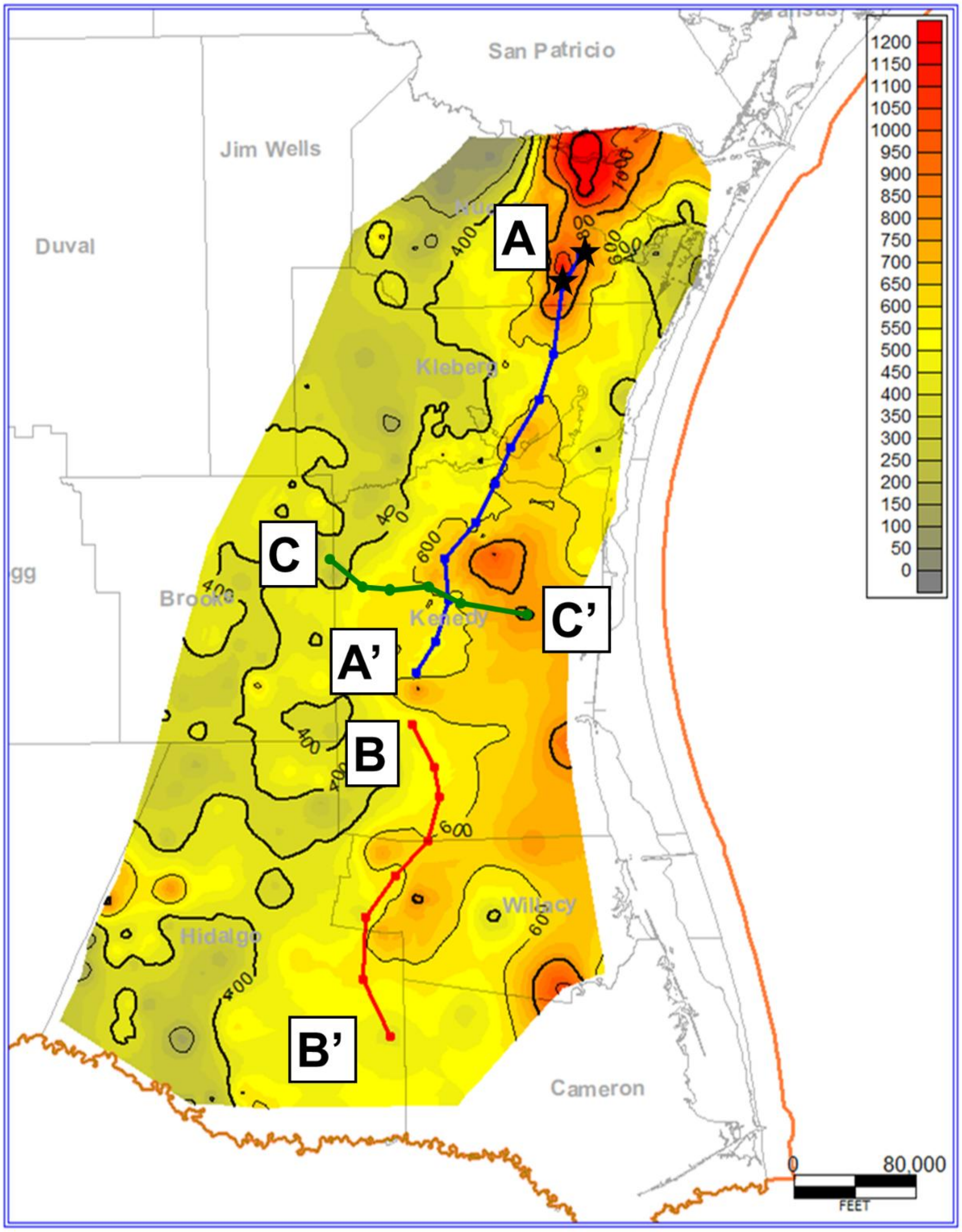

Figure 29. Net sandstone map of Zone 3 with locations of cross-section AA’, BB’, and CC’. The black stars indicate the location of the example logs.

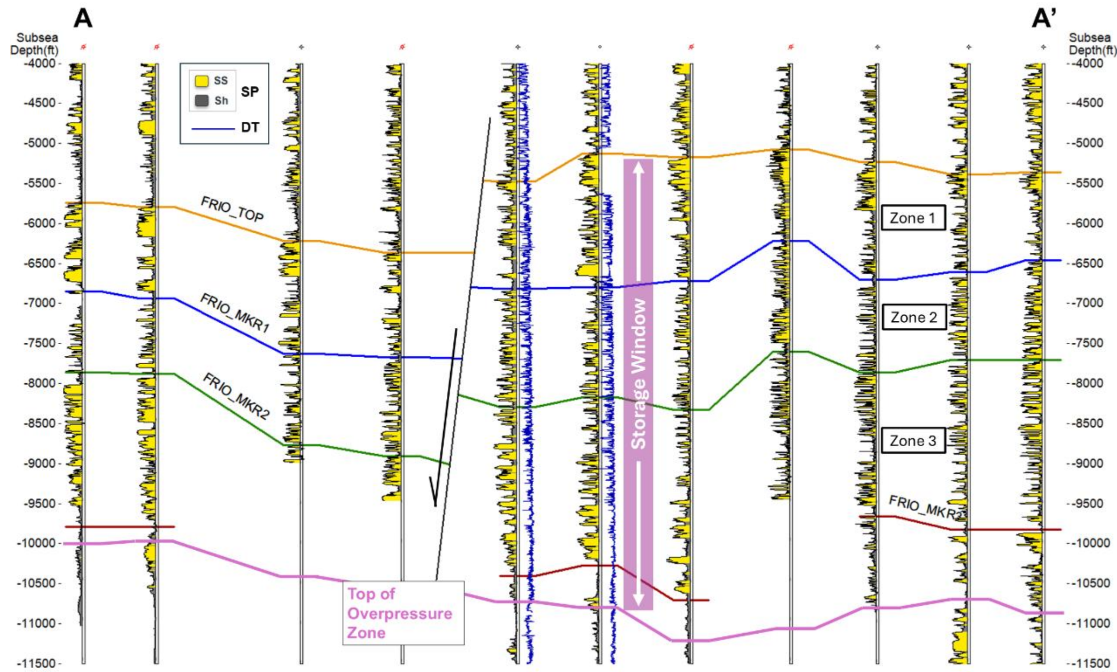

Figure 30. Cross-section AA' showing SP logs, sonic logs, Frio subdivision markers and the extrapolated top of overpressure zone.
SP logs highlight sandstone in yellow and shale in gray with a scale range of -120 to 20 mV. Sonic logs are shown in blue with a reversed scale range of 150 to 50 μs/ft. Stratigraphic markers are traced from the two example logs in the north towards the south to illustrate the continuity of the sandy units.

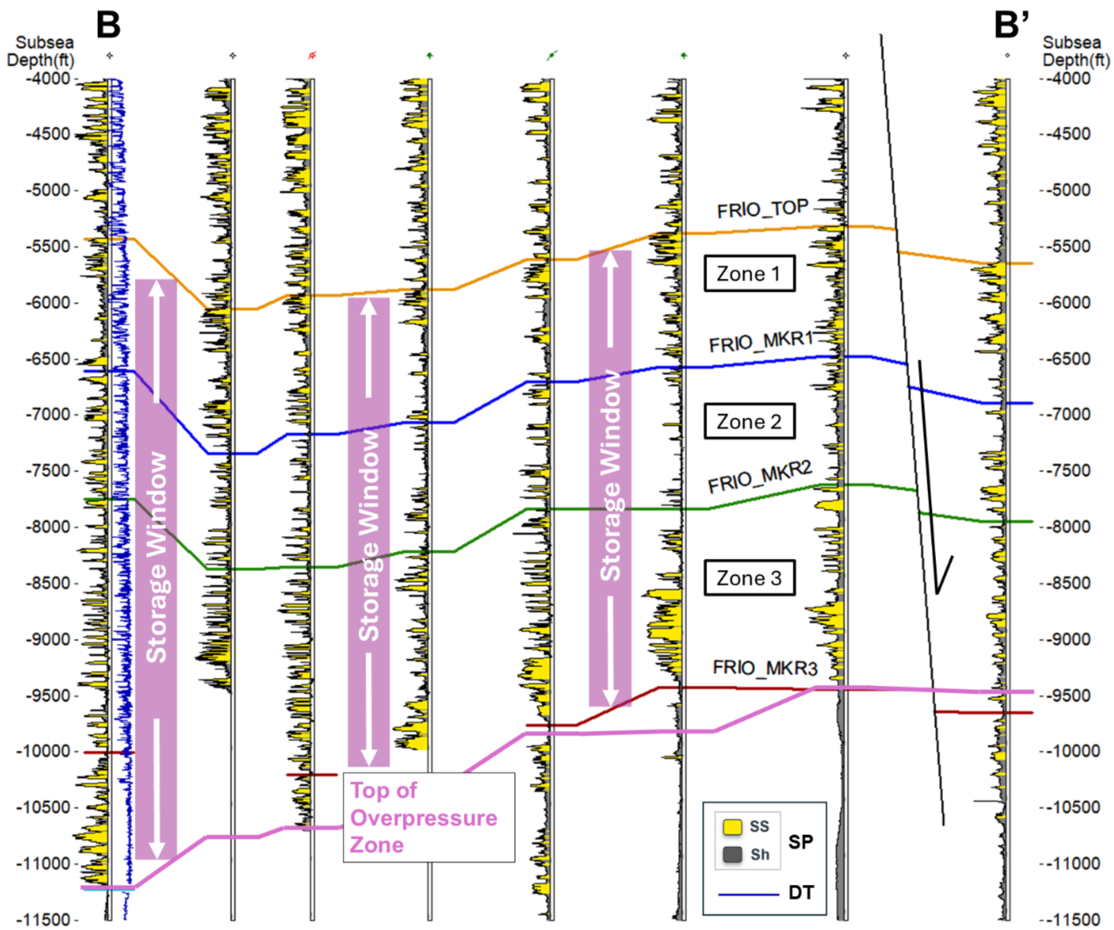

Figure 31. Cross-section BB' showing SP logs, sonic logs, Frio subdivision markers, and the extrapolated top of overpressure zone.

4.1.4 Facies Interpretation

In order to infer the depositional facies, an attempt to trace the shale continuity and sand body architecture is presented on the stratigraphic cross-sections of Figure 32 and 33. Facies interpretation has been done to define the depositional setting. In Figure 32, shale markers are highlighted in green to show the shale continuity within the central Kenedy County. In Figure 33, depositional facies interpretation is done on Zone 2 interval. On the updip of the cross-section, the channel fill deposits are observed, suggesting the presence of delta plain facies. The upward coarsening pattern of mouth bars is the main feature in the downdip, which indicates that the downdip is in a delta front setting.

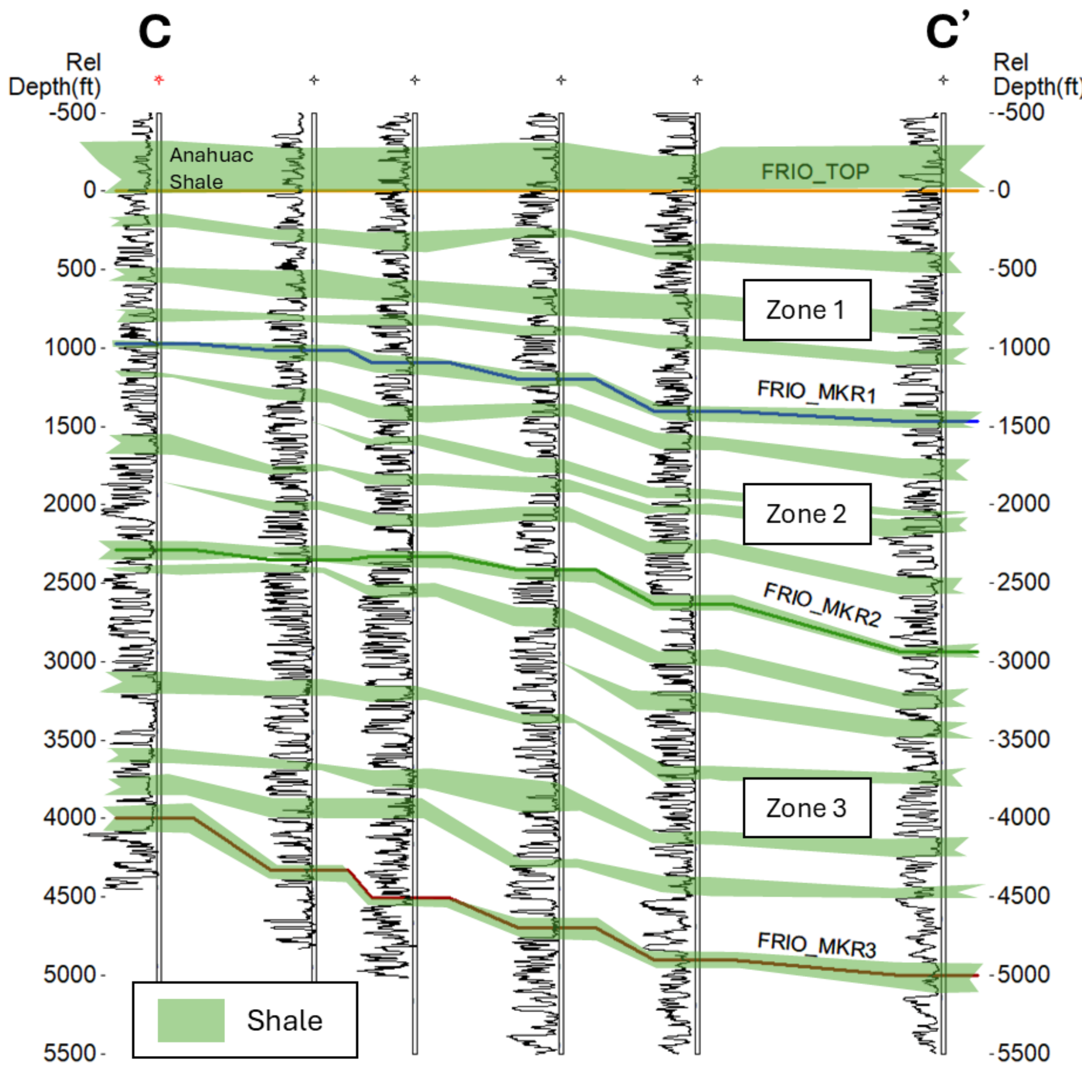

Figure 32. Dip-oriented stratigraphic cross-section CC' from the Frio Top to the bottom of Zone 3, with main shale-prone surfaces highlighted in green.

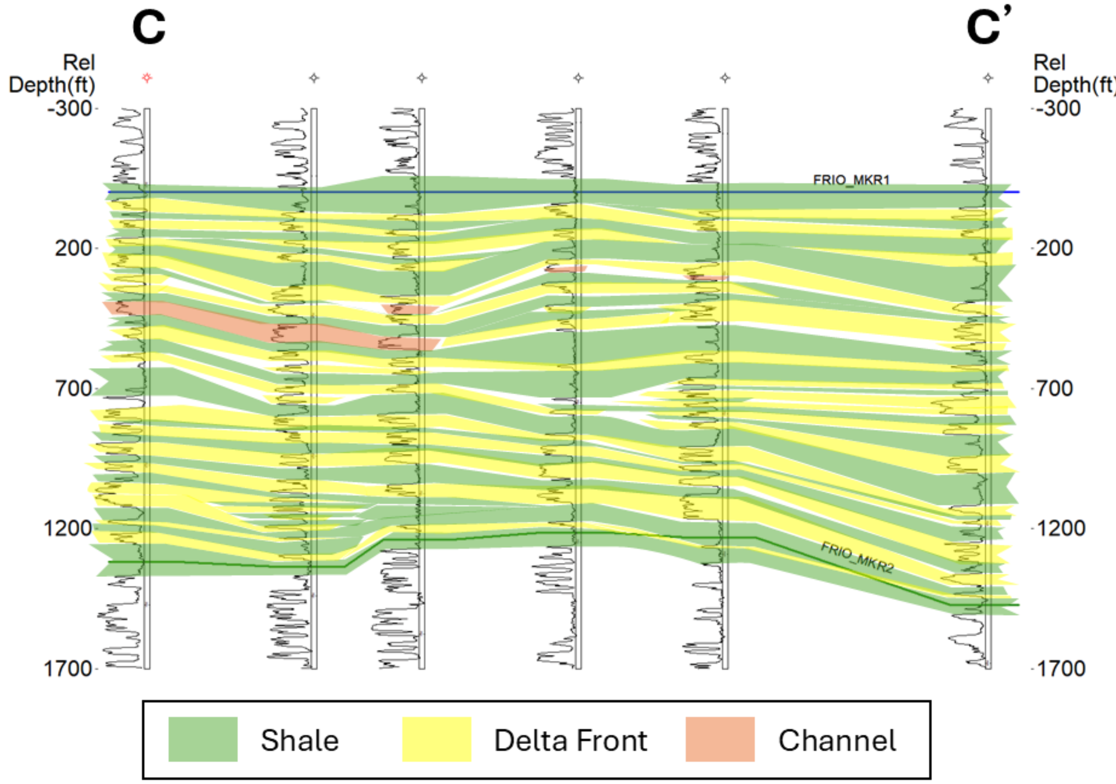

Figure 33. Dip-oriented stratigraphic cross-section CC' in Zone 2, flatten on FRIO_MKR1.
Shale is highlighted with green. Yellow indicates the presence of delta front sands. Channel fill deposits are highlighted with pink.

4.1.5 Core Descriptions

The facies variability of the lower and middle Frio Formation in South Texas is investigated in previous studies (Rogers and Ambrose, 2024; Uroza et al., 2025). Three cored wells from their study are located within the area of interest of this study, which are Union Pacific No.36 Elliff in Nueces County and Humble No. 183 Alazan in Kleberg County, and CW-1 in Kleberg. The characteristics of these wells are summarized below.

4.1.5.1 Well Union Pacific No.36 Elliff

Located in Nueces, the Union Pacific No.36 demonstrates the floodplain paleogeographic trend in the middle Frio section. The depth interval of this core data starts from the base depth of 5755ft and ends at 5680 ft and is also identified as the top of Zone 3 according to the reservoir subdivision of this study. The sandstone- percent value of the core is generally around 10%; nevertheless, a 75 ft section consists of more than 80% of sandstone (Rogers and Ambrose, 2024).

This core description (Figure 34) is divided into the lower and upper sandy section. The lower section (5725 ft – 5755 ft) is consisted of very fine- to fine-grained sands with clay nodules and interbedded with mudstone and root traces, interpreted as crevasse-splay and splay-channel deposits. A 35 ft thick fluvial channel-fill deposits of fine- to medium-grained sandstones beds overlain the lower section subsequently. Each sandstone bed in this section is scour-based and upward-fining with mudstone rip-up clast. In the upper part of the core (5680 ft – 5690 ft) represents the abandoned- channel facies, where the very fine-grained sandstone is upward-fining and then overlain by silty mudstone (Rogers and Ambrose, 2024).

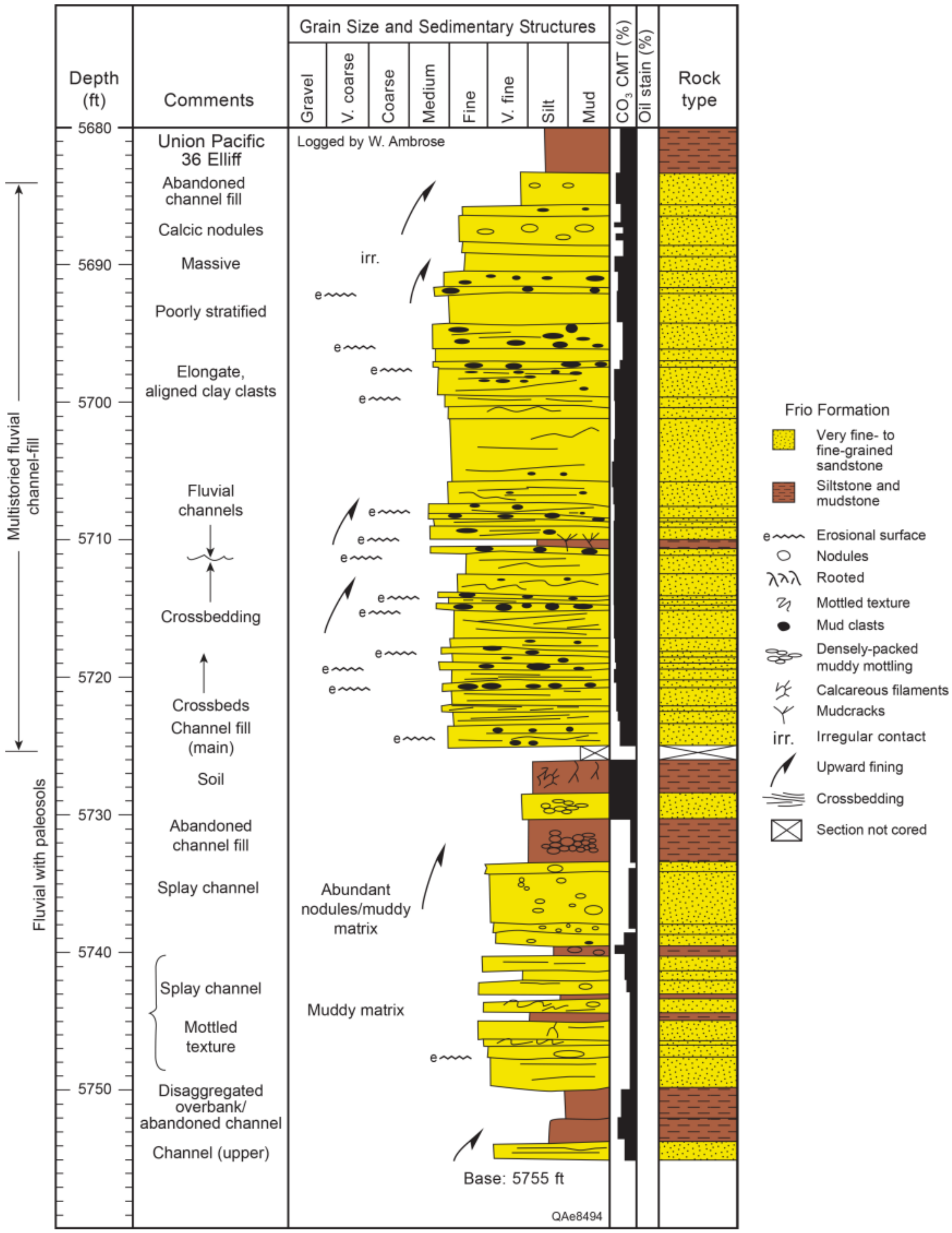

Figure 34. Core description of Union Pacific No.36 Elliff well, mostly showing the upward fining stacking patterns (Rogers and Ambrose, 2024).

4.1.5.2 Well Humble No. 183 Alazan

Located in Kleberg County, the Humble No. 183 Alazan well presents the depth interval from 7870 ft to 7910ft, which includes the northeastern margin of lower delta plain/margin paleogeographic trend in lower Frio section (Rogers and Ambrose, 2024). This core data is identified in the middle of Zone 3.

The percentage-sandstone values are less than 30% in this interval. As shown in Figure 35, between the depth interval of 7870 ft and 7910 ft, the very fine- to fine grained sandstone of the bottom beds coarsening upwards to fine- to medium-grain. According to the interpretation of the Rogers and Ambrose (2024), the delta-front deposits around 7890 ft with ripple- stratified and significantly burrowed sandstone are overlain by the channel- mouth bar facies with non-burrowed, planar-stratified sandstones at 7875 ft (Rogers and Ambrose, 2024).

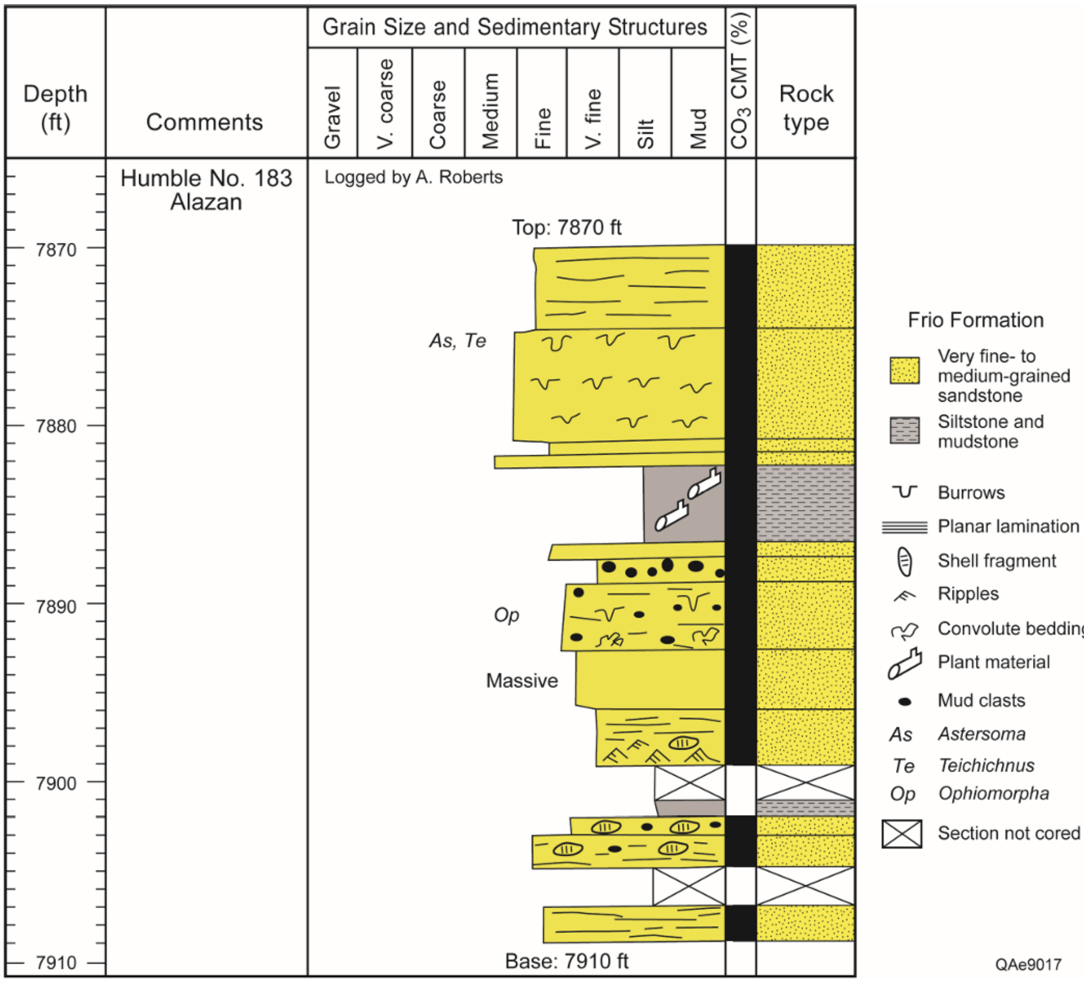

Figure 35. Core description of Humble No. 183 Alazan, recording the medial-delta-front facies of the lower Frio Formation (Rogers and Ambrose, 2024).

4.1.5.3 Well CW-1

Located in Kleberg County, close to the Humble No.183 Alazan well, core description of CW-1 well presents depth interval from 9240 ft to 9330 ft, roughly at the bottom of Zone 3. The thin sections are also included for showing the sandstone quality.

In the interval of 9240 ft to 9280 ft (Figure 36), the core description illustrates 2 upward coarsening parasequences and indicates delta-front facies developed under wave-dominant environment. At the depth of 9279.6 ft, the thin section suggests very fine sandstones with low quality. The plain light slide has no blue epoxy, since calcite cement has completely clogged the porosity. (Uroza et al., 2025)

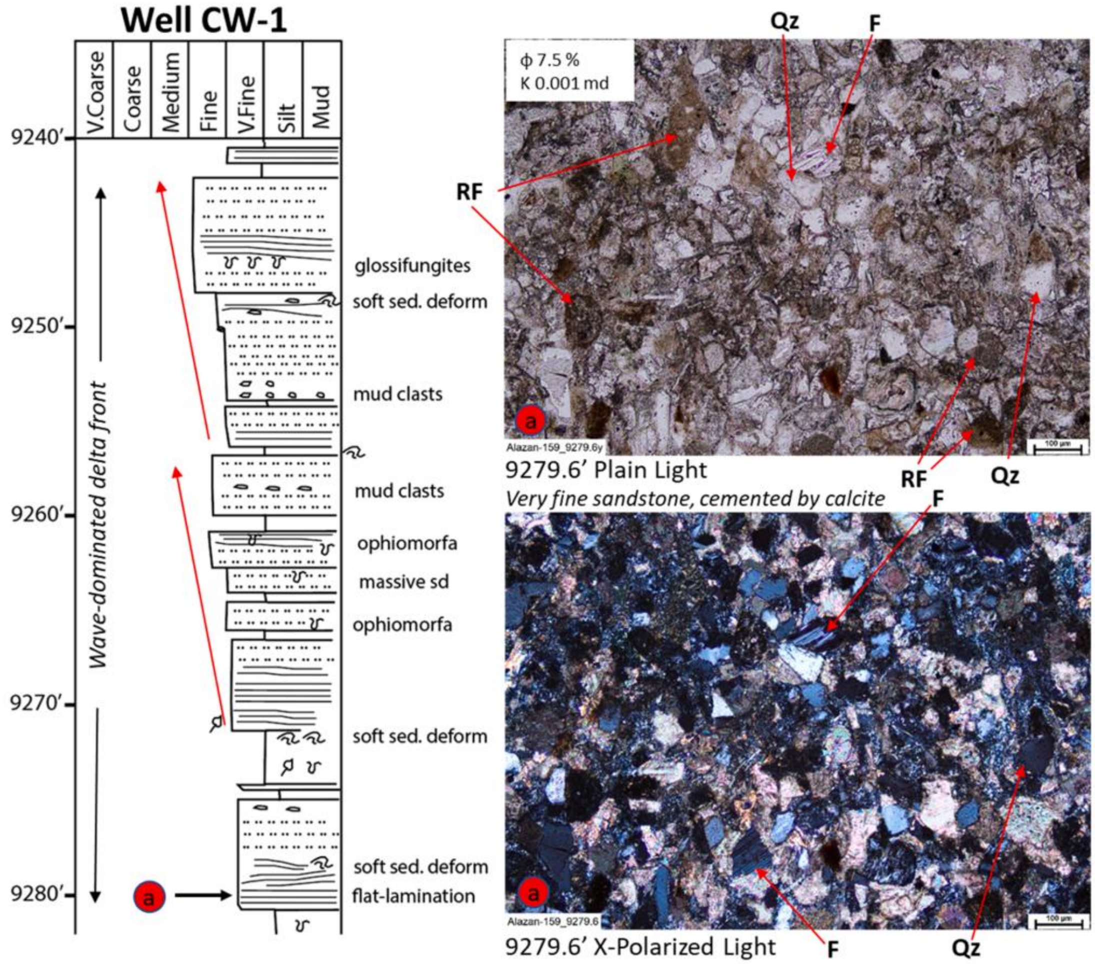

Figure 36. Sedimentological description of Well CW-1 for the depth interval of 9240 ft to 9280 ft, showing upward coarsening parasequence (Uroza et al., 2025). A thin section is shown at 9279.6 ft. The scale bar at the bottom right corner is 100 µm. RF means rock fragments, Qz means quartz, and F means Feldspar.

In the interval from 9290 ft to 9330 ft, the core description (Figure 37) exhibits upward coarsening pattern in general, with several wave/ storm structures, such as Hummocky cross-stratification, indicating that this interval belongs to a wave- dominant delta front. The thin sections taken at 9301 ft and 9303.5 ft indicate that the sandstone contains significant amount of rock fragments. Most of the quartz grains are sub-angular, while some of them are overgrown. The thin section also contains partially dissolved plagioclase feldspar. The blue epoxy indicates the presence of porosity, and the measurements of permeability and porosity are also shown in Figure 37. This section presents fair reservoir quality at such great depth and is viable for CO_2 sequestration. Within the interval 9300’ to 9310’ the rock quality has been is preserved because the hydrocarbon emplacement that has ceased diagenesis of the rock (Uroza et al., 2025).

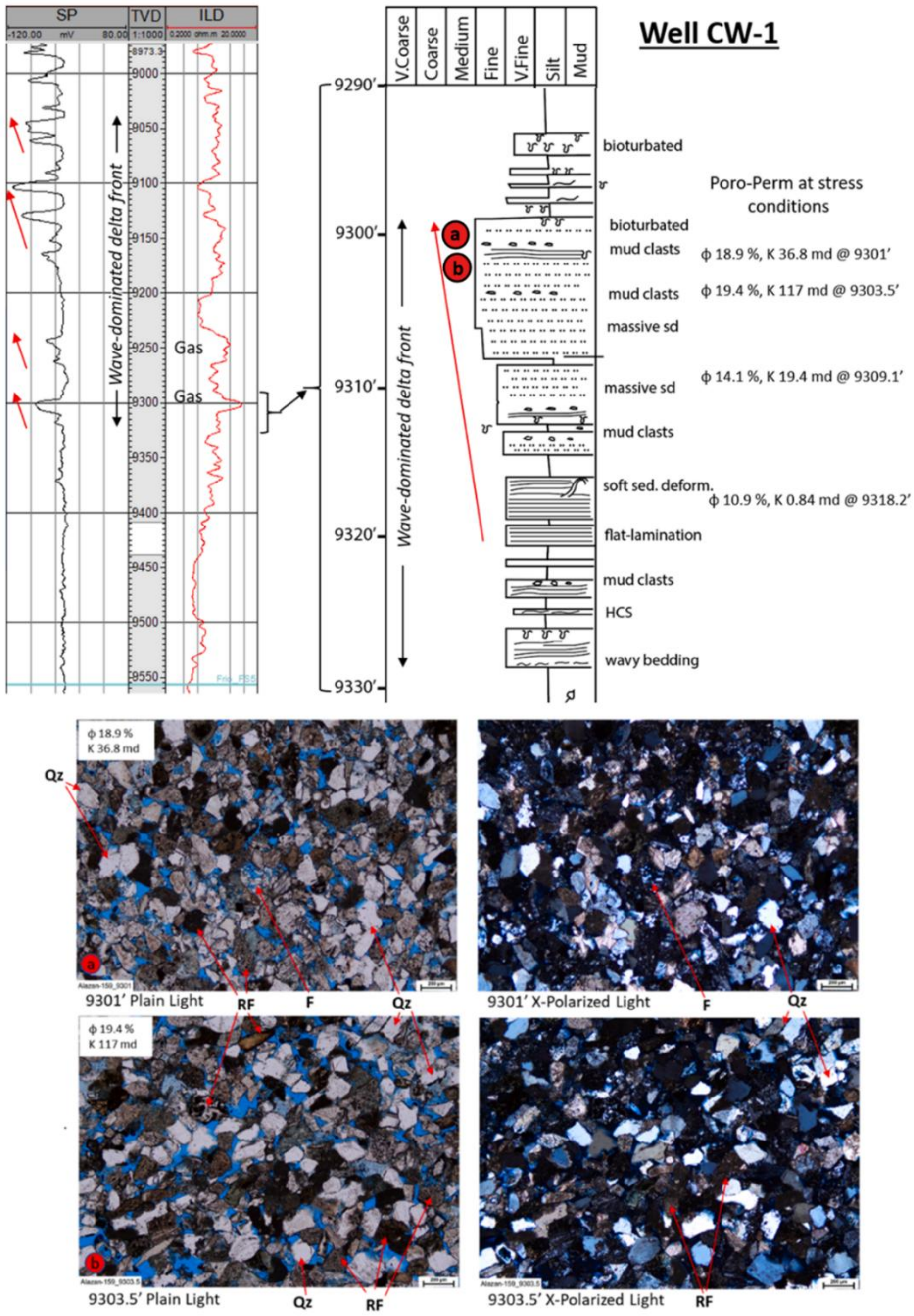

Figure 37. Sedimentological description on Well CW-1 for the depth interval of 9290 ft to 9330 ft, showing upward coarsening stacking patterns (Uroza et al.,2025). Two thin sections are obtained at 9301 ft and at 9303.5 ft. The scale bar at the bottom right conner is 200 μm. RF means rock fragments, Qz means quartz, and F means Feldspar.

4.2 Structural Analysis

Growth faulting is the most prevalent structural feature in the AOI within south Texas. These faults created structural compartmentalization and consequently created reservoirs that are bound by such faults (Brown et al., 2004; Hammes et al., 2007). Thus, it is important to understand the structure in the study area. A well-log correlation is conducted to trace the top of the Frio Formation, and to generate a structural map (Figure 38). The dipping trend of the Frio Formation is shown in the two dip-oriented cross-sections below (Figure 39 and Figure 40).

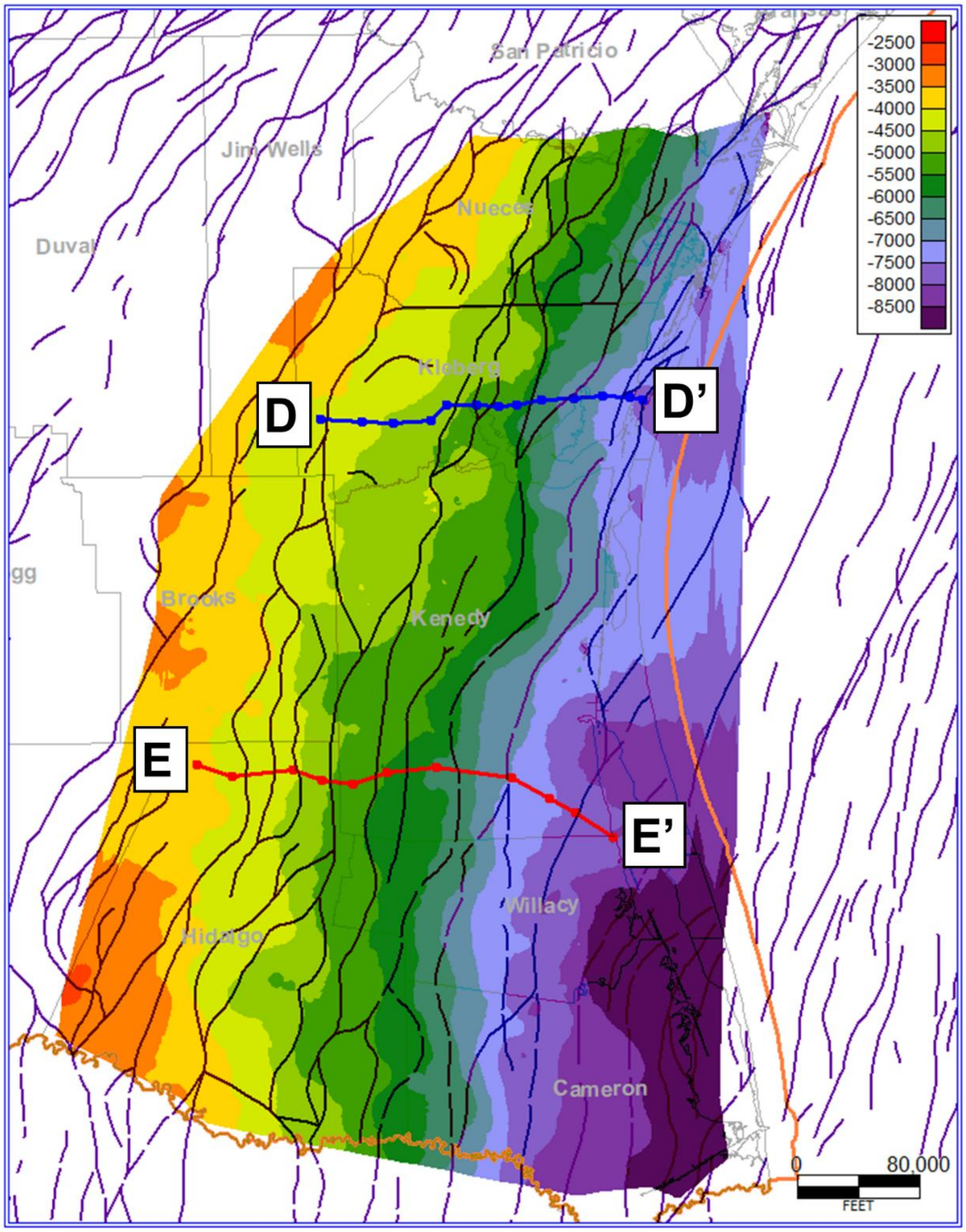

Figure 38. Structural map of the top of Frio Formation showing the location of dip-oriented cross-sections, CC' and DD'.
The dark purple lines represent the fault lines from Ewing (1991), included for comparison with the structural variation of the top of Frio Formation. The color bar on the upright indicates depth, and the orange line represents the international boundary.

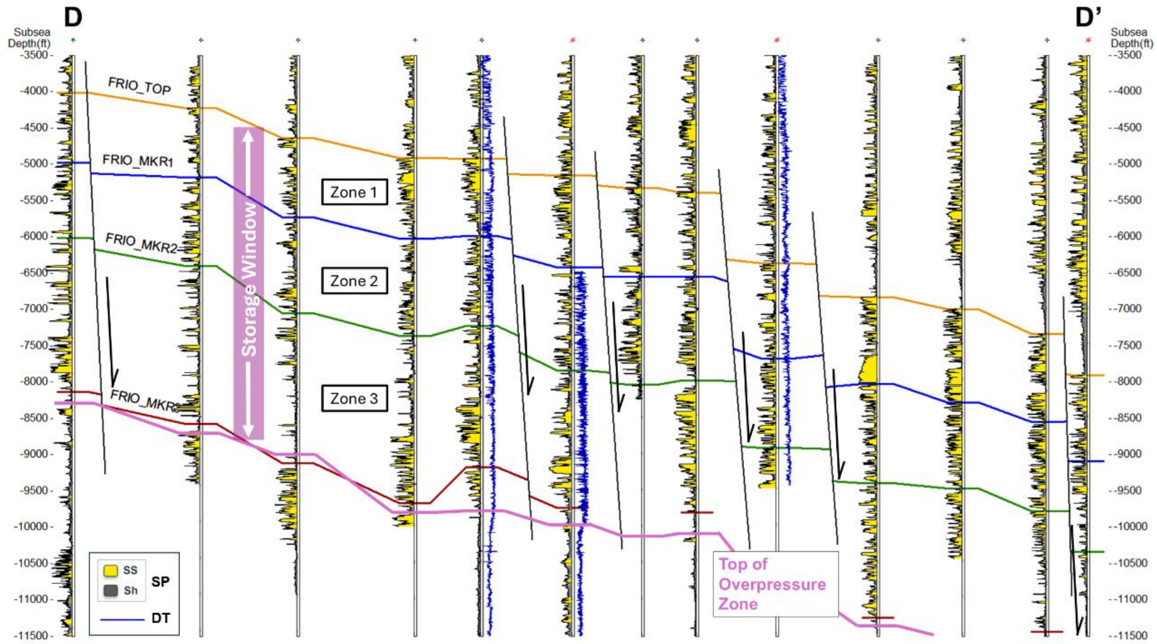

Figure 39. Dip-oriented cross-section DD' in Kleberg County, showing SP logs, sonic logs, stratigraphic well picks for the Frio section, and the extrapolated top of overpressure zone.

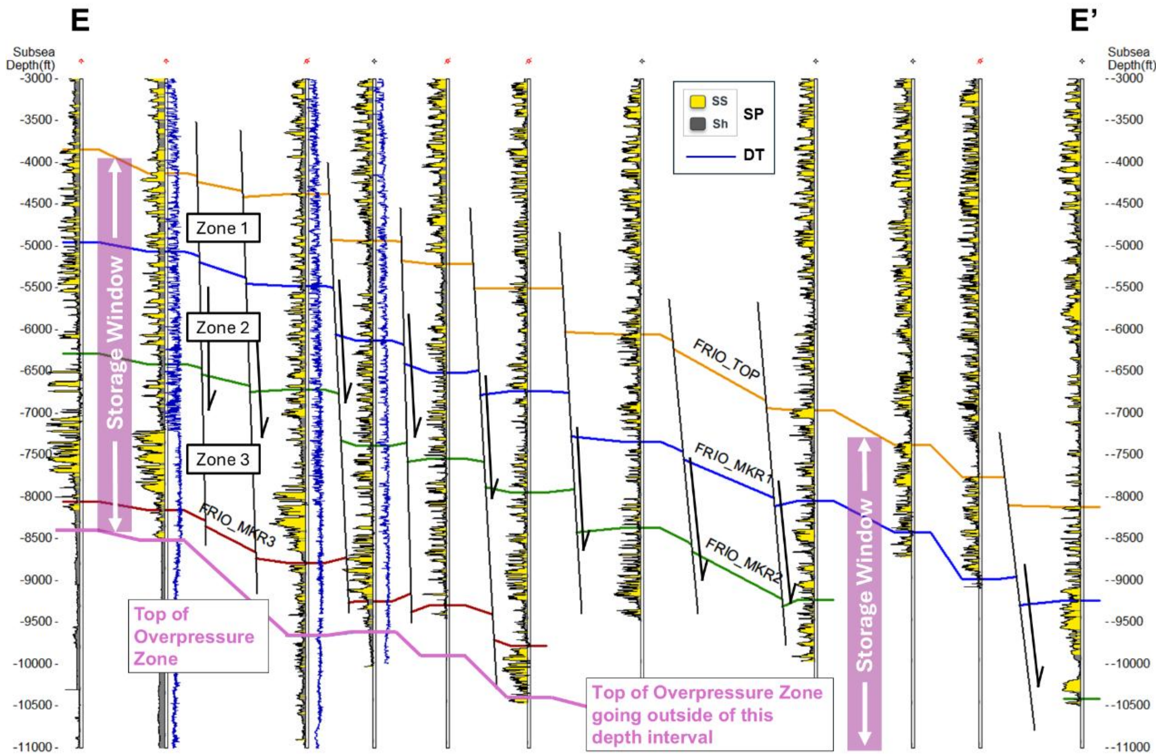

Figure 40. Dip-oriented cross-section EE' across the Hidalgo, Kenedy, and Willacy County, showing SP logs, sonic logs, stratigraphic well picks for the Frio section, and the extrapolated top of overpressure zone.

4.3 THE BASE OF USDW

In Chapter 5, this study proposes several candidate sites for CO_2 capacity and injectivity estimation. These sites are located in northeast Nueces, Kleberg, the southern Kenedy and the western Willacy Counties. This subsection summarizes the information from Figure 18 through 21 (Shi. et al., 2022) to identify which hydrostratigraphic unit contains the base of USDW in the aforementioned counties.

First, the USDW in Nueces is last seen in Chicot Aquifer, while very saline groundwater is found in most of the Nueces in Evangeline Aquifer. Second, the whole of Kleberg County has USDW deep down in Jasper Aquifer, meaning that its base is around the top of Anahuac Shale. Third, the USDW in the west side of Kenedy County is located in the Jasper Aquifer but is in Evangeline Aquifer along the coastal area of the county. Lastly, the USDW is found in Burkeville Unit around the boundary of Hidalgo and Willacy Counties, and brine is found in the next unit, which is Jasper unit.

Most of the candidate sites are approximately on the hydrostratigraphic cross-section 04, 05, and 06 (Figure 15, 16, and 17; modified from Shi et al., 2022), or very close to these cross-sections. Therefore, the site-specific depth of the USDW base for the critical pressure increase calculation is obtained from these cross-sections, and the depths are documented in the tables of EASiTool inputs in the Appendix A.

4.4 Limits of Overpressure Zone

The depth of the overpressure zone plays a major role in controlling the CO_2 storage window, which can be identified from the sonic logs. From the well log dataset, sonic logs that penetrate deeply through the FRIO_MKR3 are filtered out and used to determine the overpressure zone. A contour map (Figure 41) indicating the depth of the top of the overpressure zone is generated with 48 sonic logs that comply with the aforementioned criteria. The depth of overpressure zone basically increases gulfward. The overpressure zone also follows the stratigraphic trend and lies below Zone 3 and should not affect CO_2 injection into any targeted zones of this study.

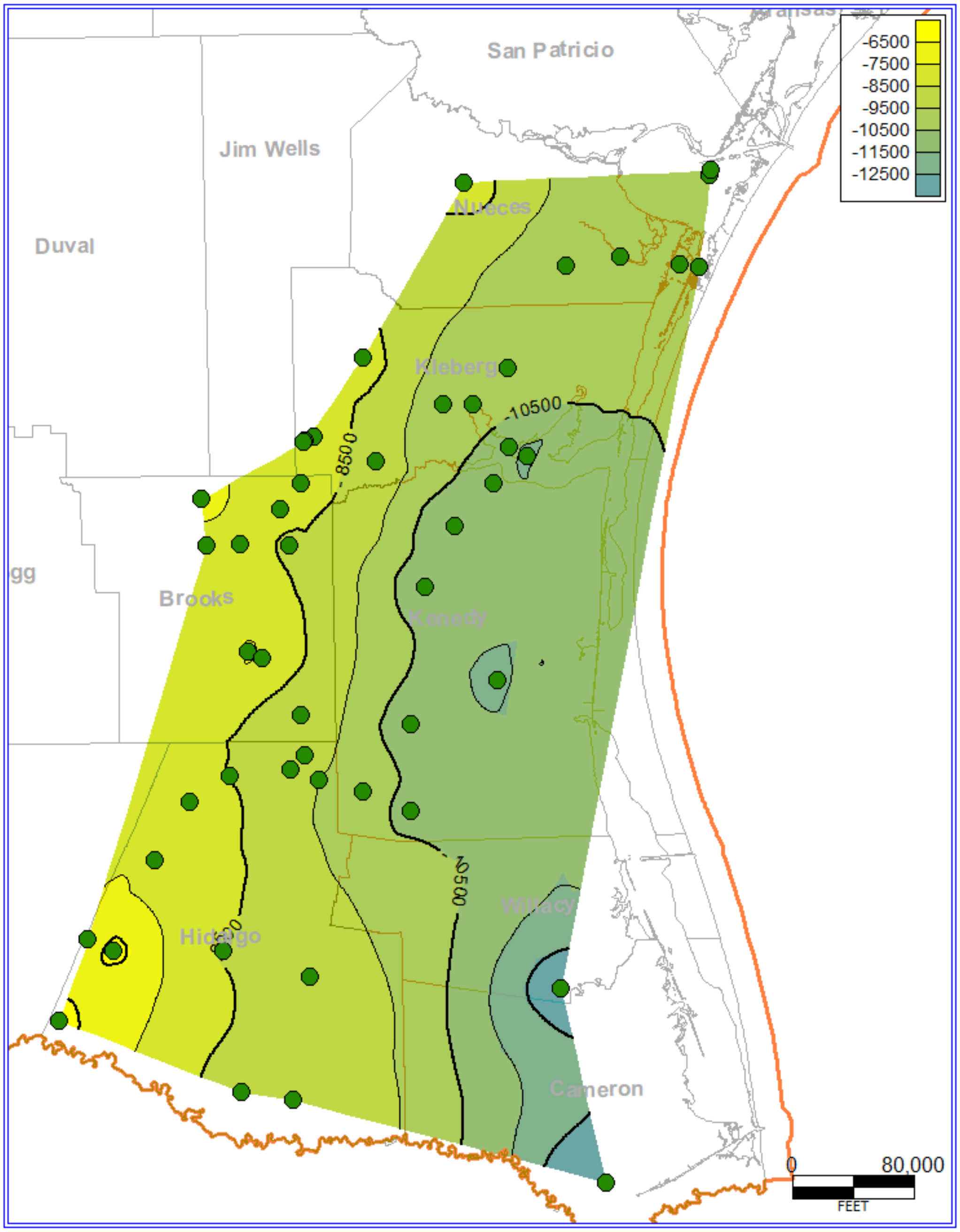

Figure 41. Depth-contour map of the top of overpressure zone.
Green dots are the location of the control points (n = 48) that are used to define the depth of overpressure zone. The color bar on the upright indicates the depth.

4.5 PERMEABILITY AND POROSITY ANALYSIS

4.5.1 Permeability and Porosity Variations with Depth

The cross plots of porosity and permeability versus depth (Figure 42, 43) are created with all the sample points available for Frio Formation (location indicated in Figure 25). In the plots, the minimum permeability and porosity at each depth both decreases with the depth, but permeability up to 100 mD and porosity up to 30% are presented between 6000 ft to 12000 ft in the subsurface.

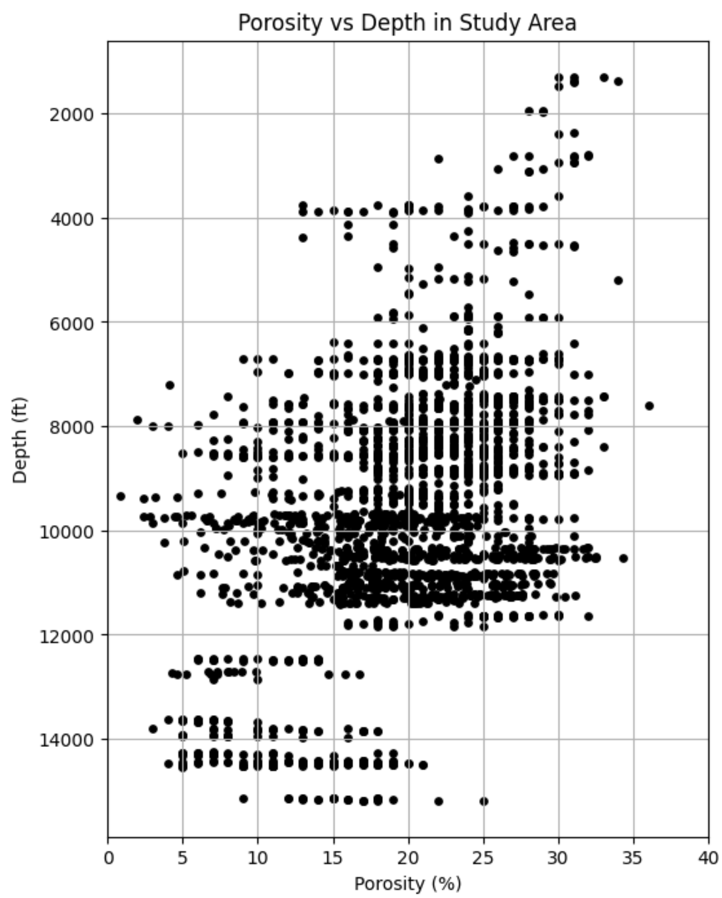

Figure 42. Cross plot of porosity versus depth with the core measurement available for this study within the study area.

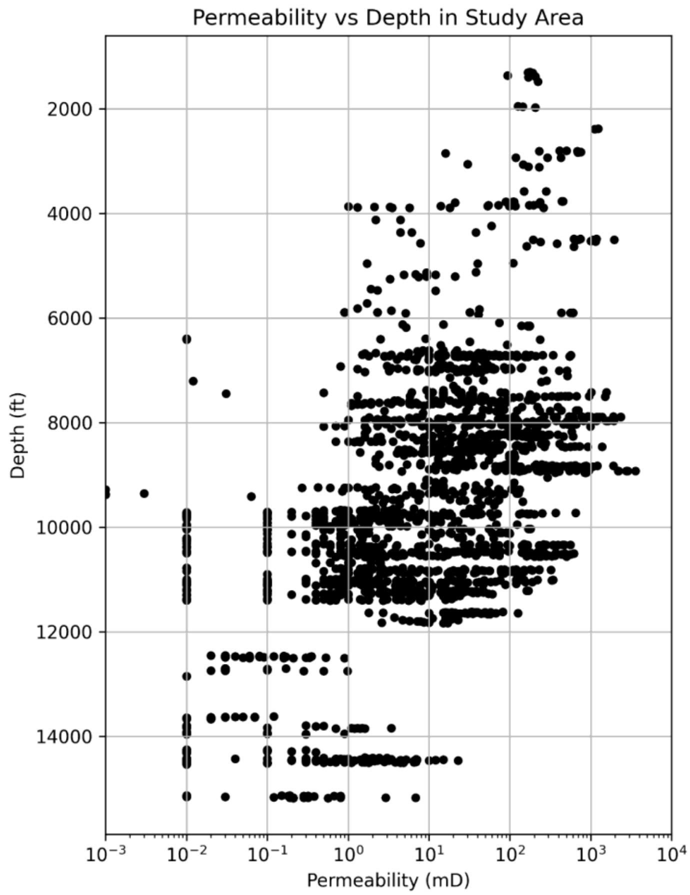

Figure 43. Cross plot of permeability versus depth with the core measurement available for this study within the study area.

4.5.2 Permeability-Porosity Evaluation

Porosity vs Permeability transforms are created for 9 locations where core-derived petrophysical measurements are available in Zone 1, 2, and 3: Cluster CW, A, B, and D, and Well C, E F, G, and H (Figure 44).

Cluster CW, consisting of Well Humble No. 183 Alazan and Well CW-1, is labeled separately and is not assigned in alphabetical order because they are obtained from a different dataset than other measurement data. Also, the core description of these two wells has been summarized earlier in section 4.1.5.

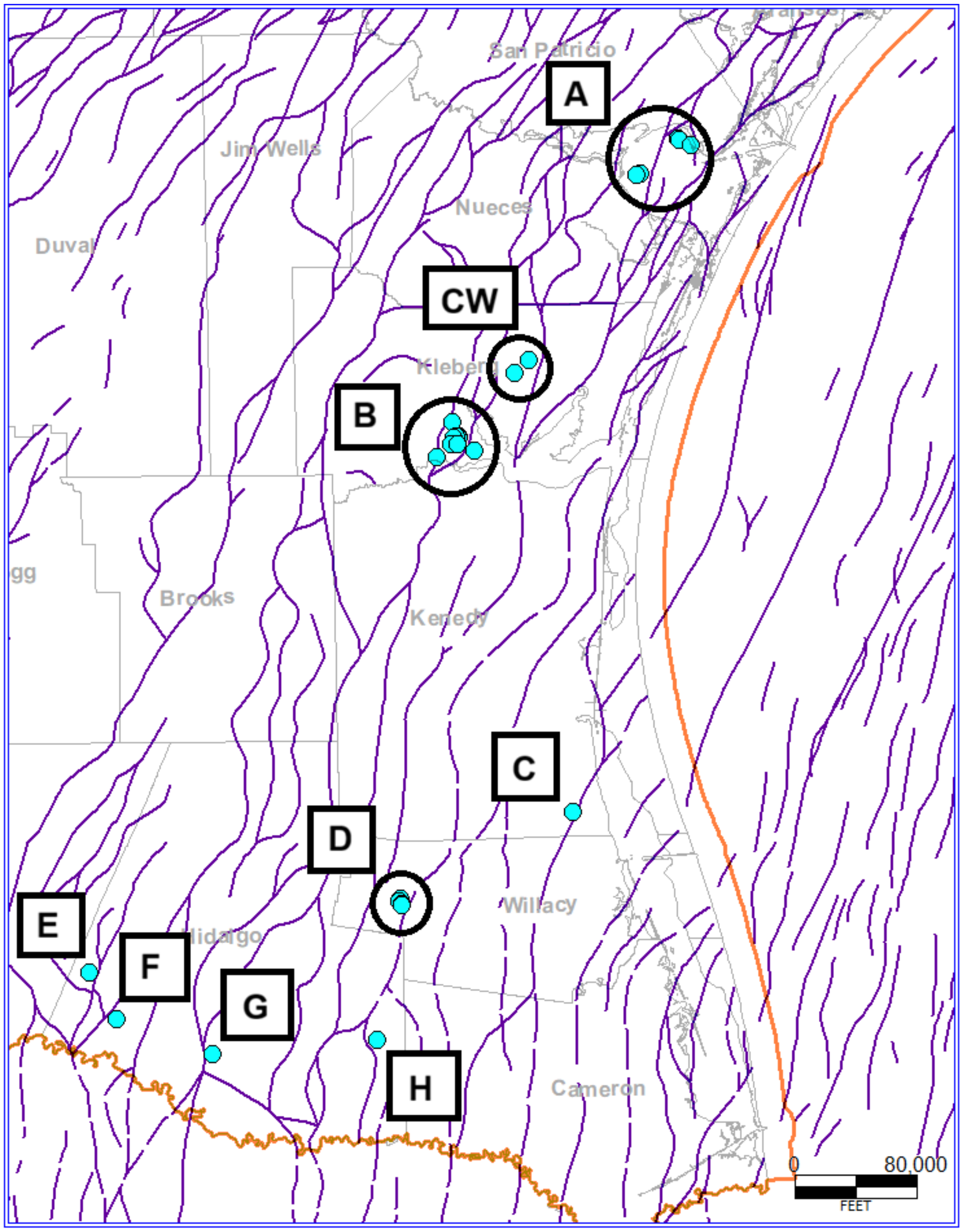

Figure 44. Location of the wells with petrophysical core data available in Zone 1, 2, or 3. One cored well is located in southwestern Kenedy County, four are located in Hidalgo County, and four clusters of cored wells occur in Corpus Christi Bay, Baffin Bay, central Kleberg County and the western Willacy County. The light blue dots represent cored wells, and the orange line marks the international boundary. Fault traces from Ewing (1991) are shown to partially indicates structural compartments. The code letter for each analysis is labeled A through H, while Cluster CW is named separately.

4.5.2.1 Permeability and Porosity Variations along the Strike- Orientation of the Study Area

Cluster A, Cluster CW, Cluster B, Well C and Cluster D are used to perform Permeability-Porosity evaluation along the strike-orientation. In the crossplot of the petrophysical data (Figure 45 through 51), sample points identified by the stratigraphic units of Zone 1 to Zone 3 are color-coded. Generally, Zone 1 and Zone 2 are more similar speaking of their trendline nearly coinciding in Cluster A, Well C, and Cluster D. The trendline of Zone 3 is found always slightly above and to the left of Zone 1 and Zone 2.

The plots below also show that the cored wells from Cluster A and B exhibit the high permeability values between 100 and 1000 millidarcies(mD), with some values exceeding this range. In contrast, permeability only reaches 700 mD in Cluster D and even remains below 70 mD in Well C. Furthermore, porosity in Humble No.183 Alazan, Well CW-1 and Well C never exceed 0.25, while it reaches around 0.30 in other three locations.

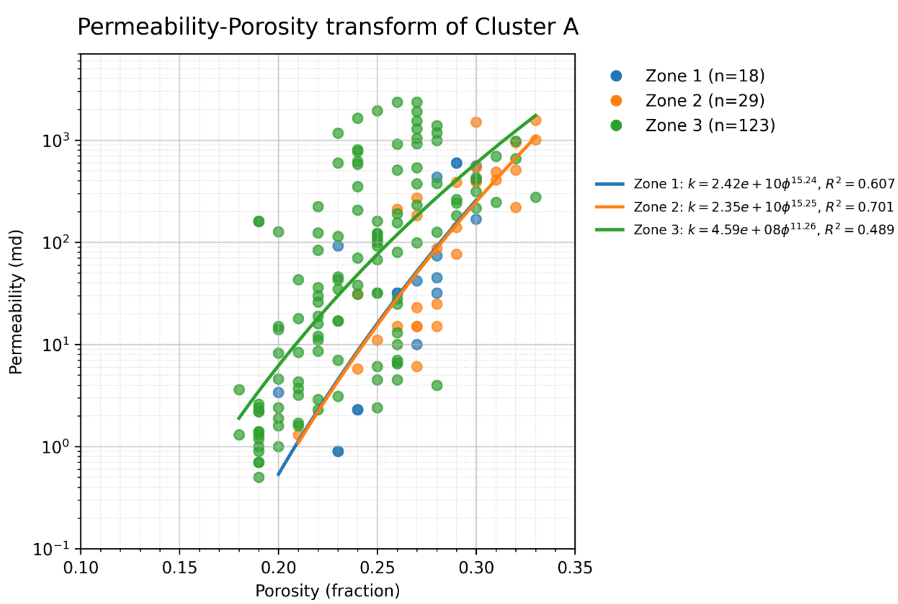

Figure 45. Permeability versus porosity transform for Zone 1, Zone2, and Zone 3 of the cored wells in Cluster A.

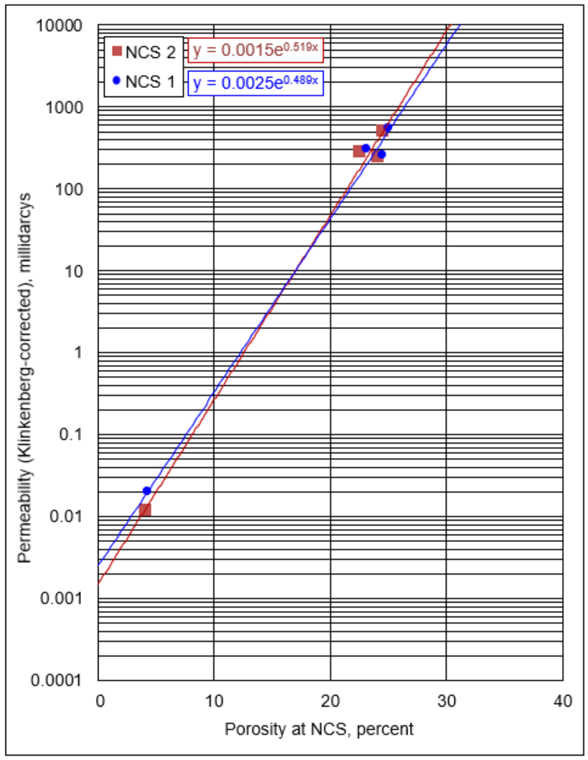

Figure 46. Klinkenberg permeability versus porosity transform of Humble No.183 Alazan of Cluster CW in Zone 2, under two net confining stress (NCS) (BEG internal dataset).
NCS1 is 800 psi, and NCS2 is 2450 psi.

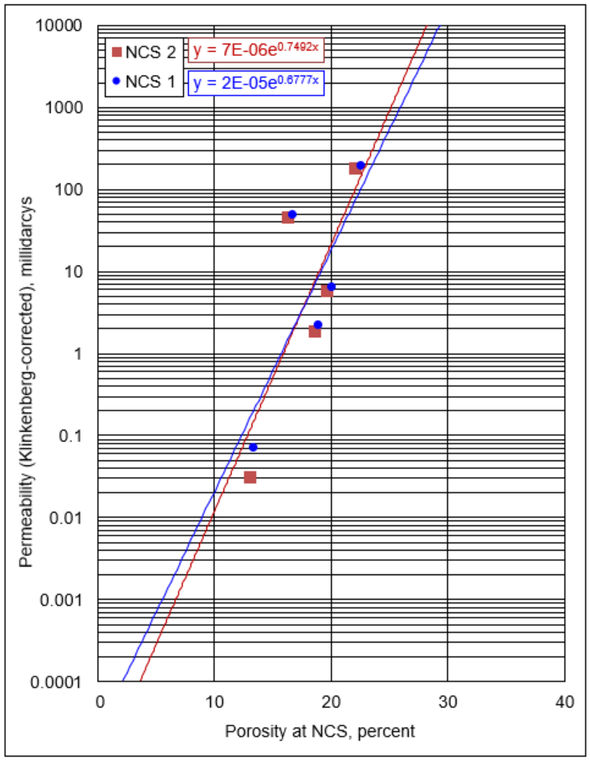

Figure 47. Klinkenberg permeability versus porosity transform of Humble No.183 Alazan of Cluster CW in Zone 3, under two net confining stress (NCS) (BEG internal data).
NCS1 is 800 psi, and NCS2 is 2450 psi. (Modified from.)

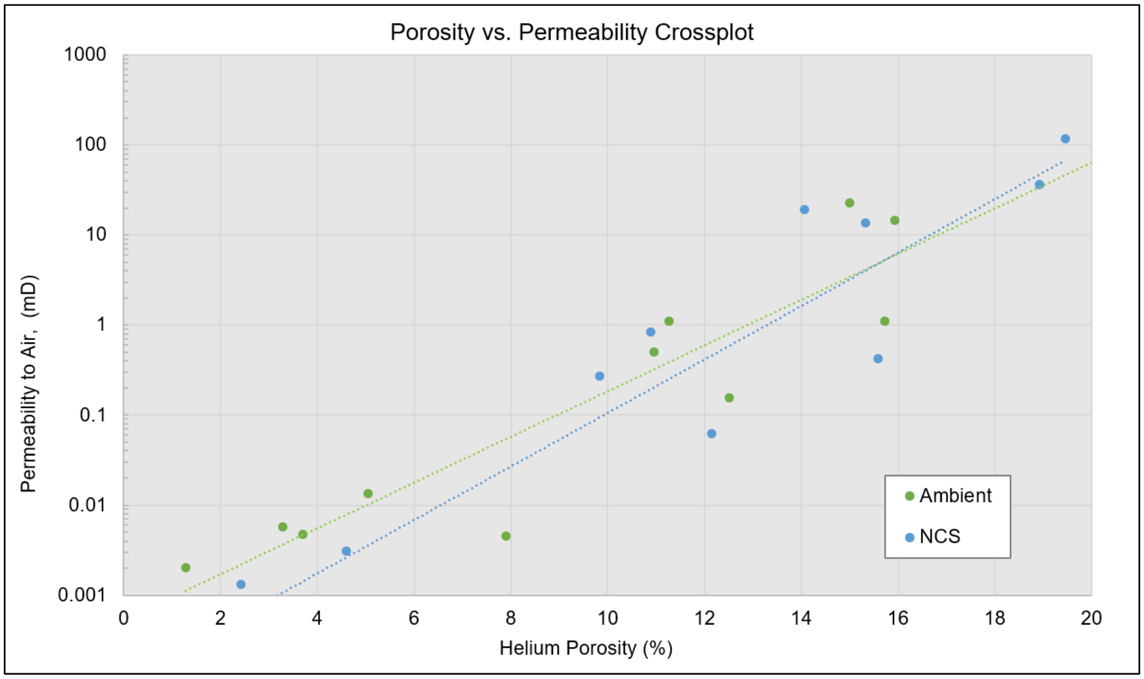

Figure 48. Permeability to air versus porosity transform for Zone 3 of Well CW-1 of Cluster CW tested under the NCS of 3750 psi (BEG internal data).

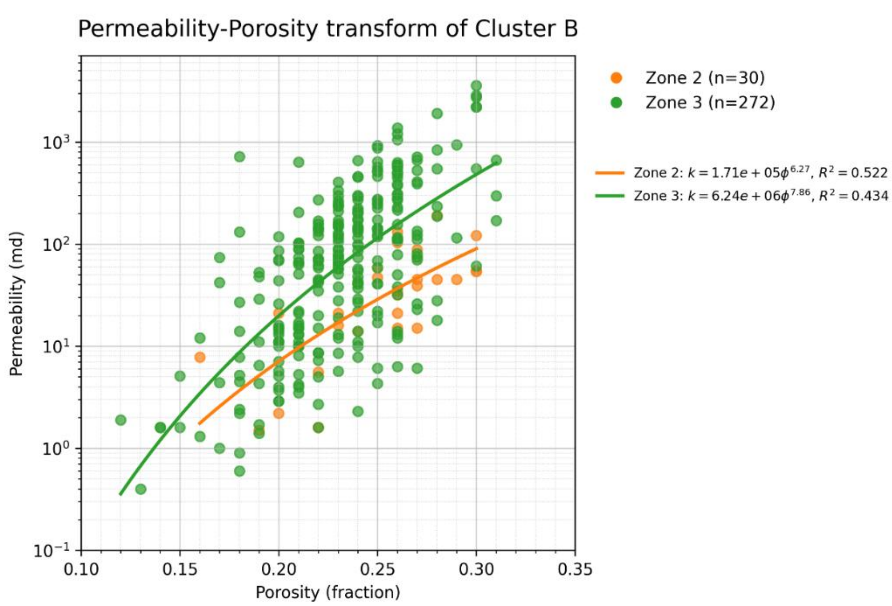

Figure 49. Permeability versus porosity transform for Zone 2 and Zone 3 of the cored wells in Cluster B.

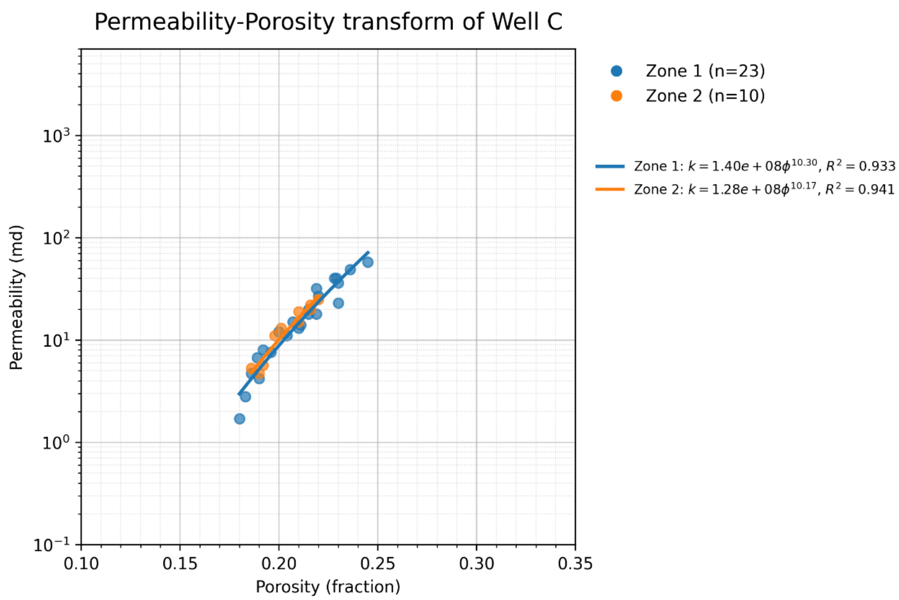

Figure 50. Permeability versus porosity transform for Zone 1, Zone 2 of the cored wells in the Well C.

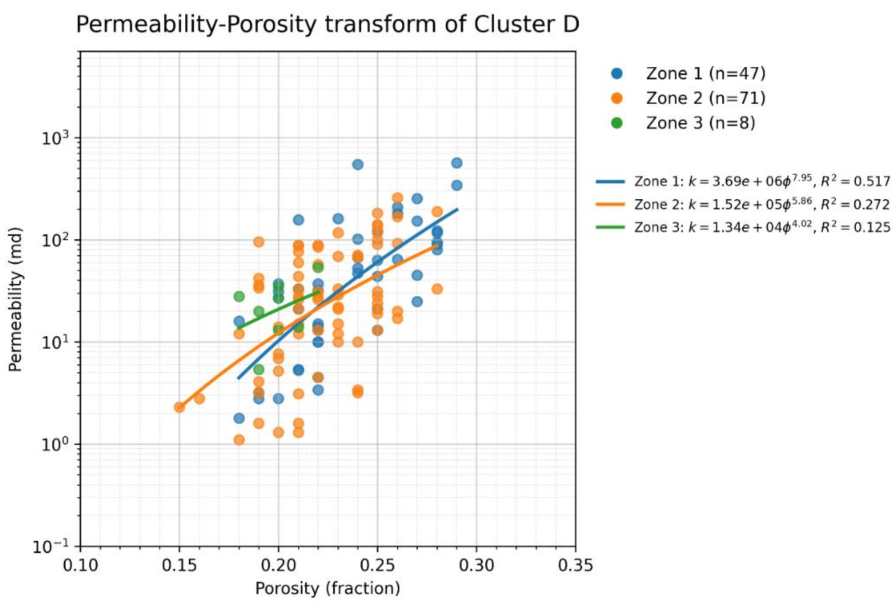

Figure 51. Permeability versus porosity transform for Zone 1, Zone 2, and Zone 3 of the cored wells in Cluster D.

The statistics of permeability and porosity data by zone are organized below in Table 1, 2, and 3. Average porosity decreases towards the south in every zone, whereas the permeability distribution cannot be simply concluded.

In Zone 1 and Zone 2, permeability is highest at Cluster A in Nueces County, decreases towards Well C in the southern Kenedy County and slightly increases at Cluster D in Willacy County again. This increase is expected because Cluster D is located updip of Well C, and belongs to a more proximal facies.

As for in Zone 3, Cluster B has the higher permeability than Cluster A. Cluster CW presents poorest reservoir quality with representative permeability values below 1 mD and porosity around 0.12. This is also expected because Cluster CW samples are derived from a distal facies.

Zone 1	**Permeability (mD)**			**Porosity**		
	-1sd	Geometric Mean	+1sd	-1sd	Mean	+1sd
Cluster A	3.47	31.45	285.40	0.23	0.26	0.29
Cluster CW	-	-	-	-	-	-
Cluster B	-	-	-	-	-	-
Well C	5.54	14.14	36.08	0.18	0.21	0.23
Cluster D	8.24	35.71	154.70	0.17	0.21	0.26

Table 1. Statistical summary of permeability and porosity for Zone 1 sandstones. Permeability is reported as geometric mean with ±1 standard deviation. Porosity is reported as average with ±1 standard deviation. Standard deviations of samples less than 10 are not on the table.

Zone 2	Permeability (mD)			Porosity		
	-1sd	Geometric Mean	+1sd	-1sd	Mean	+1sd
Cluster A	14.51	98.85	673.49	0.23	0.27	0.31
Cluster CW	-	25.58	-	-	0.19	-
Cluster B	8.00	28.21	99.46	0.22	0.25	0.28
Well C	6.43	12.03	22.53	0.19	0.20	0.22
Cluster D	5.54	22.09	88.10	0.15	0.20	0.25

Table 2. Statistical summary of permeability and porosity for Zone 2 sandstones. Permeability is reported as geometric mean with ±1 standard deviation. Porosity is reported as average with ±1 standard deviation. Standard deviations of samples less than 10 are not present on the table.

Zone 3	Permeability (mD)			Porosity		
	-1sd	Geometric Mean	+1sd	-1sd	Mean	+1sd
Cluster A	3.91	41.38	437.86	0.17	0.22	0.27
Cluster CW	-	0.36	-	-	0.12	-
Cluster B	9.47	57.22	345.83	0.15	0.21	0.26
Well C	-	-	-	-	-	-
Cluster D	-	20.23	-	-	0.17	-

Table 3. Statistical summary of permeability and porosity for Zone 3 sandstones.

Table 3. Statistical summary of permeability and porosity for Zone 3 sandstones. Permeability is reported as geometric mean with ±1 standard deviation. Porosity is reported as average with ±1 standard deviation. Standard deviations of samples less than 10 are not present on the table.

4.5.2.2 Permeability and Porosity Variations along the Dip- Orientation in Hidalgo County

In Hidalgo County, there are four cored wells aligned perpendicular to the shoreline. Each of them sits within a different structural compartment, separated by more than one fault. These cored wells have limited samples in each identified zone. As shown in the permeability-porosity transform and the statistical summary table below (Figure

52, 53, 54, and Table 4), the petrophysical properties vary significantly between the compartments. Zone 1 and Zone 2 are overlapping in the permeability-porosity plot of Well H, but are significantly separated in Well E. Moreover, permeability exceeding 1000 mD are found in Zone 1 of Well E, while the same zone in Well H only shows 10-ish mD. The Zone 3 samples of Well F are only about 10 mD, while the samples of Well G exhibits permeability around 200 mD. Such a huge variation without any pattern being observed may be caused by the limitation of data samples.

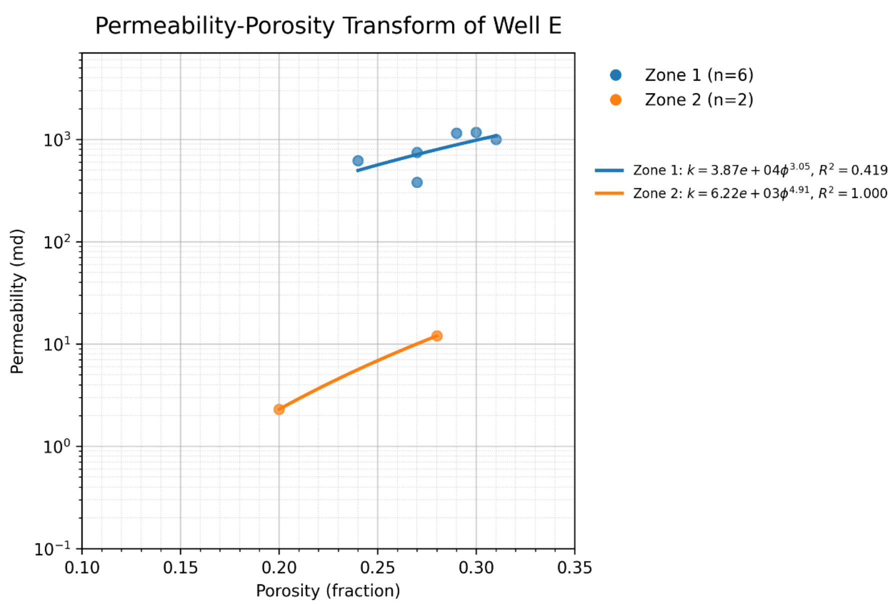

Figure 52. Permeability versus porosity transform for Zone 1 and Zone 2 of Well E.

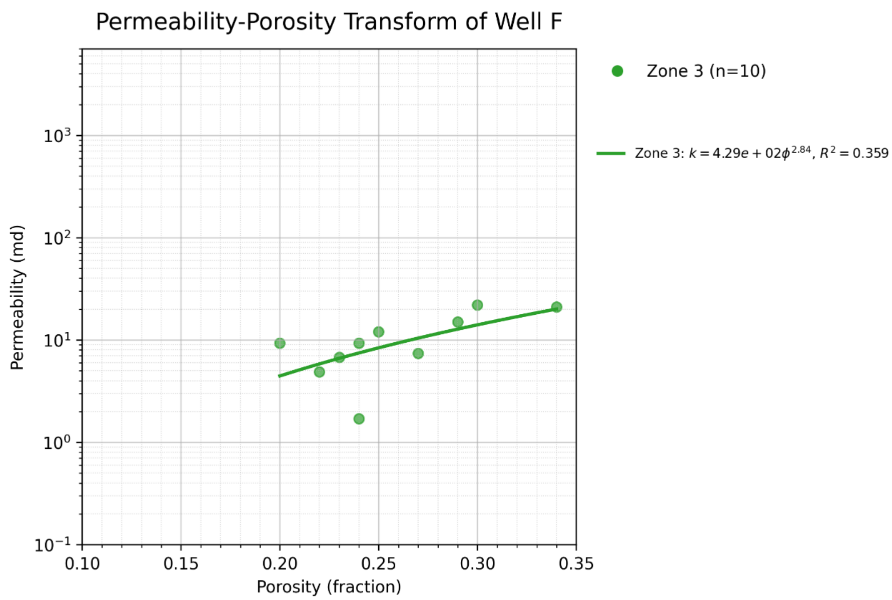

Figure 53. Permeability versus porosity transform for Zone 3 of Well F.

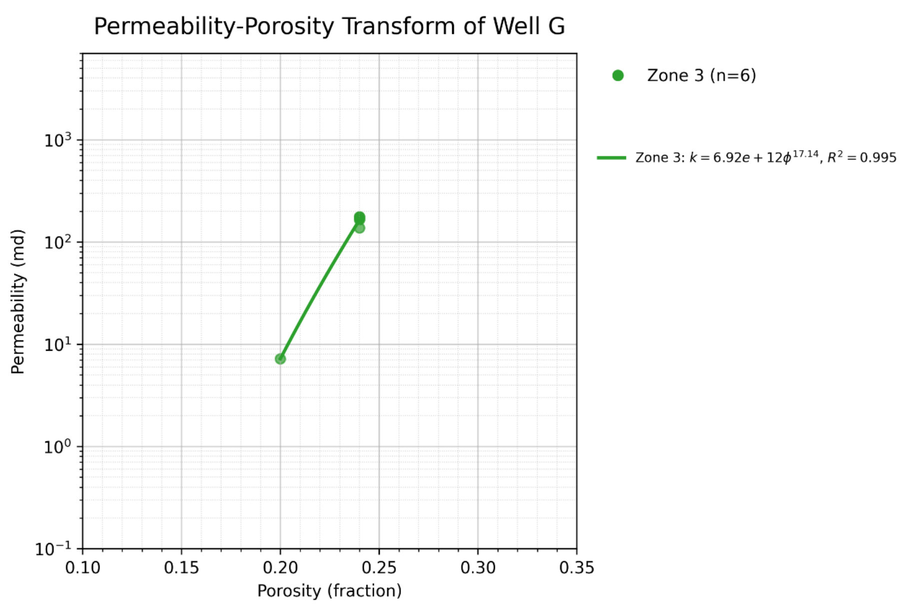

Figure 54. Permeability versus porosity transform for Zone 3 of Well G.

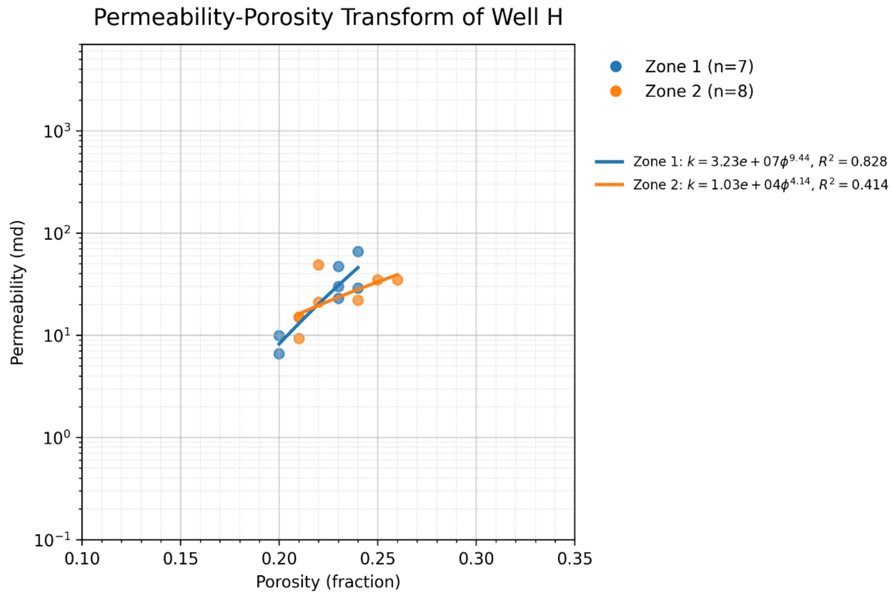

Figure 55. Permeability versus porosity transform for Zone 1 and Zone 2 of Well H.

Zone	Representative Value	Well E	Well F	Well G	Well H
1	Geometric Mean Permeability (mD)	786.21	-	-	23.58
	Mean Porosity	0.28	-	-	0.22
2	Geometric Mean Permeability (mD)	5.25	-	-	22.15
	Mean Porosity	0.07	-	-	0.22
3	Geometric Mean Permeability (mD)	-	8.87	163.96	-
	Mean Porosity	-	0.26	0.24	-

Table 4. Statistical summary of permeability and porosity data in Well E, F, G, H. Permeability is reported as geometric mean and porosity is reported as average. Standard deviation is not included in this table because it is not reliable when there are less than 10 samples points.

Chapter 5: CO_2 Storage Capacity Estimation

The selection of the injection sites for capacity estimation is based on the net sand thickness, and the avoidance in legacy wells in or near the reservoir area, and the availability of core data for understanding reservoir properties.

Taking all of the criteria above into consideration, four sites are proposed for assessment. Their names are simply adopted from the counties where they belong. They are 1. Site N (Nueces) 2. Site WK (West Kleberg) 3. Site KK (Kleberg and Kenedy) 4. Site KND (Kenedy) 5. Site W (Willacy), and their locations are outlined on the map below (Figure 56.) in red.

Without site specific seismic data, the boundary of the reservoirs is simply defined according to the fault lines from Ewing (1991); however, whether the faults actually act as a lateral seal remains uncertain. Since all the selected sites are not fully bounded by the faults and their cross-sections have shown that the sandstones do not pinch out within their compartments, the capacity estimations are all tested with both open and closed boundary scenarios.

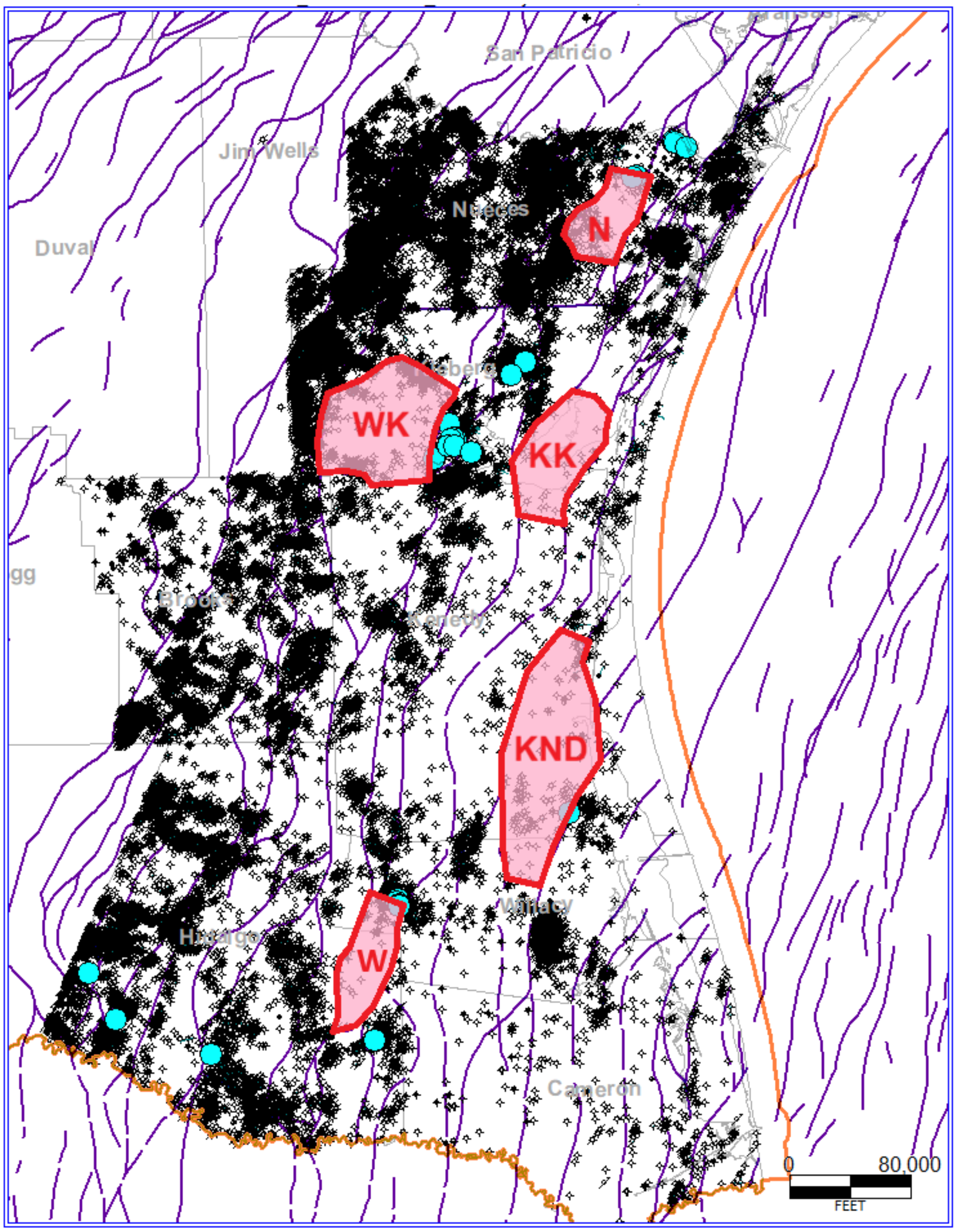

Figure 56. Location map of the proposed sites, outlined in red with their names. The black well symbols represent the location of the available legacy wells to this study. Bright blue dots represent the location of core-derived petrophysical data available in Zone 1, 2, and 3.

Storage capacity corresponding to 25 injection wells is selected as base cases for presentation in this chapter. The capacity curves vs injection wells typically flatten beyond this point in most of the site cases. The plateauing behavior is found in nearly all sites and indicates that increasing number of injection wells to above 25 does not efficiently increase capacity. Sensitivity simulations are also performed with an assumption of 25 injection wells to compare the probability distribution to the base cases.

The summary estimation results are presented on a site-by-site basis below, including the injectivity in the forms of the product of reservoir permeability and thickness, the deterministic storage capacity with 25 injection wells and the results of Monte Carlo simulations. These values provide an efficient first-order assessment of engineering feasibility on implementing geological CO_2 sequestration at a given site. Additionally, a table of the ranked proposed sites ranked on the basis of total injectivity and total capacity under closed boundary condition is presented.

The input parameters for the use of EASiTool and the original output figures generated by EASiTool are included in the Appendix A, including capacity vs number of injection wells, the AOR range estimation with probability, the sensitivity tornado chart, and the Monte Carlo simulation for sensitivity analysis.

5.1 SITE N

The estimated injectivity and capacity of Site N is summarized in Table 5. This site is located in the northeast of Nueces County, as known as the Corpus Christi Bay. There are cored wells within the reservoir area, so the EASiTool inputs for this site are calculated from local measurement.

As shown in the sand maps (Figure 57), the reservoir is bounded by faults on the left and right of the compartment, leaving the injected fluids with exits on the north and south sides. Thanks to the stacked barrier, the sand maps and cross-sections indicate the presence of high sand content and well continuity in all three zones within the compartment (Figure 58 and 59). Hence, this site is capable of providing stack storage.

Site N	Zone 1	Zone 2	Zone 3	Total
Injectivity (kh, darcy·m)	4.65	13.67	9.58	27.90
Open boundary capacity (MMT)				
Deterministic (25 wells)	51	90	125	266
P10	255	579	926	—
P50	99	197	327	—
P90	32	66	75	—
Closed boundary capacity (MMT)				
Deterministic (25 wells)	12	8	17	37
P10	22	20	38	—
P50	13	10	21	—
P90	4	3	5	—

Table 5. Injectivity and estimated storage capacity for Site N under open and closed boundary conditions.
Deterministic results are calculated with the representative values for reservoir properties, whereas the percentile-based probability is derived from Monte Carlo simulation.

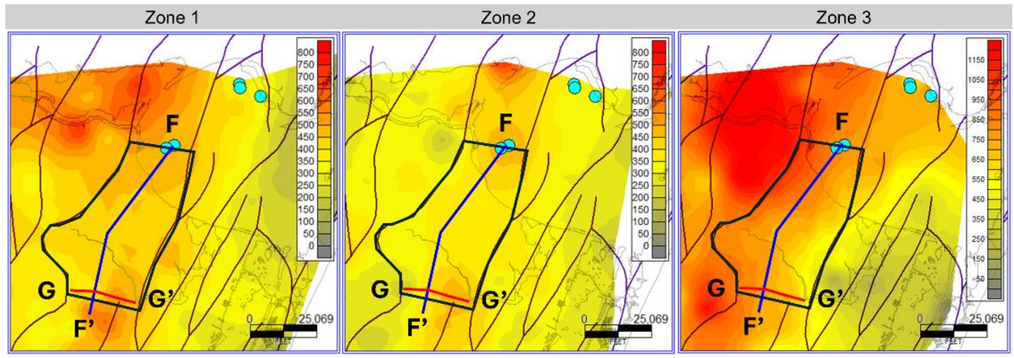

Figure 57. Net sand maps of Corpus Christi Bay, with reservoir area of Site N outlined by a black polygon.
Bright blue dots indicate the location of core data used for this site. The location of cross-sections FF' (Figure 58) and GG' (Figure 59) are labeled on the maps.

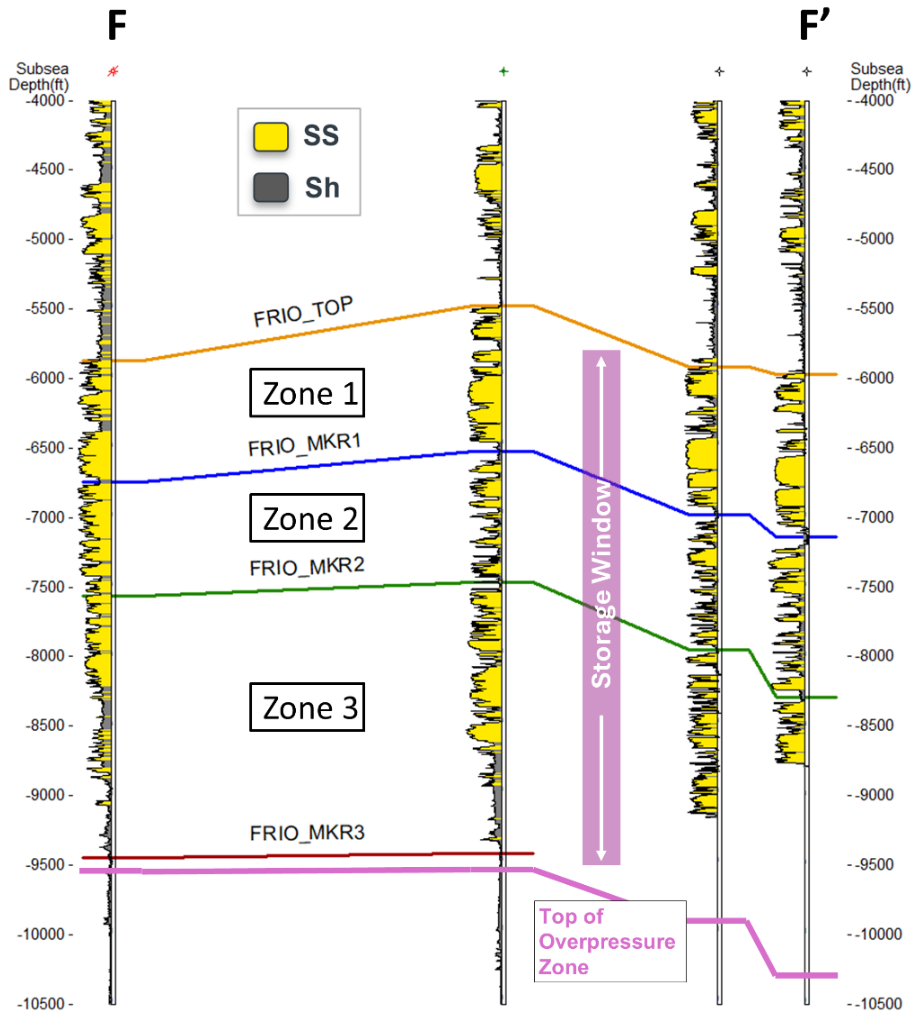

Figure 58. Strike-oriented cross-section FF' in Site N, showing SP logs, reservoir zones, and the extrapolated top of overpressure zone.

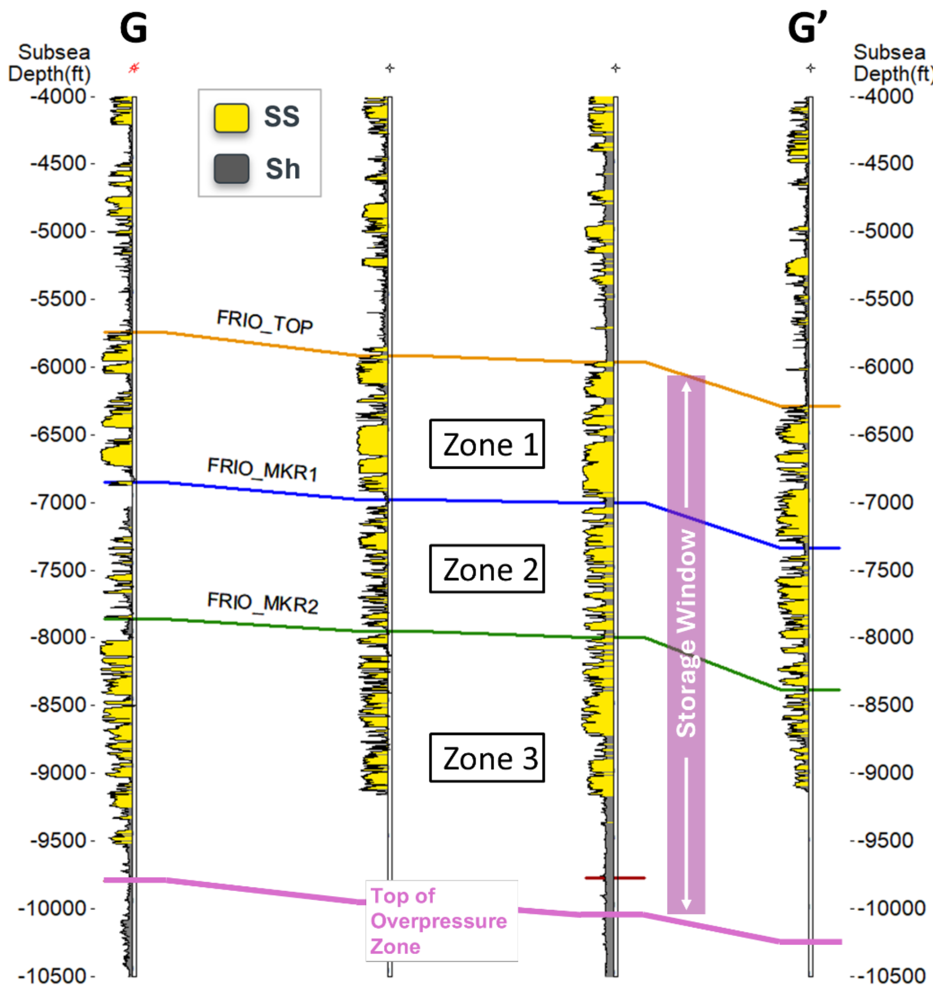

Figure 59. Dip-oriented cross-section GG' in Site N, showing SP logs, reservoir zones, and the extrapolated top of overpressure zone.

5.2 Site WK

The estimation results of Site WK are summarized in Table 6. Site KW is located in a wide compartment in the west Kleberg County, bounded by two normal faults on its west and east side (Figure 60). There are also two minor fault structures on its north and south side, that may serve as an obstacle for fluid flow but are not completely blocking the paths because they are not intersecting with the major faults on the west and east. Good reservoir connectivity is observed in Zone 1, Zone 2 and the lower half of Zone 3 (Figure 61 and 62). Despite pinching out in the middle of the compartment (shown in Figure 62), the sandstones are still connected in the peripheral areas.

Core data are not available within the reservoir area; however, such data is available in a nearby compartment located to the east. In this study, the porosity and permeability are assumed to be approximately the same when the sandstones belong to the same stratigraphic unit and occur in close proximity. Therefore, the reservoir properties for this storage capacity estimation are taken from the nearby compartments. In contrast, compartment- specific properties, such as initial pressure and temperature are calculated with the general gradients described earlier in methodology.

Any data for Zone 1 is not available. Since Zone 1 and Zone 2 exhibit similar reservoir properties in the permeability-porosity transforms along the coast, the porosity and permeability values from Zone 2 is used for calculation of Zone 1 at this site.

Site WK	Zone 1	Zone 2	Zone 3	Total
Injectivity (kh, darcy·m)	3.20	2.67	5.63	11.50
Open boundary capacity (MMT)				
Deterministic (25 wells)	82	95	214	391
P10	168	191	674	—
P50	100	119	367	—
P90	62	62	174	—
Closed boundary capacity (MMT)				
Deterministic (25 wells)	54	53	64	117
P10	77	74	93	—
P50	55	54	64	—
P90	36	37	40	—

Table 6. Injectivity and estimated storage capacity for Site WK under open and closed boundary conditions.

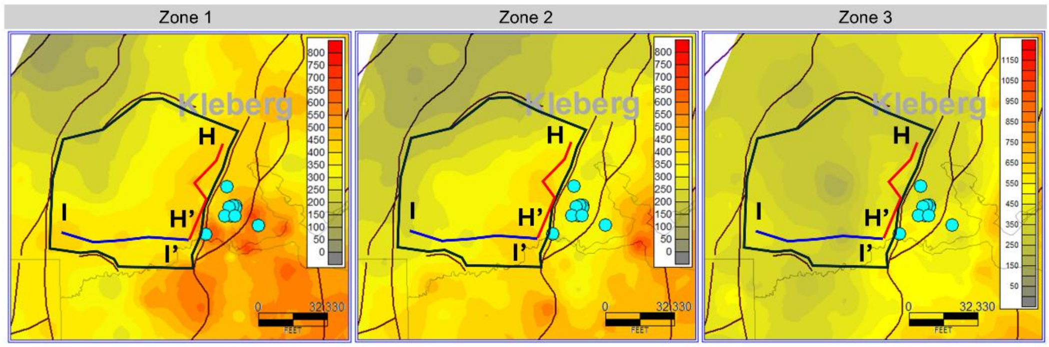

Figure 60. Net sand maps of the western Kleberg County with the reservoir area of Site WK outlined by a black polygon.
Bright blue dots indicate the location of core data used for this site. The location of cross-sections HH' (Figure 61) and II' (Figure 62) are labeled on the maps.

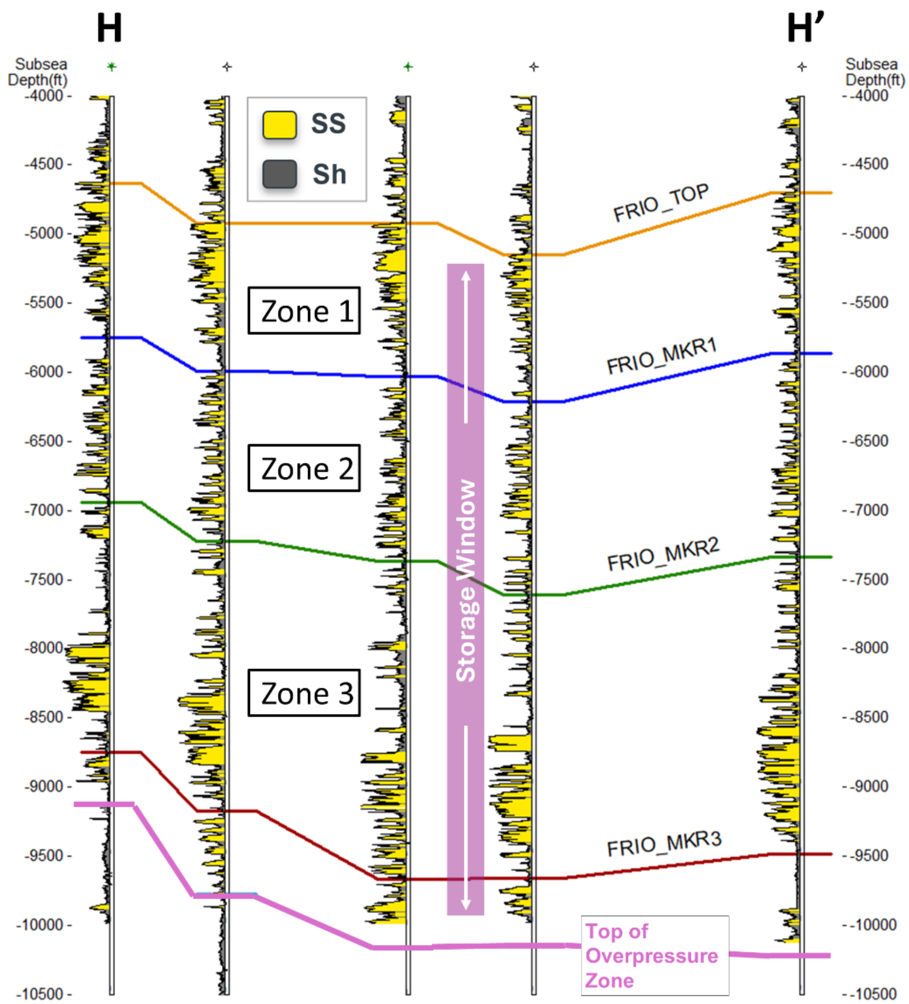

Figure 61. Strike-oriented cross-section HH' in Site WK, showing SP logs, reservoir zones, and the extrapolated top of overpressure zone.

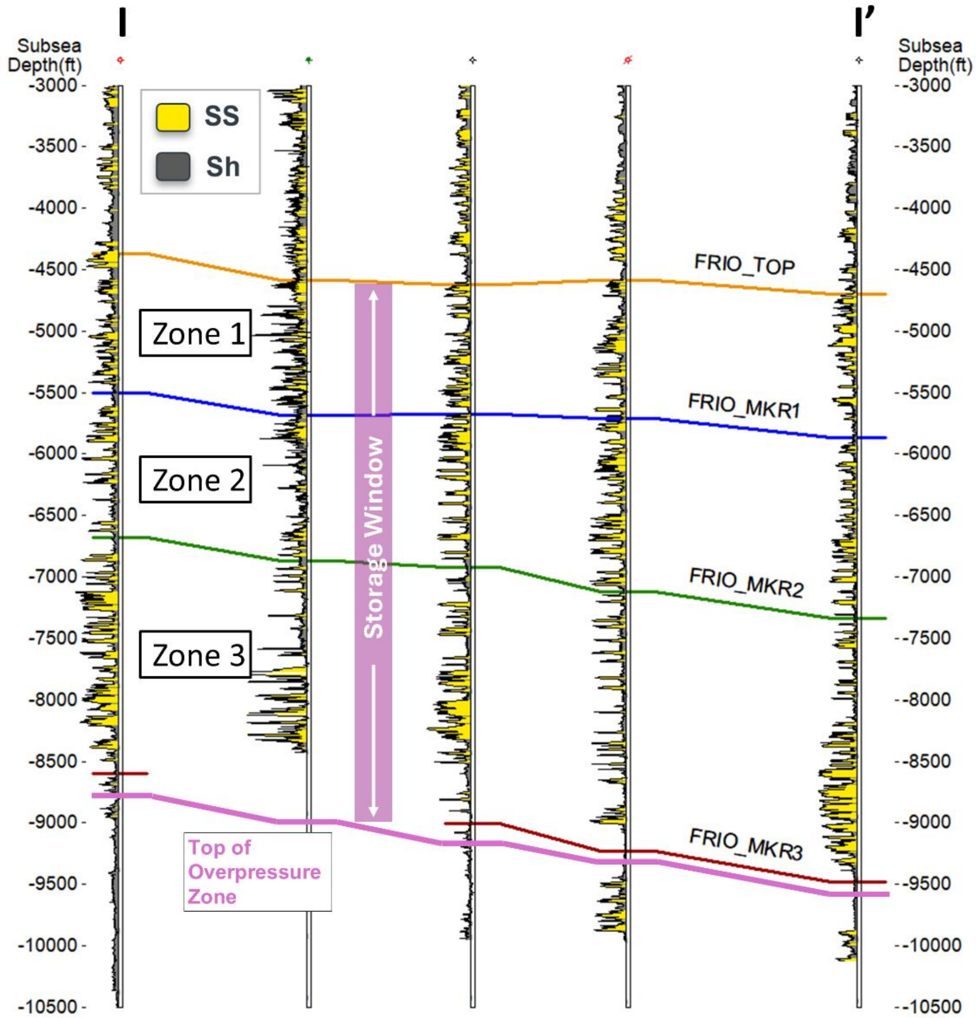

Figure 62. Dip-oriented cross-section II' in Site WK, showing SP logs, reservoir zones, and the extrapolated top of overpressure zone.

5.3 Site KK

The estimation results for Site KK are summarized in Table 7. This site is located in the coastal area on the edge of Kleberg and Kenedy Counties, known as the Baffin Bay. The reservoir area has semi-closed boundaries determined by faults extending in north-south direction. As shown in the net sand maps (Figure 63), the sand depocenter was mostly in Kenedy County in Zone 3. Later in Zone 1 and Zone 2, the depocenter shifts north to the Baffin Bay, where the sandstones are the thickest. The SP log cross sections indicate good reservoir connectivity in all three zones (figure 64 and 65).

Site KK faces the same limitation in core data availability as Site WK. Although no local core measurement data is available within this site, a nearby cluster of core data is present to the west. Therefore, the EASiTool inputs for this site are derived from the nearby compartment, consistent with the approach used for Site WK.

Site KK	Zone 1	Zone 2	Zone 3	Total
Injectivity (kh, darcy·m)	3.31	3.61	8.60	15.52
Open boundary capacity (MMT)				
Deterministic (25 wells)	135	190	439	764
P10	316	447	1558	—
P50	186	237	837	—
P90	94	138	400	—
Closed boundary capacity (MMT)				
Deterministic (25 wells)	57	72	66	195
P10	78	103	90	—
P50	55	77	66	—
P90	38	50	44	—

Table 7. Injectivity and estimated storage capacity for Site KK under open and closed boundary conditions.

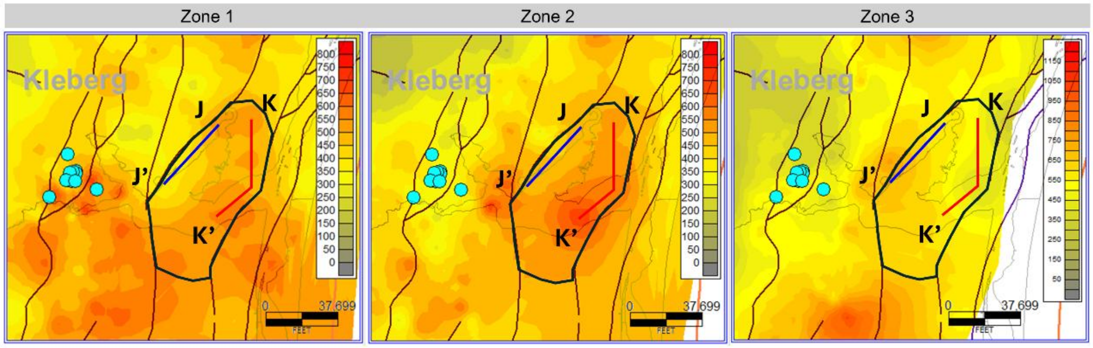

Figure 63. Net sand maps of Baffin Bay with the reservoir area of Site KK outlined by a black polygon.
Bright blue dots indicate the location of core data used for this site. The location of cross-sections JJ' (Figure 64) and KK' (Figure 65) are labeled on the maps.

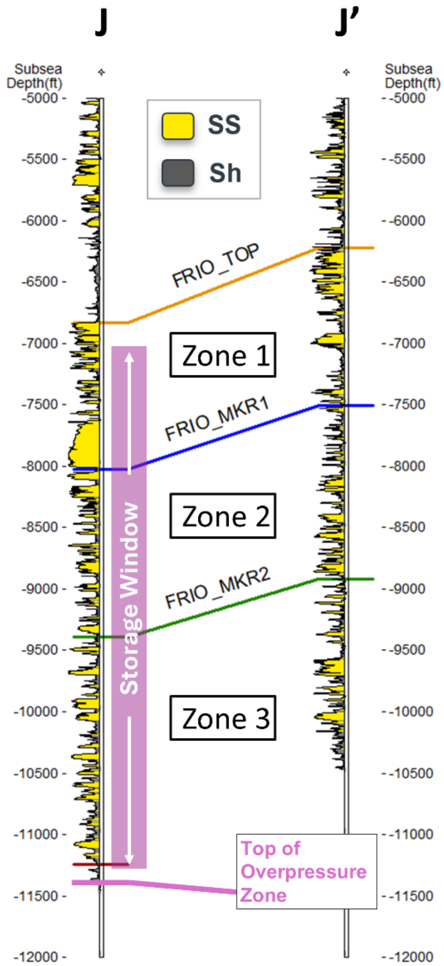

Figure 64. Strike-oriented cross-section JJ' on the left of the Site KK, showing SP logs, reservoir zones, and the extrapolated top of overpressure zone.

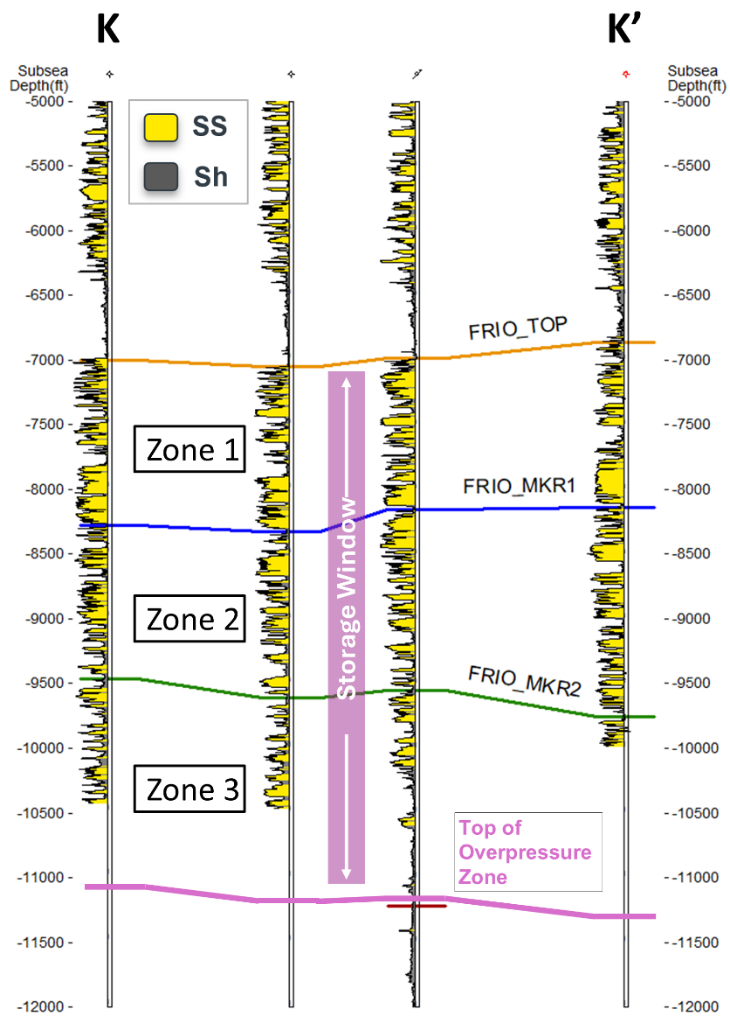

Figure 65. Strike-oriented cross-section KK' on the right side of the Site KK, showing SP logs, reservoir zones, and the extrapolated top of overpressure zone.

5.4 Site KND

The estimation results of Site KND are presented in Table 8. This site is located in the south boundary of Kenedy County, while a part of this site extends in the Willacy County. Being in the extensive sand rich facies of the Norias delta system (Galloway et al, 1982a), site KND has the most significant amount of sandstone in the study area. Every zone within the reservoir area has considerable sand thickness (Figure 66). Reservoir connectivity could be observed from the strike-oriented cross-section (Figure 67). Also, the reservoir area is the largest among all the candidate sites due to the distance between the faults.

The aforementioned conditions should be favorable for storage capacity; nevertheless, the permeability in this area are fairly poor, which is the lowest among all the candidates. According to the available local core data on this site, the geometric mean permeability in this site is 14 and 12 respectively in zone 1 and zone 2. There is no core measurement data available for zone 3, so the capacity of zone 3 of this site is estimated with the data from zone 2.

Site KND	Zone 1	Zone 2	Zone 3	Total
Injectivity (kh, darcy·m)	2.08	2.17	2.85	7.10
Open boundary capacity (MMT)				
Deterministic (25 wells)	139	184	281	605
P10	236	288	447	—
P50	157	198	295	—
P90	95	130	194	—
Closed boundary capacity (MMT)				
Deterministic (25 wells)	99	132	188	420
P10	139	179	261	—
P50	101	132	184	—
P90	67	88	133	—

Table 8. Injectivity and estimated storage capacity for Site KND under open and closed boundary conditions.

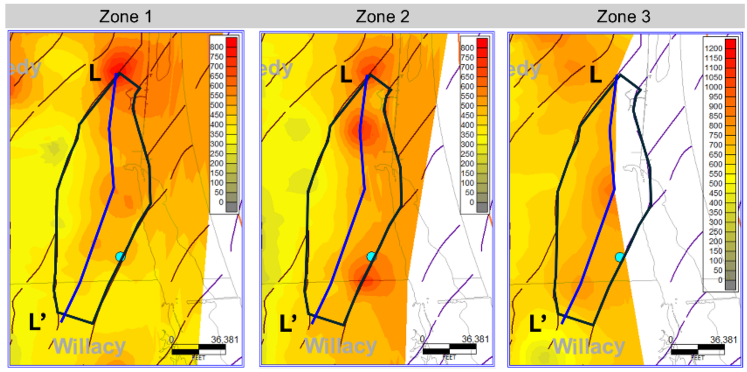

Figure 66. Net sand maps of the coastal Kenedy with the reservoir area of Site KND outlined by a black polygon.
Bright blue dots indicate the location of core data used for this site. The location of cross-sections LL' (Figure 67) is labeled on the maps.

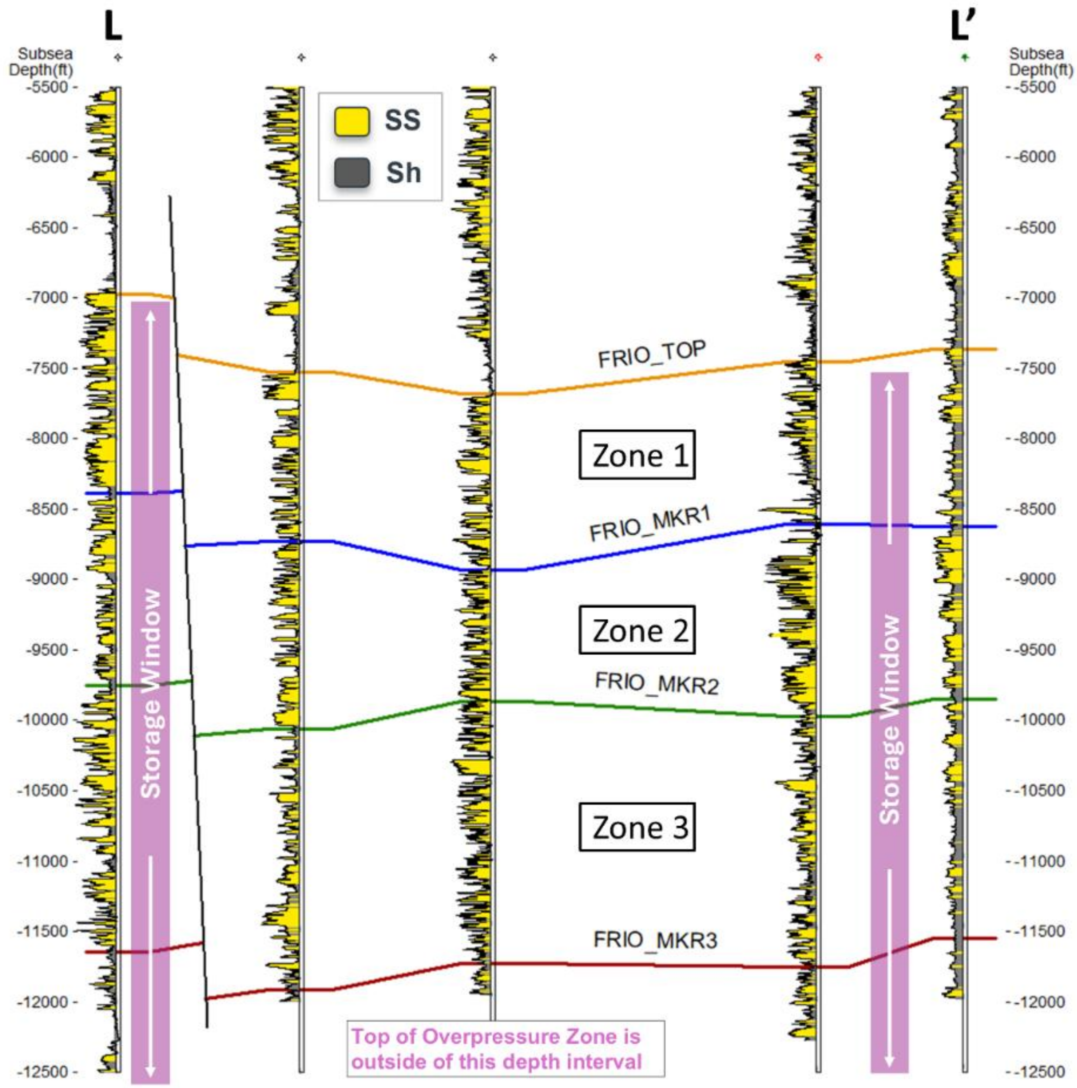

Figure 67. Strike-oriented cross-section LL' in KND site, showing SP logs, the reservoir zones, and the extrapolated top of overpressure zone.

5.5 SITE W

The estimation results of Site W are summarized in Table 9. This site is located at the boundary of Willacy and Hidalgo counties. This reservoir area is bound by two faults, which intersect each other in their south end (Figure 68). If the faults serve as a seal, the only exit for fluids would be in the north of the area. According to the cross-sections (Figure 69), there are barely any sandstones in Zone 1 and Zone 2. In contrast, thick sandstones are presented at the bottom of the zone 3. The core measurements are available in this area. Hence, all reservoir properties are derived from the local core measurements.

Site W	Zone 3
Injectivity (kh, darcy·m)	3.48
Open boundary capacity (MMT)	
Deterministic (25 wells)	97
P10	182
P50	96
P90	39
Closed boundary capacity (MMT)	
Deterministic (25 wells)	28
P10	44
P50	27
P90	12

Table 9. Injectivity and estimated storage capacity for Site W under open and closed boundary conditions.

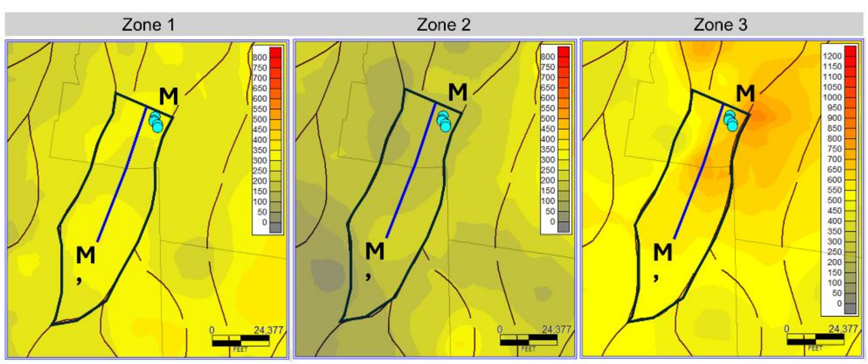

Figure 68. Net sand maps of the western Willacy County with the reservoir area of Site W outlined by a black polygon.
Bright blue dots indicate the location of core data used for this site. The location of cross-sections MM' (Figure 69) are labeled on the maps.

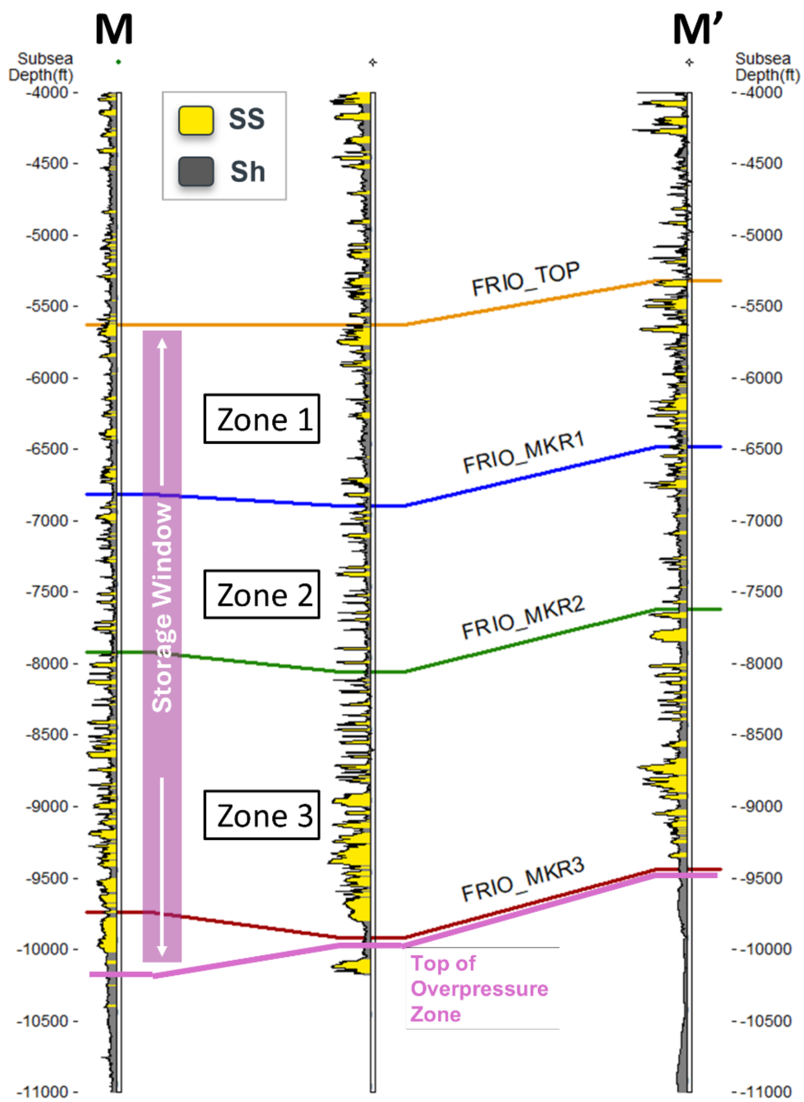

Figure 69. Strike-oriented cross-section MM' of Site W, showing SP logs, reservoir zones, and the extrapolated top of overpressure zone.

5.6 Summary of the Estimation Results

The estimated injectivity and capacity under closed boundary conditions of the five proposed sites are summarized and ranked in Table 9. These sites are categorized into 3 types of reservoirs according to the reservoir classification developed by Hoffman et al. (2015) and their approximate location on the permeability-thickness crossplot is shown below in Figure 70. The three sites in the northern study area are viable for commercial projects while the other two sites in the southern study area are only suitable for low volume storage.

Site	Total Injectivity (darcy-meter)	Injectivity Type	Injectivity Ranking	Total Closed-Boundary Capacity (MMT)	Capacity Ranking
N	27.90	2	1	37	4
WK	11.5	2	3	117	3
KK	15.52	2	2	195	2
KND	7.10	3	4	420	1
W	3.48	3	5	28	5

Table 10. Summary of estimated injectivity and CO_2 storage capacity for the five proposed sites, with rankings.

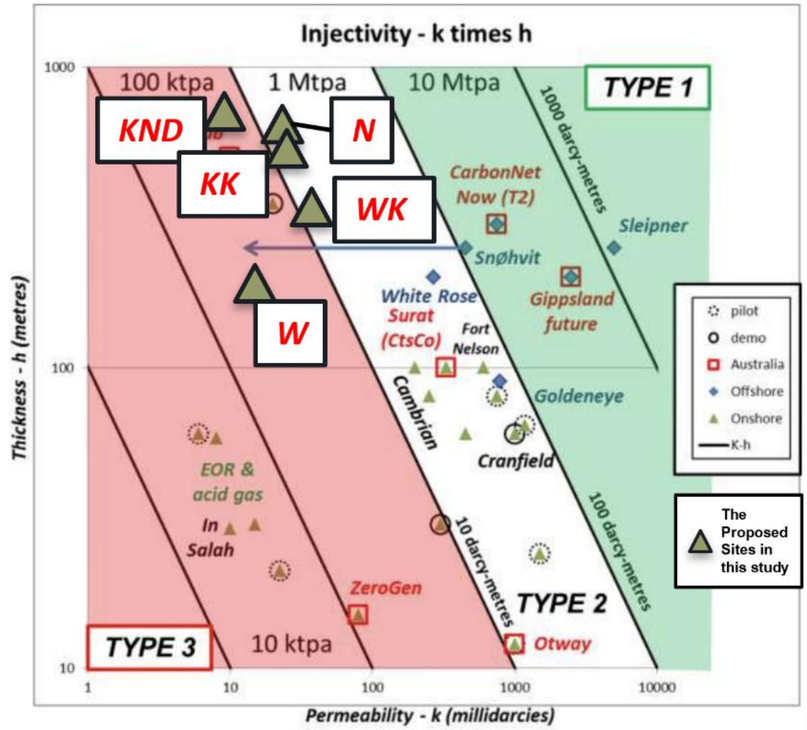

Figure 70. Injectivity of the proposed sites indicated on the permeability-thickness crossplot by Hoffman et al. (2015)

Chapter 6: Discussion

6.1 Regional Geological Implications for CO_2 Storage in South Texas

Good injectivity and effective storage, the presence of a confining system, sufficient reservoir thickness and good reservoir quality are the primary concerns for stakeholders during exploration stage. This study serves the purpose of preliminary regional screening for the CO_2 sequestration potential in the Frio Formation of South Texas. These geologic factors are evaluated accordingly to better identify the potential of Frio saline reservoirs for injectivity and storage.

6.1.1 Regional Sandstone Distribution of South Texas Frio

The well-log correlations and the three reservoir zones are developed independently by this study. The interpretated gross depositional environment (GDE) on the sand maps of these zones was guided by the regional framework built by Galloway et al. (1982a) and Rogers and Ambrose (2024). The sandstone distribution presented in the net sand maps (Figure 27, 28, and 29) correspond closely with the findings in these previous studies and indicates four main depositional systems that contain high sand content in the South Texas Frio.

The massive and blocky sand content found in Eastern Nueces County in Zone 1 and Zone 3 is interpreted to represent the Greta Barrier/ Strandplain System. The delta-shaped thick sandstone accumulation shifting around the present-day Baffin Bay throughout three zones is interpreted as the proximal delta front of Norias Delta System. Speaking in a chronological order, the main depocenter (Snedden & Galloway, 2019) is originally at the central Kenedy County in Zone 3 and later shifts northward toward present-day Baffin Bay area during Zone 2 and Zone 1.

The wide band of thick sand beneath the current coastline of Kenedy and Willacy counties is interpreted as the proximal delta front. The belt-shaped sand distribution observed around the eastern Brooks County across all zones is considered as the channel fill deposits within the delta plain (Galloway et al., 1982a; Rogers and Ambrose, 2024). These interpretations with the permeability and porosity representative values at available locations are visualized on the sand maps (Figure 71, 72, 73), for discussing the relationship between gross depositional environments and reservoir quality.

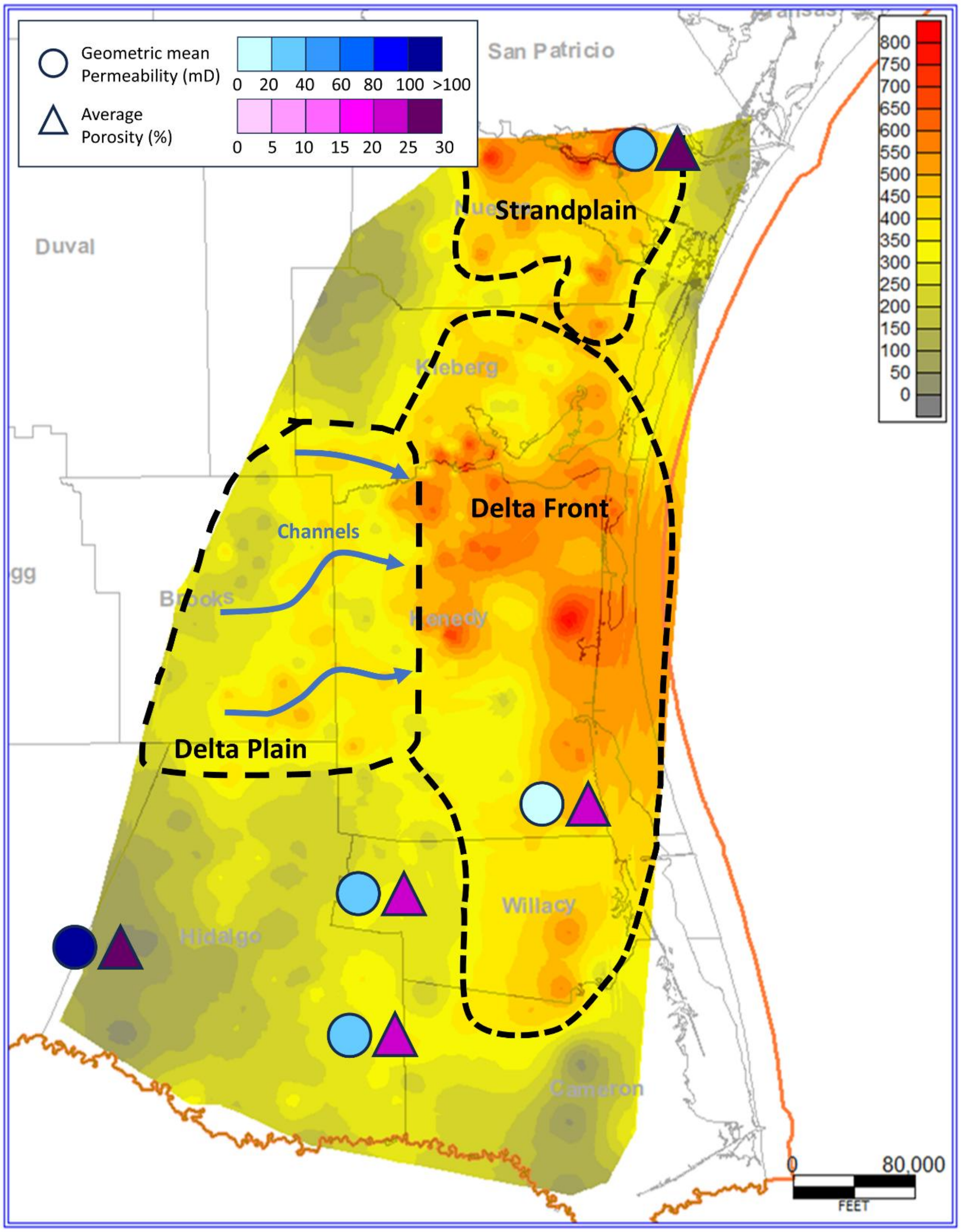

Figure 71. Zone 1 sand map with interpretations of gross depositional environments and with the distribution of representative permeability and porosity values. Circle indicates permeability while triangle indicates porosity.

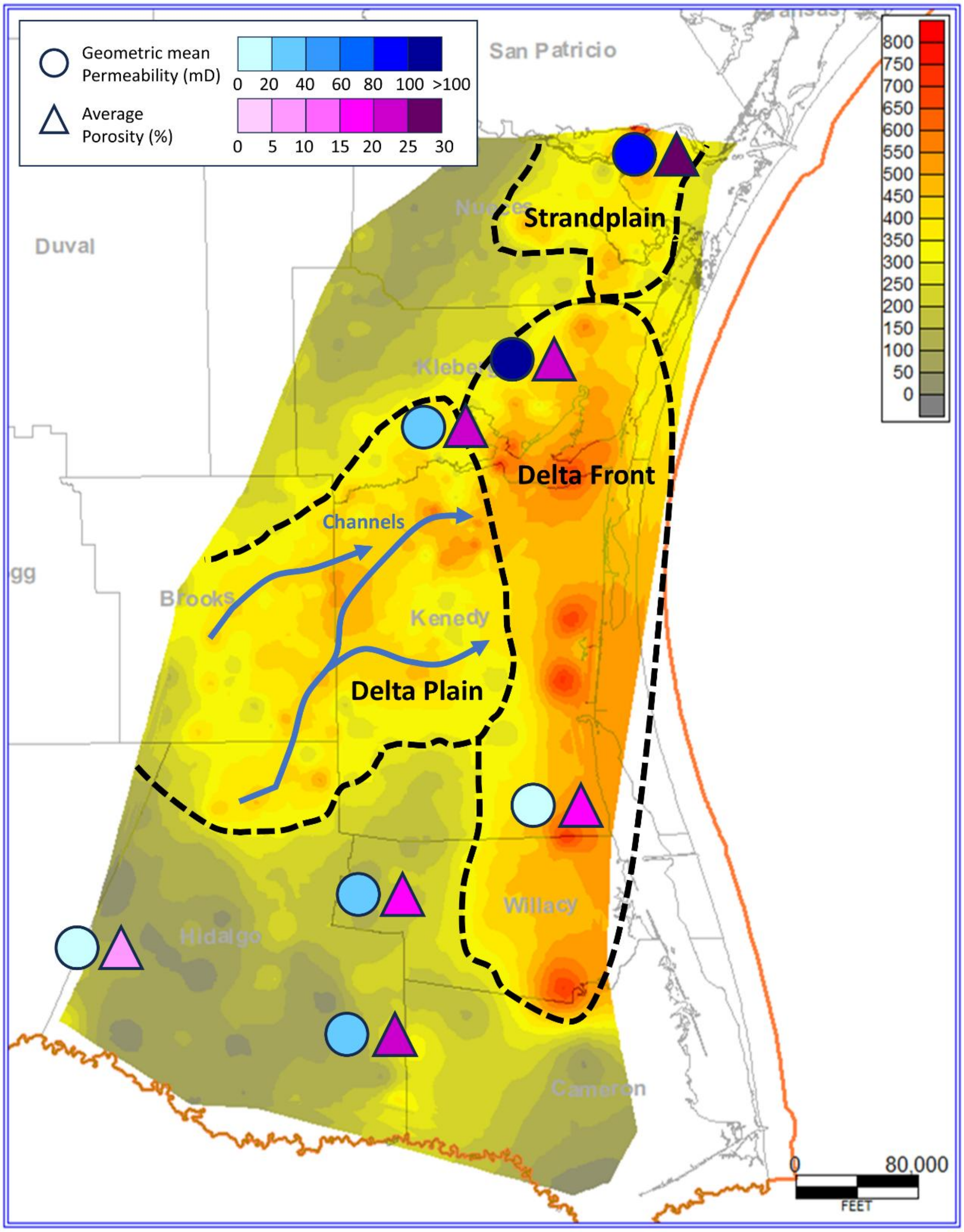

Figure 72. Zone 2 sand map with interpretations of gross depositional environments and with the distribution of representative permeability and porosity values. Circle indicates permeability while triangle indicates porosity.

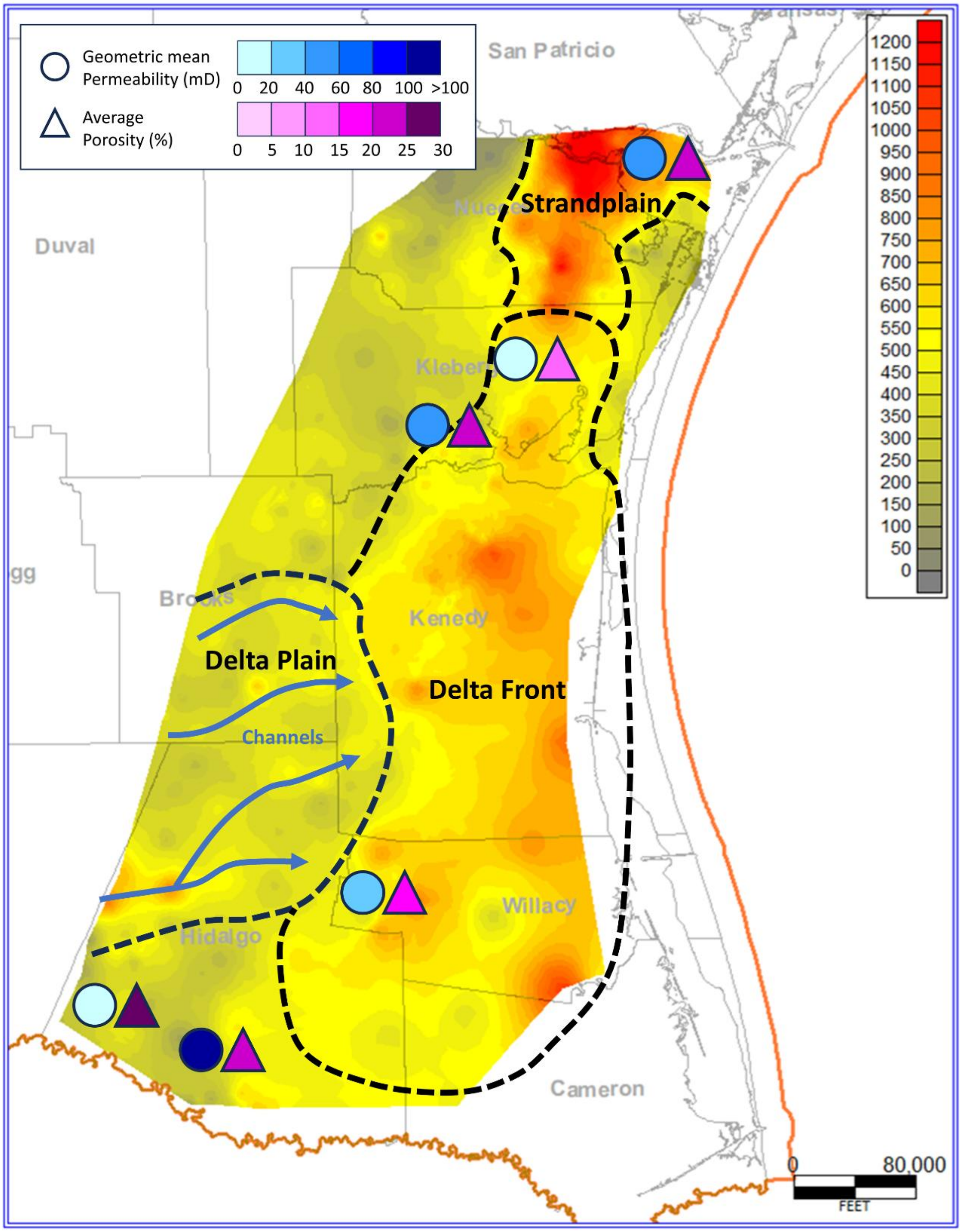

Figure 73. Zone 3 sand map with interpretations of gross depositional environments and with the distribution of representative permeability and porosity values. Circle indicates permeability while triangle indicates porosity.

6.1.2 Spatial Variation of Reservoir Properties

The permeability- porosity evaluation in Chapter 4 presented the variation of rock quality by reservoir zones. Figure 71, 72, and 73 show the interpreted sand maps with the distribution of reservoir properties, which is further discussed below in terms of depth, and in strike and dip orientation.

6.1.2.1 Permeability and Porosity Variation with Depth

The permeability-porosity transforms generally suggest that the Zone 1 and Zone 2 have similar reservoir properties, whereas Zone 3 lies above and to the left of Zone 1 and Zone 2, as shown in Figure. 45, 49, 50, and 51 in section 4.5.2. This observation may indicate that rock characteristics are different in Zone 3 than in the other two zones.

Vertically, average porosities in Zone 1 are similar to Zone 2 and are reduced in Zone 3, as this trend is observed across the study area. Notably, the permeability-porosity cross plots for Cluster A and B, in Nueces and Kleberg Counties, shows the presence of porosity greater than 25% in Zone 3. These porosities are possibly associated with the secondary porosity or/and microporosity. According to Loucks et al. (1984), quartz and carbonate cementation could reduce the porosity to 10% but may be reversed by the secondary dissolution that could restore porosity up to 30% at the bottom of the intermediate subsurface diagenesis zone. In Figure 74., the porosity versus depth cross plot aligns with Louck's findings and demonstrates that many porosities ranging from 0.15 to 0.30 are present in the lower half of the intermediate subsurface diagenesis zone, which approximately overlaps with Zone 3.

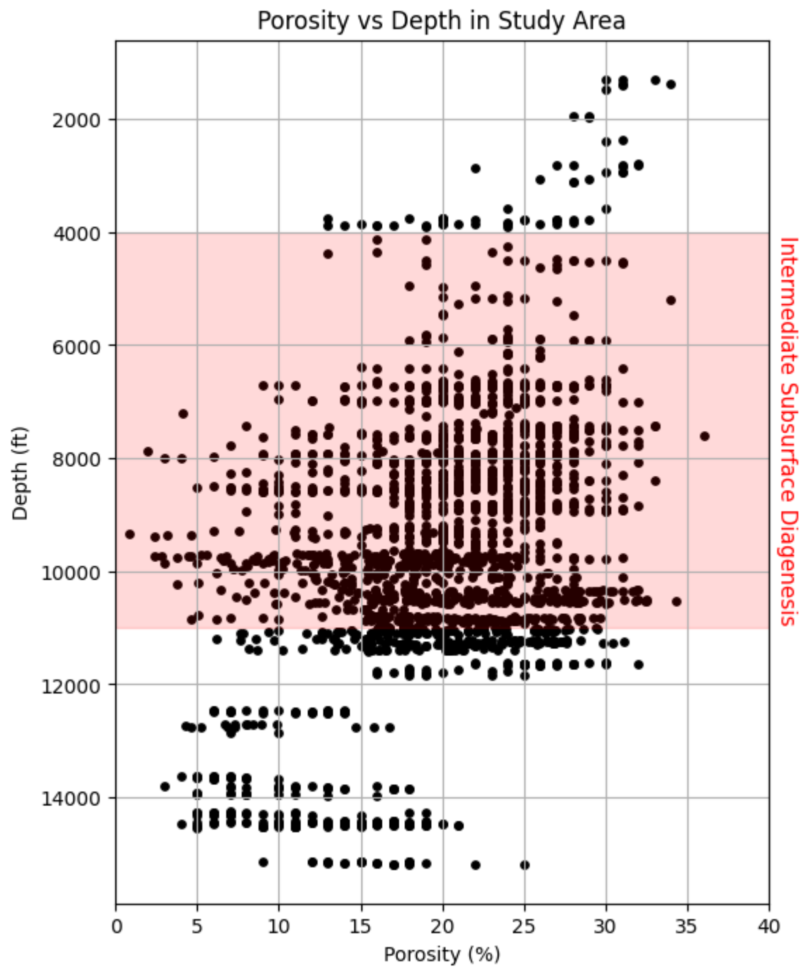

Figure 74. Cross plot of porosity versus depth with the available core measurement. Intermediate subsurface diagenesis zone defined by Loucks et al. (1984) is highlighted in pink.

In contrast, the vertical variation of average permeabilities does not have a clear common trend across the study area. For example, the highest average permeability is found in Zone 2 of Cluster A in Nueces County and in Zone 3 of Cluster B in Kleberg County. Nevertheless, the overall permeability variation with depth still exhibits similar patterns like porosity does. In the permeability versus depth cross plot (Figure 75), the minimum permeability decreases with depth, while good permeability between 20 to

1000 mD is present in the interval from 8000 ft to 12000 ft. This depth interval overlaps with the bottom of Zone 3 and intermediate subsurface diagenesis zone. However, secondary porosity doesn't usually increase permeability (Uroza, personal communication). Therefore, the mechanism of permeability preservation remains unclear.

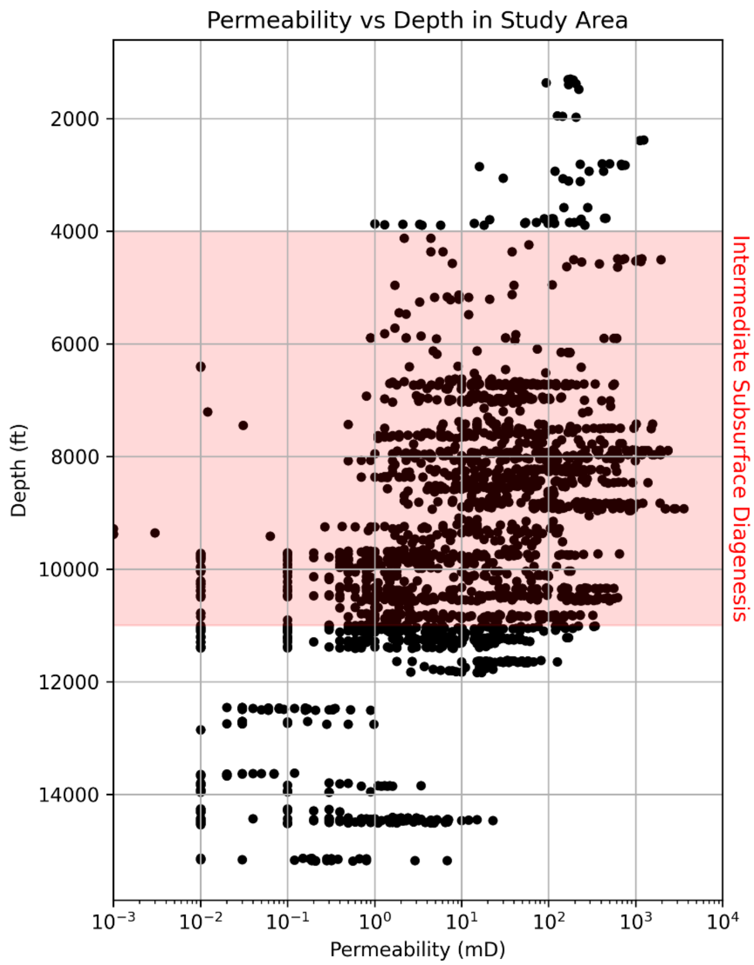

Figure 75. Cross plot of permeability versus depth with the available core measurement. Intermediate subsurface diagenesis zone is highlighted in pink.

To summarize, the secondary porosities could provide additional storage spaces if they are connected, and the preserved permeabilities could also be promising for injecting in Zone 3. Not only these conditions in Zone 3 sandstones are favorable for CO_2 sequestration but their greater depth may also reduce the area of review and improve USDW protection.

6.1.2.2 Variation along Strike:

Cluster A, Cluster CW, Cluster B, well C and Cluster D are distributed parallel to the gulf coastline, demonstrating the reservoir quality variation along the structural strike. Aerially, the overall reservoir quality in the north is better than in the south on a regional scale. Table 1 to 3 have shown that the porosity is best preserved in the northern study area and gradually decrease toward the south, whereas the permeability does not exhibit a clear trend.

In the depth interval of Zone 1 and Zone 2, Well C in Kenedy County, which should belong to the delta-front facies, exhibits the lowest reservoir quality. The permeability obtained from Well C is lower than that of Cluster D in Willacy County (Figure 71, and 72), even though Cluster D is located closer to the provenance of carbonate debris. This observation can be interpreted as a result of compaction with depth, because the same zone at Well C is about 1500-2000 ft deeper than at Cluster D.

In Zone 3, a similar contrast is observed between two nearby well clusters. Cluster CW in central Kleberg County and B in Baffin Bay are approximately 7000 ft apart and are both at the intersection of where the proximal delta front grades into the strandplain, as identified on the interpreted sand maps (Figure 73). However, Cluster CW has its geometric mean permeability smaller than 1mD, while the Cluster B reaches almost 60 mD.

6.1.2.3 Variation along Dip:

There are 4 cored wells available in Hidalgo County: Well E, F, G, and H arrange along the structural dip towards the Gulf Coast. These cores are identified to be in the floodplain facies according to the paleogeography trend proposed by Rogers and Ambrose (2024). As shown in Figure 71 to 73, the permeability-porosity evaluation of these cores indicates that there is no clear spatial variation pattern found in Hidalgo County, as the samples identified as same stratigraphic zones are exhibiting significant difference in reservoir quality. The limitation on data availability could be the cause of difficulties in looking for variation trends.

6.1.2.4 Summarization for Spatial Variation of Reservoir Properties

Comparing all cored data together, several samples from Well E surprisingly show better reservoir quality than Well C and Cluster D in the wave-reworked delta front, even though Well E are closer to the source of the volcanic ash and carbonate fragments. Since Well E is located in the delta plain, its samples with good reservoir properties are likely to be preserved by distributary or fluvial channels, where sandstones should be coarser and is favorable to develop permeability. To summarize, the porosity variation with depth can be understood as a result of compaction and its variation along the coastal counties aligns with depositional facies. However, the mechanism of preservation on permeability remains unclear as it does not suggest any trends regarding depth, depositional facies, or the distance to the provenance.

6.2 IMPLICATIONS OF CAPACITY ESTIMATION ON THE CANDIDATE SITES

After screening for the areas with less legacy wells and available core data, Site N, Site WK, Site KK, Site KND and Site W were proposed for evaluating their suitability for CO_2 injection. The results of these sites are discussed individually below. It should be noted that a more realistic capacity estimation would require the use of seismic data to assist with confirming the subsurface structures. Without access to this information, storage capacity is estimated under both boundary conditions to present best- and worst-case scenarios.

6.2.1 Site N

Located on the Greta Barrier/ Strandplain, Site N has thick and blocky sandstones with good continuity. Moreover, its reservoir quality is the best among all the candidate sites reaching permeability of 98 mD in Zone 2. Site N presents total injectivity of 27.9 darcy-meter, the highest among all proposed sites, and is classified as Type 2 reservoir based on Hoffman et al. (2015), indicating its suitability for developing into commercial projects. Optimistically, its estimated capacity of 266 MMT under open boundary scenario could accommodate approximately 20 years of CO_2 emissions from the reported large facilities in Nueces County, based on their combined annual emissions of about 14 MMT in 2023 obtained from the EPA FLIGHT dataset (2026a). In contrast, the capacity of 37 MMT calculated with closed boundary conditions appears limited but could still provide 20-year storage for point-source emissions below 1.8 MMT per year, such as Corpus Christi Energy Center, which reported annual emissions of 1.4 MMT in 2023 (EPA FLIGHT database, 2026a).

6.2.2 Site WK

The reservoir quality in Kleberg County is relatively moderate within study area. However, located on the edge of the Norias delta system, the net sand thickness on Site WK is the thinnest among all sites, only presenting around 100m in each zone. Thus, this site proposed a total injectivity of 11.5 darcy-meters, almost being classified as a Type 3 reservoir due to the limited sand thickness. The biggest advantage of this site is its large reservoir area, more than 500 km^2, remaining the capacity to reach 391 MMT and 117 MMT under open and closed boundary scenarios, respectively. There is only one reported large facility in Kleberg County, that is King Ranch Gas Plant which emitted about 0.24 MMT of CO_2 in 2023. Site WK is not only able to accommodate the emission from this local gas plant, but it has sufficient spaces for CO_2 storage from direct air capture (DAC) projects or any future carbon-emitting facilities.

6.2.3 Site KK

Site KK is the closest to the depocenter of the Norias delta system, with its Zone 2 sandstones being in the proximal delta front facies. Hence, it also presents one of the highest net sand thicknesses and considerable storage capacity even though the reservoir quality and reservoir area remain moderate. Its total injectivity is 15.52 darcy-meters, identified as a Type 2 reservoir which has potential for commerciality. The estimated capacity reaches 764 MMT and 195 MMT under open and closed boundary scenarios, respectively. Same as Site WK, there are not many large emissions nearby, and DAC projects or CO_2 transported through pipelines should be suitable for this site. For example, project 1PointFive has been in cooperation with King Ranch in Kleberg County to develop a DAC sequestration hub (1PointFive, 2026).

6.2.4 Site KND

Located in the sand-rich distal delta front facies in the coastal part of Kenedy County, Site KND also owns a significant amount of net sand content. Additionally, it has the largest reservoir compartment among all candidate sites. These advantages cancel out the negative effect of its poor reservoir quality on the estimated storage capacity, achieving 605 MMT with open boundary and 420 MMT with closed boundary. Remarkably, its capacity difference between 2 boundary conditions is the least due to the large reservoir area. However, this site is a Type 3 reservoir due to low injectivity of 7.1 darcy-meters and may only be viable for small injection rates. There is not any large facility in Kenedy County, and the only emission source nearby is the KMBP Brooks County Station that emitted 15273 MT of CO_2 reported in 2023 (EPA FLIGHT dataset). Site KND could take the emissions from nearby counties or from DAC.

6.2.5 Site W

Most of the sandstones pinched out in Zone 1 and Zone 2 in Site W, so only the capacity of Zone 3 is estimated. Also, it is the only site that does not serve as stack storage. With moderate sand thickness, moderate size of reservoir area, and reservoir quality lower than the sites in Kleberg, the capacity of Site W is estimated to assess how much storage capacity could still be achieved under these less ideal conditions. The capacity with open boundary is 97 MMT and with closed boundary it is 28 MMT. Although there are not any large facilities in Willacy County, there are 9 in Hidalgo and 3 in Cameron County that together emitted 3.4 MMT of CO_2s in 2023 (FLIGHT by EPA, 2026a). Even with the worst case of a 28MMT capacity, Site W could still provide storage for adjacent counties for 9 years. Considering its low injectivity, matching with a single point source emission is viable, such as Calpine Hidalgo Energy Center that emitted about 1MMT CO_2 in 2023, allowing for approximately 28 years of injection.

6.2.6 Total Storage Capacity of All Proposed Sites

Summing up the estimates from all sites, the total storage capacity is 2173 MMT under open boundary conditions and 797 MMT under closed boundary conditions. Based on annual emissions from the large facilities reported in 2023 within the study area (FLIGHT by EPA, 2026a), this capacity is sufficient to store at least 45 years of local large-scale CO_2 emissions.

6.3 General Observations from Storage Capacity Estimation

While estimating the capacities for each site, several behavior patterns are observed across the candidates and are synthesized below for providing insights into the storage capacity in the South Texas Frio.

First, the P50 capacity with open boundary condition from the Monte Carlo simulations is found higher than the corresponding base-case estimate for most sites in this study. Considering the variation of permeability contributes the most sensitivity to storage capacity in most cases with open boundary conditions, this discrepancy may reflect the log-normal distribution of permeability values used in the simulations. The Monte Carlo simulation output figures (Appendix A) also show a right-skewed distribution that align with the log-normal distributional permeability data.

Secondly, area of review (AOR) is a major concern among the proposed sites. As the critical pressure increase at every site in each zone calculated to be below 1Mpa, the plots of AORs with probability generated by EASiTool (Appendix A) indicate that most of the mean AOR estimates exceed the corresponding reservoir areas. This result may be attributed to a deeper USDW base, as in Site WK and Site KK, where the UDSWs are found in Jasper Aquifer and the Anahuac Shale is the only confining unit separating USDW from the injection zones (Shi et al., 2022). It may also be related to the relatively small brine salinity assumed in the calculations, as direct salinity measurement from the upper Frio is unavailable and the salinities recorded at the shallowest available depth is instead adopted in the calculation.

Having small critical pressure increase and large AOR is found particularly common when injecting into Zone 1, likely because it is close to the base of USDW. Nonetheless, capacity estimates for the selected sites in Zone 1 are still presented in this study to evaluate the overall storage potential of Frio sandstones. However, it should be noted that a larger AOR would increase costs for investigating, mitigating, and monitoring the legacy wells, thereby reducing the net present value (NPV) of a CO_2 sequestration project.

Lastly, it is well understood that the site with the greatest injectivity is not necessarily the one with the largest storage capacity. A site with lower injectivity may still surpass others in terms of capacity when it is associated with a sufficiently large reservoir. This relationship is demonstrated in the comparison of Site N and Site KND in Table 10.

As the thickness-permeability product represents the most fundamental reservoir properties controlling injectivity, the capacity estimation further incorporates the influence of reservoir area and boundary conditions. Consequently, the size of compartment and boundary conditions becomes essential to determine the potential of an injection site, especially in Frio Formation in South Texas. This is because the results have suggested that a larger reservoir compartment is able to compensate for the suboptimal reservoir quality and achieve effective storage capacity, as demonstrated by Site WK and Site KND.

6.4 GEOLOGICAL UNCERTAINTY IN STORAGE CAPACITY ESTIMATION

According to Uroza (personal communication) and the observation on the cores of Humble No.183 Alazan and CW-1, it is found in core data from the South Texas that the Frio sandstones could have significant variation of permeability within several feet. The light grayish calcite cement with diameter around 10 to 20 centimeters took place randomly and it is distributed non- homogeneously in the core (Figure 76). Also, the permeability-porosity data also shows that reservoir quality could vary within a short distance vertically or aerially. Such uneven distribution of reservoir quality has also been observed with the Cluster CW and Cluster B in Kleberg County, and with the wells (Well E, F, G, H) in Hidalgo County. Therefore, this study suggests that there is a good chance that better reservoir properties are present but may not be recorded by the current limited data.

As for the faults from Ewing (1991), these faults are assumed to be a lateral seal and used to define the boundary of the reservoir area of the proposed sites in this study. Nevertheless, if seismic data or further investigations suggest that the sandstones are connected, there could be a larger compartment to hold more capacity, as explained previously.

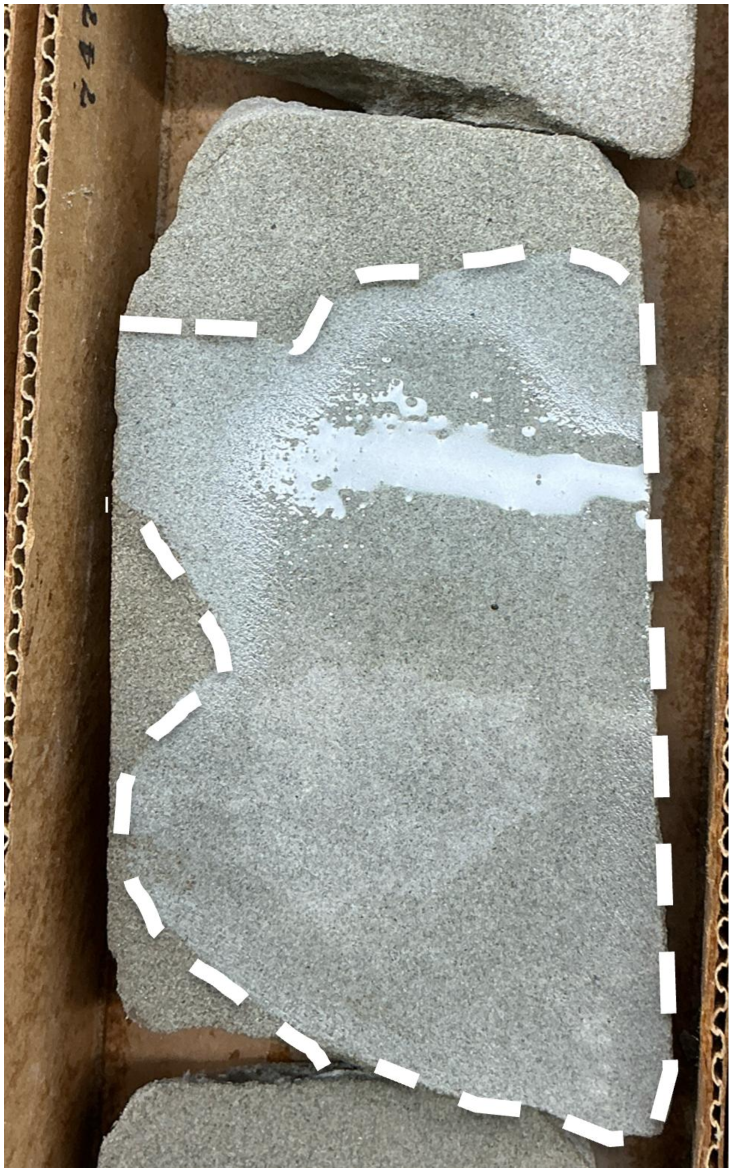

Figure 76. Calcite cement (outlined with white dash line) observed in the core of Humble No.183 in Kleberg County at 7478 ft, photographed in the BEG Core Research Center.

Chapter 7: Conclusion

This study aimed to understand the distribution of Frio sandstone reservoirs and the impact of its reservoir quality on CO_2 injection, as well as to propose the potential of CO_2 storage viability within the South Texas area.

The results of the geological characterization show that relatively good sandstone continuity and sufficient net sand contents occur within the Greta Barrier/ Strandplain in Nueces and Northen Kleberg Counties, and the delta front of the Norias delta system along the coast of Kleberg, Kenedy, and Willacy Counties. Meanwhile, the delta plain and its marginal areas also contain a fair number of sandstones with decent quality for injectivity. Regarding the reservoir quality, the mechanism controlling its spatial variation remains unclear, although few trends have been observed. Speaking of areal variation generally, the porosity decreases towards the south, and the permeability is typically better in the northern half of the study area since the southern half contains more poor values. Vertically, secondary porosities and good permeabilities are found to take place largely in Zone 3 within the study area, reviving the reservoir quality.

In summary, reservoir quality in Zone 1 and Zone 2 are feasible for injections but should be careful with the issue of small critical pressure increase which would result in large area of review (AOR). Zone 3 is also viable because CO_2 injection into this zone could have less impact on AOR due to its greater depth.

The South Texas Frio sandstones are overall associated with less favorable reservoir quality due to diagenetic process, and the results of the storage capacity estimation also indicate that their capacities are relatively limited compared to the conventional standards. In spite of these constraints, the proposed sites have proved their capability to at least accommodate local CO_2 emissions or for DAC projects and for future increased emissions from new facilities. From the observation on capacity estimation across all sites, it is also concluded that targeting CO_2 sequestration in a larger reservoir compartment could be a feasible strategy in South Texas to offset the decreased capacity caused by poor permeability.

This study obtained the capacity estimations with conservative assumptions and scenarios but results still presents promising storage potential. Therefore, the findings of this study suggest that the Frio Formation in South Texas has the potential for CO_2 sequestration. The actual capacity could even be more optimistic than the results because they are calculated based on limited core data and limited structural interpretation. Further seismic investigations are required to better delineate the reservoir compartments and to understand their dimensions. In addition, reservoir properties derived from site-specific core data within target reservoir would improve the accuracy of the storage capacity estimation. Future work may investigate the mechanisms of how diagenesis controls the spatial variation of reservoir quality via petrography analysis.

Appendix A – EASiTool Simulation Input and Results for Each Site

A.1 Site N

A.1.1 Simulation Input

EASiTool inputs	Site N								
Reservoir area (square kilometer)	174								
depth of USDW base (m)	243.84 (at the base of Chicot Aquifer)								
	Zone 1			Zone 2			Zone 3		
Representative Depth (m)	1921.92			2222.72			2648.42		
Critical pressure increase (MPa)	0.36			0.39			0.36		
	min	base	max	min	base	max	min	base	max
Initial Pressure (MPa)	24.22	24.71	25.20	28.46	29.96	31.45	33.21	34.95	36.70
Net sand thickness (m)	128.23	147.83	167.43	91.26	138.30	185.35	222	231.95	241
Porosity	0.23	0.26	0.29	0.23	0.27	0.31	0.17	0.22	0.27
Permeability (md)	3.47	31.45	285.40	14.51	98.85	673.49	3.91	41.38	437.87
Temperature (C)	75.62	77.17	78.71	81.49	85.78	90.07	96.88	101.98	107.07
Salinity (mol/kg)	1.37	1.40	1.43	1.40	1.37	1.43	1.37	1.40	1.43
Maximum allowable injection pressure (MPa)	23.61	27.77	31.94	27.30	32.12	36.94	32.53	38.27	44.01

Table A-1 Simulation input parameters for Site N

A.1.2 Output Figures

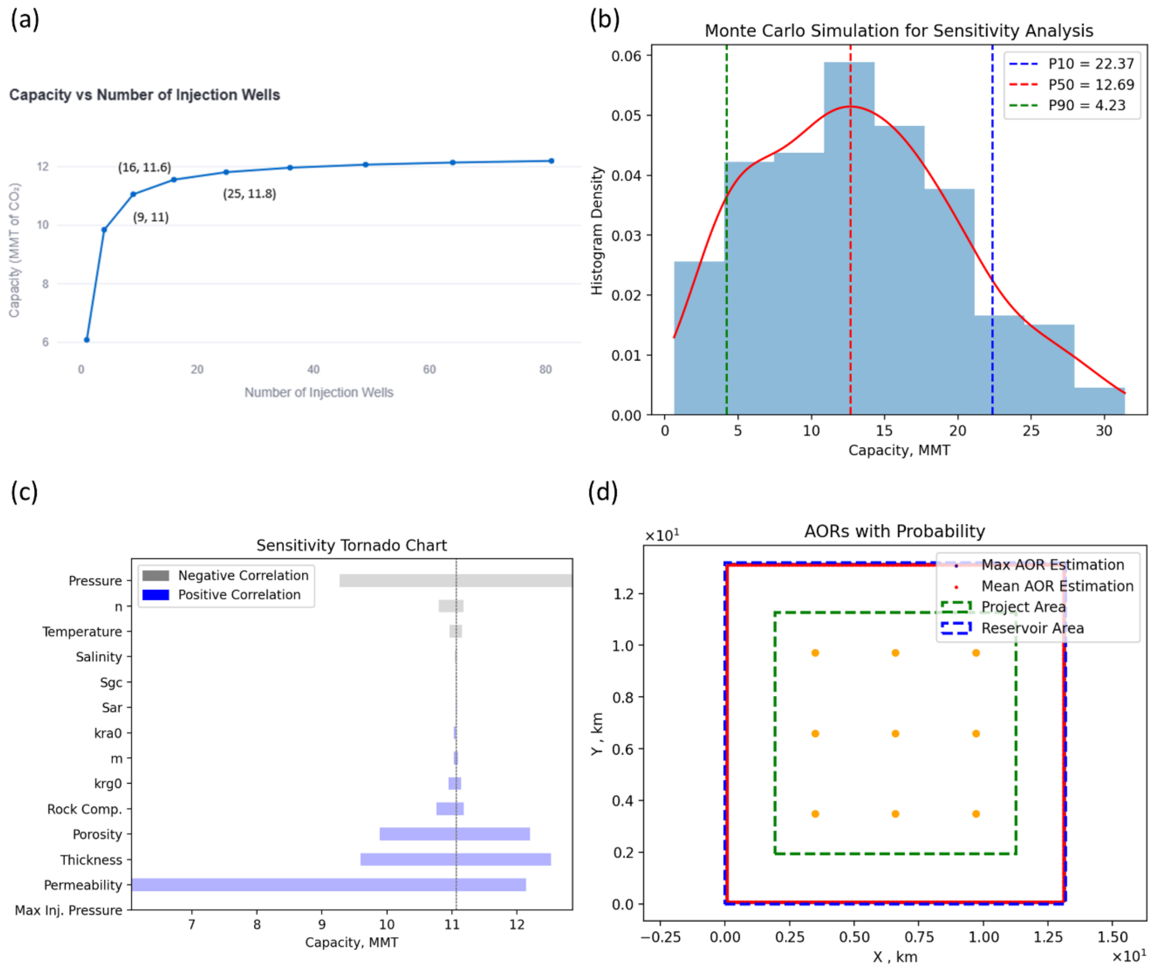

Figure A-1. EASiTool simulation outputs for the reservoir in Zone 1 at Site N under closed-boundary conditions:
(a) capacity vs. number of injection wells; (b) Monte Carlo simulation for sensitivity analysis; (c) sensitivity tornado chart; (d) AORs with probability.

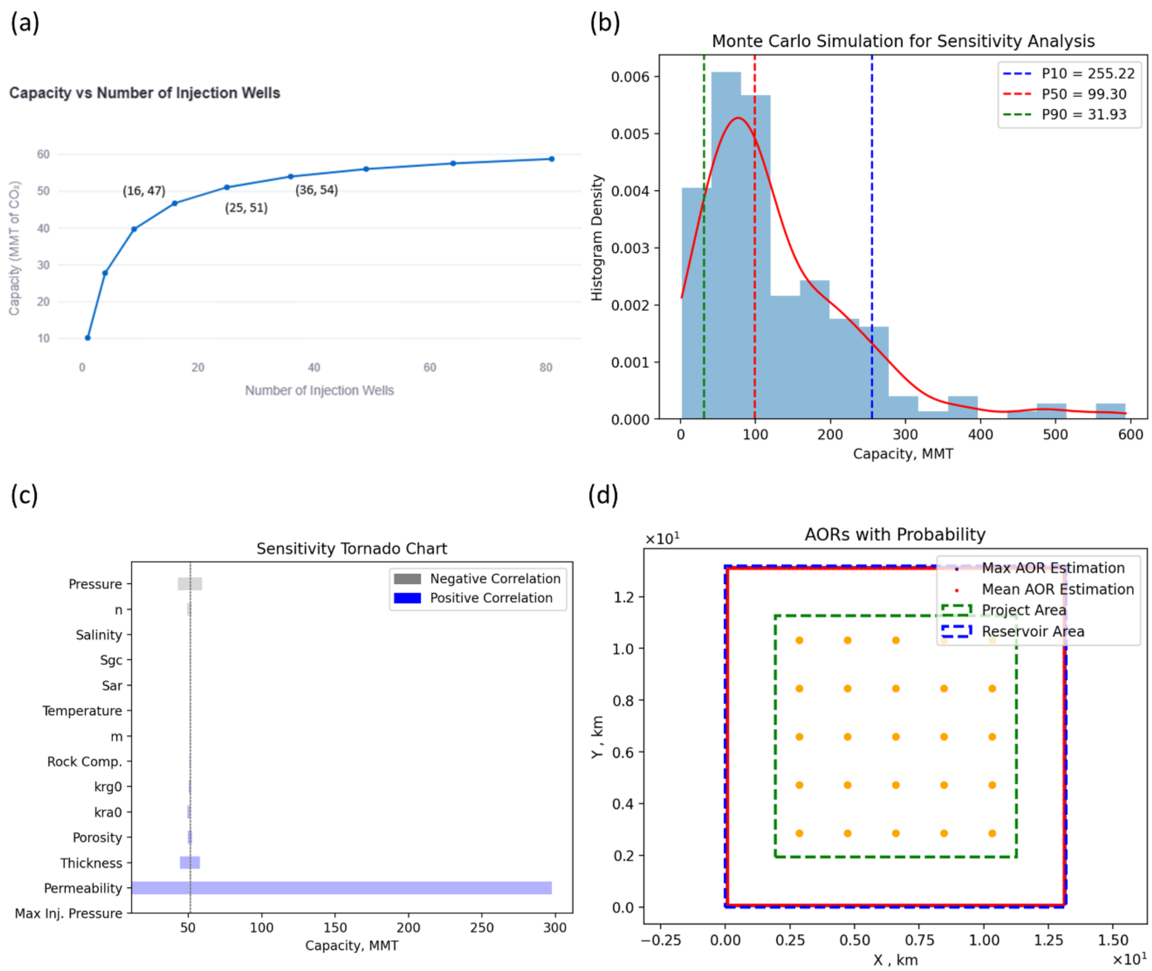

Figure A-2. EASiTool simulation outputs for the reservoir in Zone 1 at Site N under open -boundary conditions:
(a) capacity vs. number of injection wells; (b) Monte Carlo simulation for sensitivity analysis; (c) sensitivity tornado chart; (d) AORs with probability.

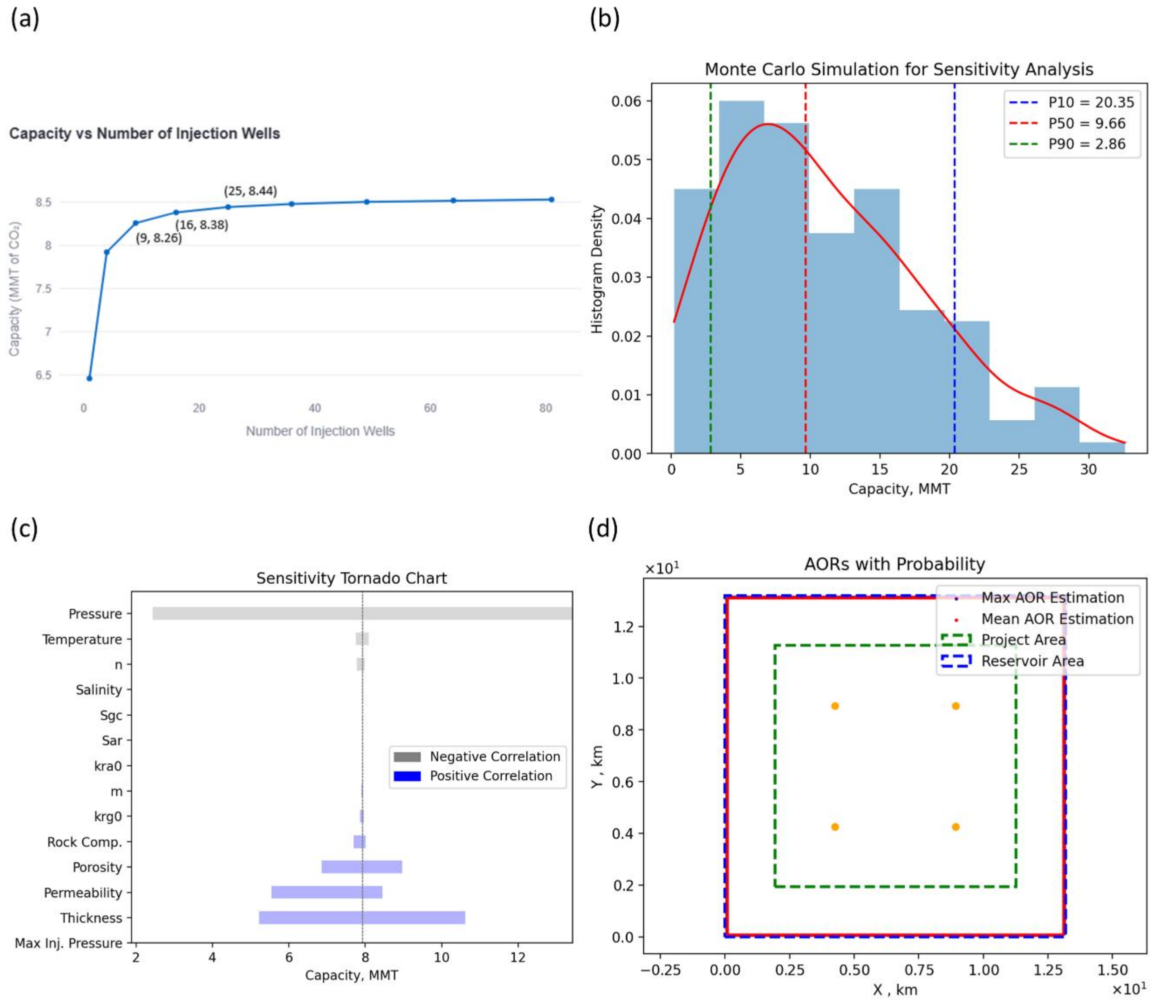

Figure A-3. EASiTool simulation outputs for the reservoir in Zone 2 at Site N under closed-boundary conditions:
(a) capacity vs. number of injection wells; (b) Monte Carlo simulation for sensitivity analysis; (c) sensitivity tornado chart; (d) AORs with probability.

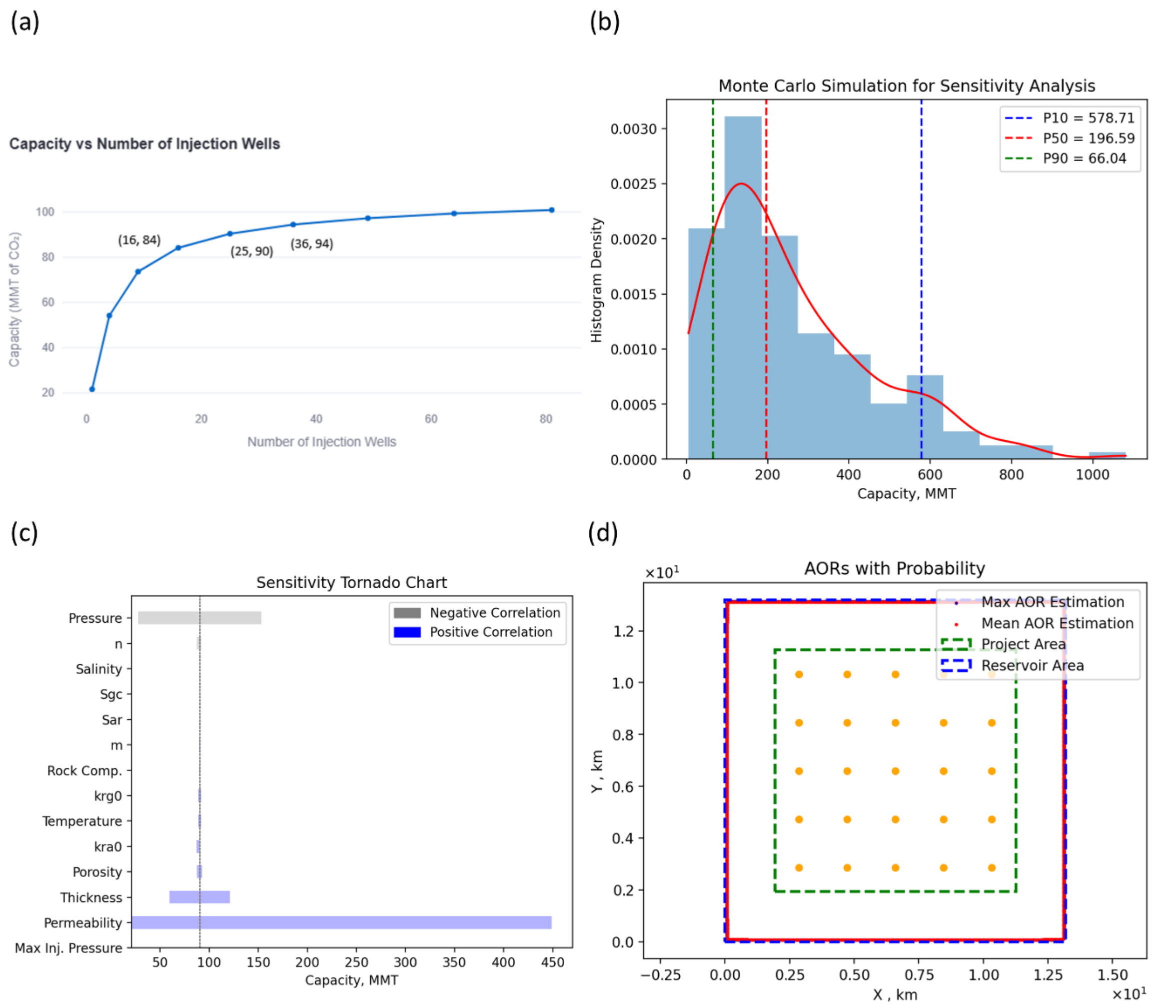

Figure A-4. EASiTool simulation outputs from for the reservoir in Zone 2 at Site N under open-boundary conditions:
(a) capacity vs. number of injection wells; (b) Monte Carlo simulation for sensitivity analysis; (c) sensitivity tornado chart; (d) AORs with probability.

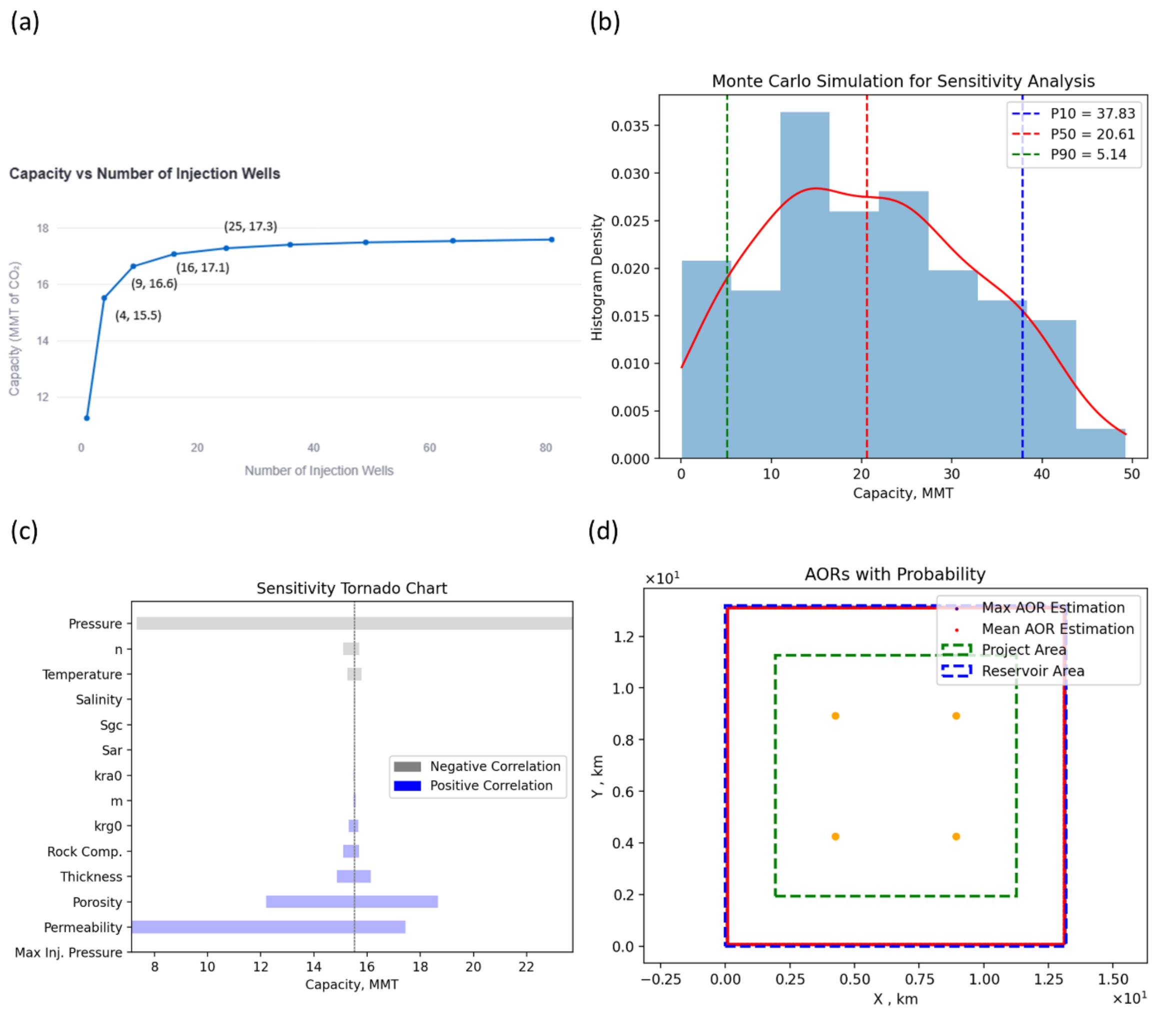

Figure A-5. EASiTool simulation outputs for the reservoir in Zone 3 at Site N under closed-boundary conditions:
(a) capacity vs. number of injection wells; (b) Monte Carlo simulation for sensitivity analysis; (c) sensitivity tornado chart; (d) AORs with probability.

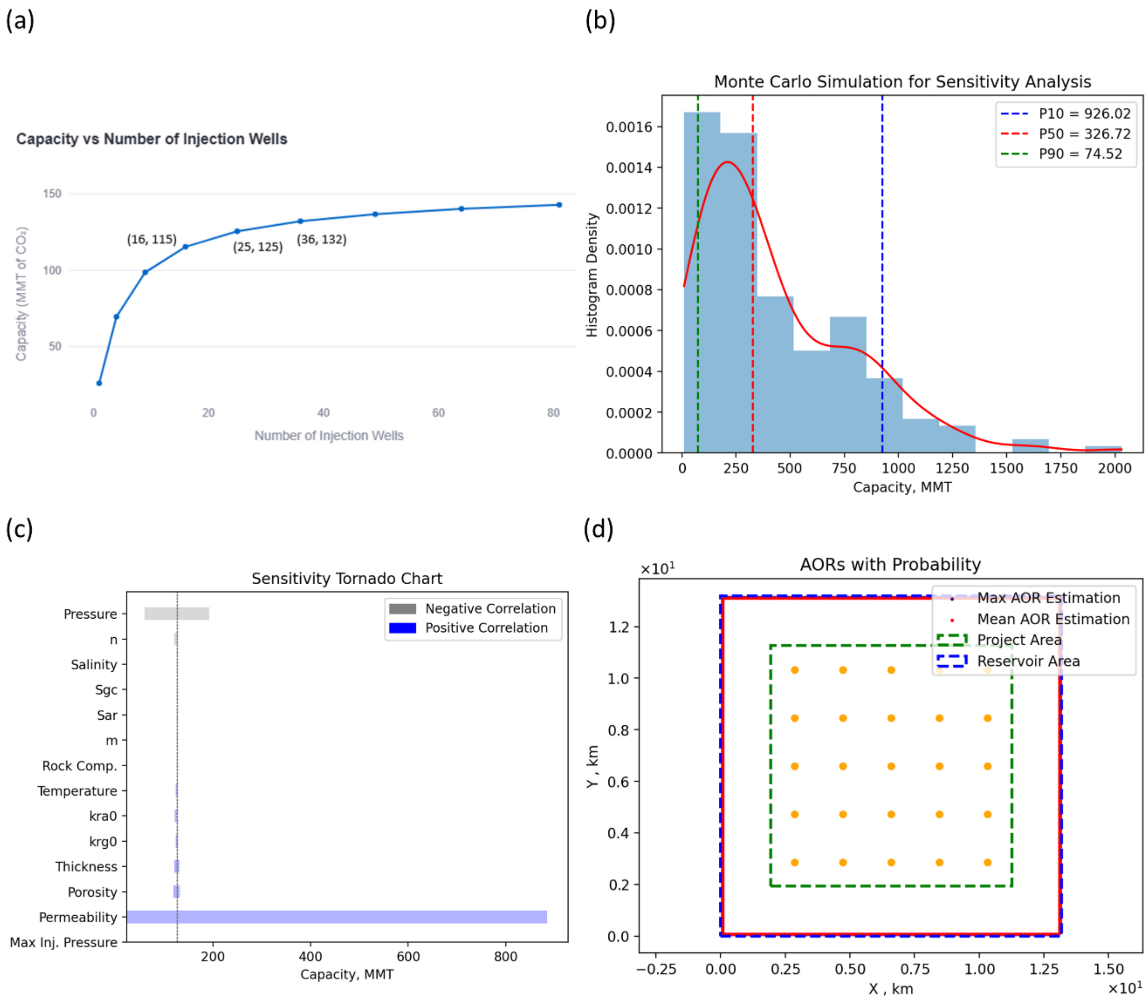

Figure A-6. EASiTool simulation outputs from for the reservoir in Zone 3 at Site N under open-boundary conditions:
(a) capacity vs. number of injection wells; (b) Monte Carlo simulation for sensitivity analysis; (c) sensitivity tornado chart; (d) AORs with probability.

A.2 SITE WK

A.2.1 Simulation Input

EASiTool inputs	Site WK								
Reservoir area (square kilometer)	528.61								
depth of USDW base (m)	1275.36 (at the base of Jasper Aquifer)								
	Zone 1			Zone 2			Zone 3		
Representative Depth (m)	1548.08			1907.89			2408.21		
Critical pressure increase (MPa)	0.064			0.12			0.12		
	min	base	max	min	base	max	min	base	max
Initial Pressure (MPa)	15.95	16.28	13.61	19.67	20.07	20.47	24.82	25.33	25.84
Net sand thickness (m)	86.24	113.39	140.53	67.09	94.24	121.38	62.94	98.34	133.75
Porosity	0.22	0.25	0.28	0.22	0.25	0.28	0.15	0.21	0.26
Permeability (md)	8.00	28.21	99.46	8.00	28.21	99.46	9.47	57.22	345.83
Temperature (C)	39.26	40.06	40.86	60.40	61.63	62.86	70.76	72.21	73.65
Salinity (mol/kg)	1.37	1.40	1.43	1.37	1.40	1.43	1.37	1.40	1.43
Maximum allowable injection pressure (MPa)	19.01	22.37	25.73	23.43	27.57	31.70	29.58	34.80	40.02

Table A-2 Simulation input parameters for Site WK

A.2.2 Output Figures

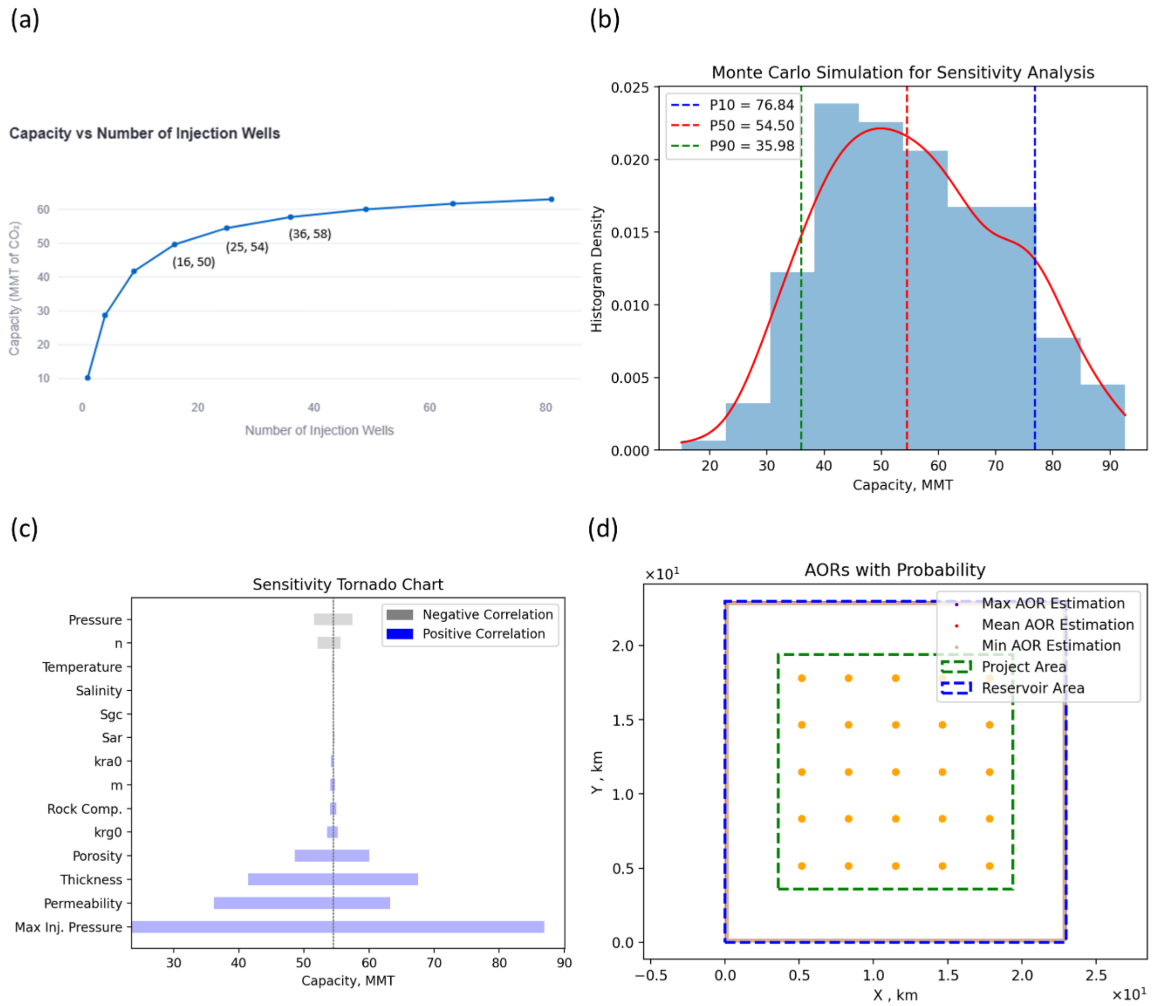

Figure A-7. EASiTool simulation outputs for the reservoir in Zone 1 at Site WK under closed-boundary conditions:
(a) capacity vs. number of injection wells; (b) Monte Carlo simulation for sensitivity analysis; (c) sensitivity tornado chart; (d) AORs with probability.

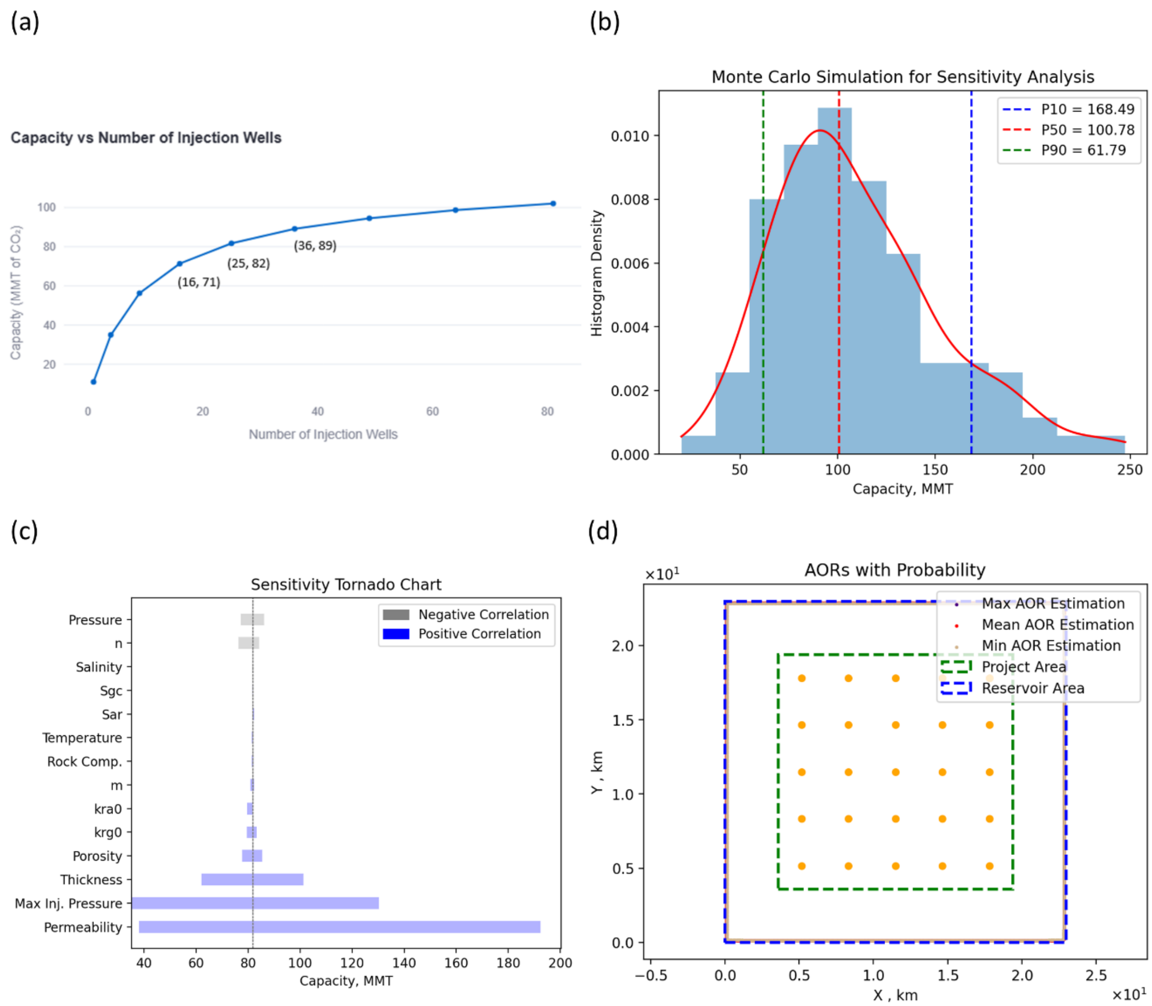

Figure A-8. EASiTool simulation outputs for the reservoir in Zone 1 at Site WK under open-boundary conditions:
(a) capacity vs. number of injection wells; (b) Monte Carlo simulation for sensitivity analysis; (c) sensitivity tornado chart; (d) AORs with probability.

(a)

(b)

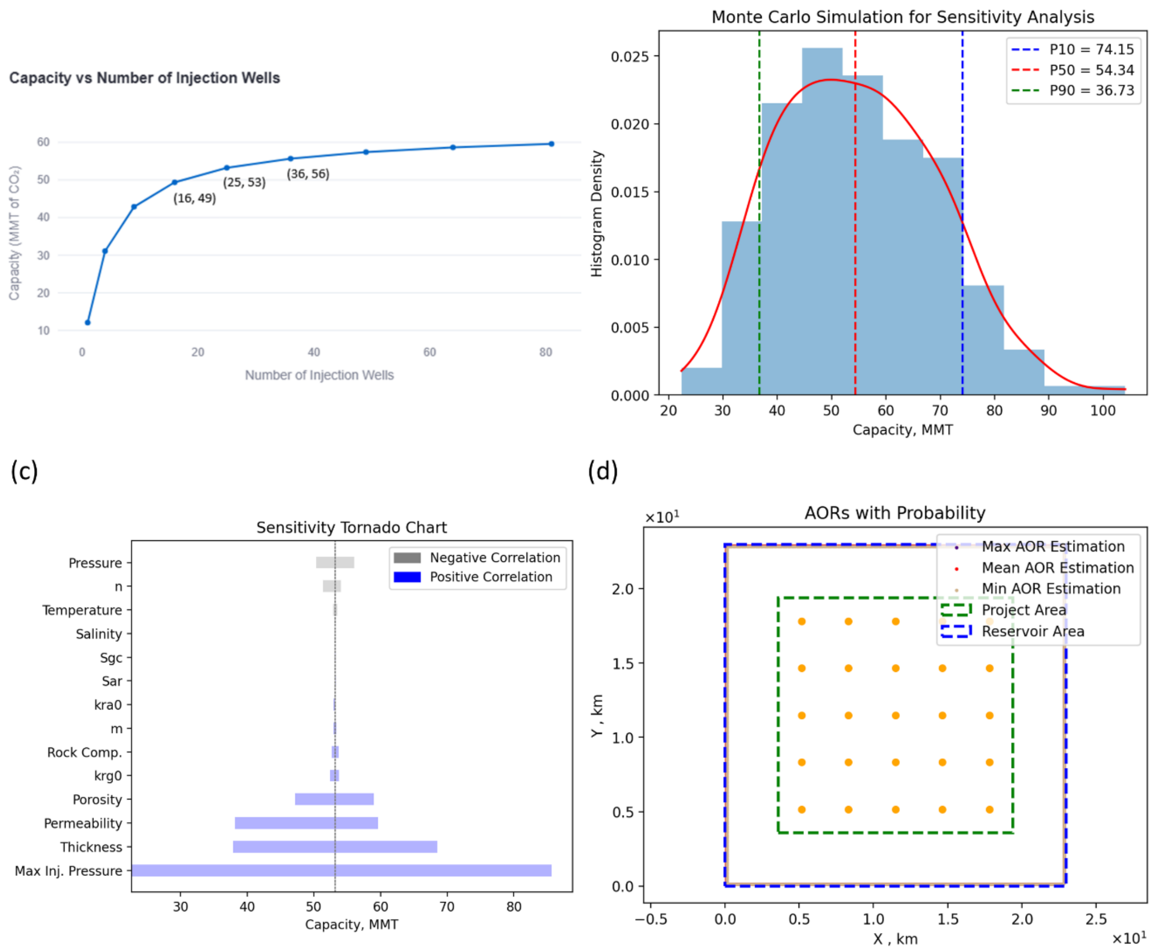

(c)

(d)

Figure A-9. EASiTool simulation outputs for the reservoir in Zone 2 at Site WK under closed-boundary conditions:
(a) capacity vs. number of injection wells; (b) Monte Carlo simulation for sensitivity analysis; (c) sensitivity tornado chart; (d) AORs with probability.

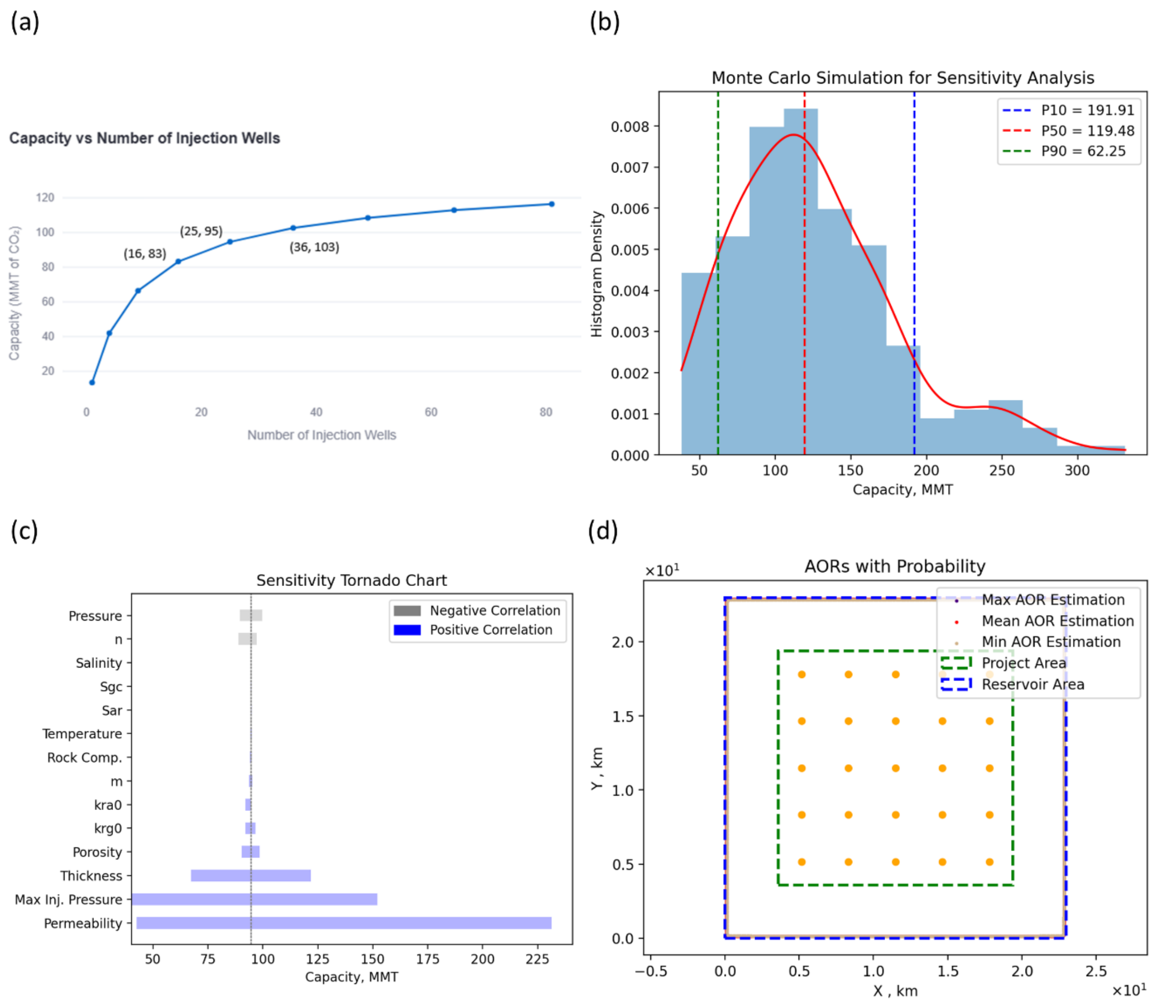

Figure A-10. EASiTool simulation outputs for the reservoir in Zone 2 at Site WK under open-boundary conditions:
(a) capacity vs. number of injection wells; (b) Monte Carlo simulation for sensitivity analysis; (c) sensitivity tornado chart; (d) AORs with probability.

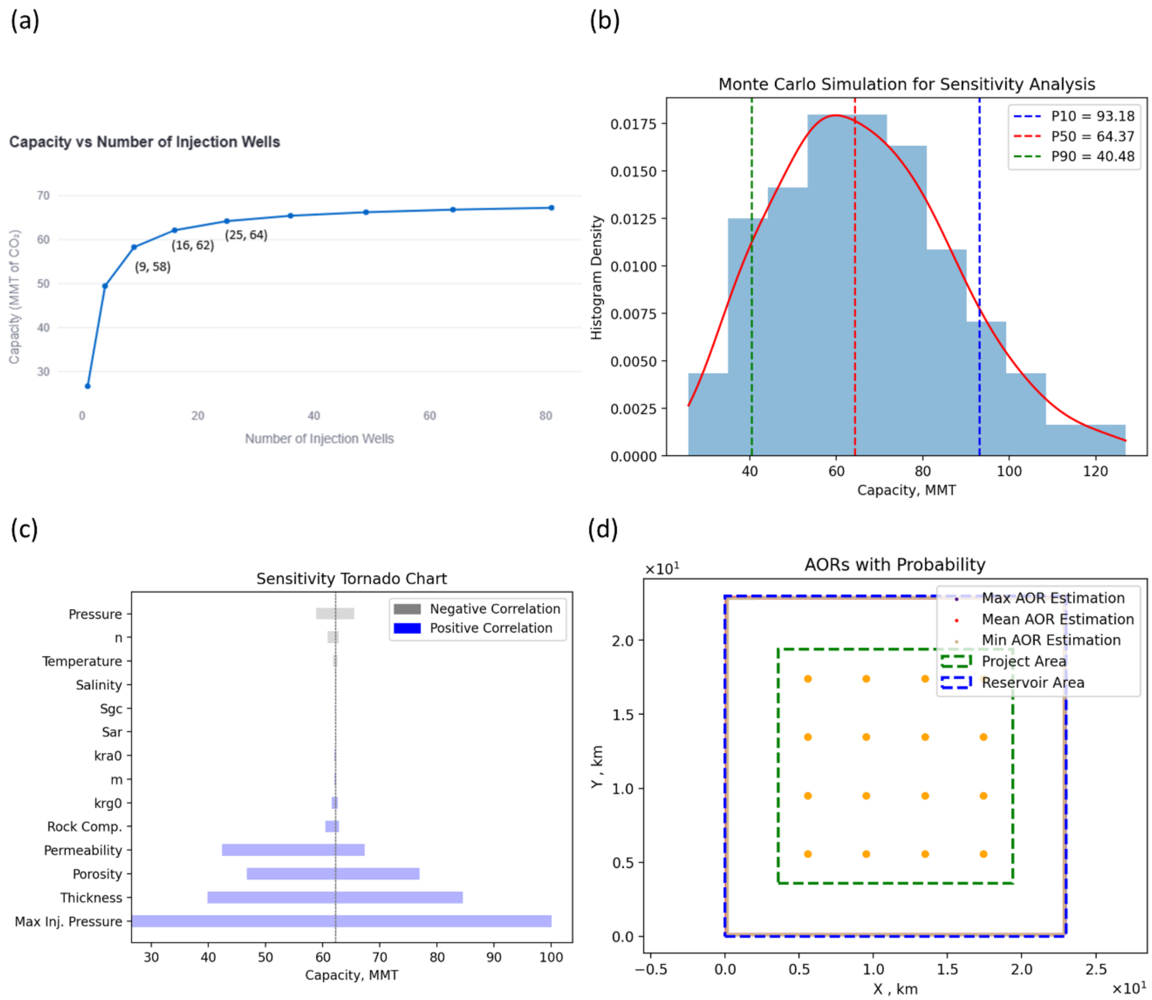

Figure A-11. EASiTool simulation outputs for the reservoir in Zone 3 at Site WK under closed-boundary conditions:
(a) capacity vs. number of injection wells; (b) Monte Carlo simulation for sensitivity analysis; (c) sensitivity tornado chart; (d) AORs with probability.

(a)

(b)

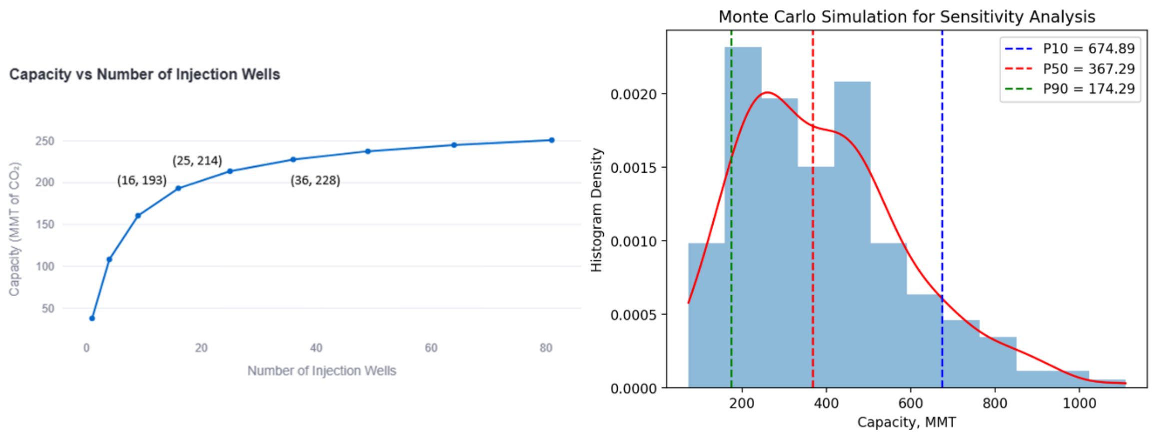

(c)

(d)

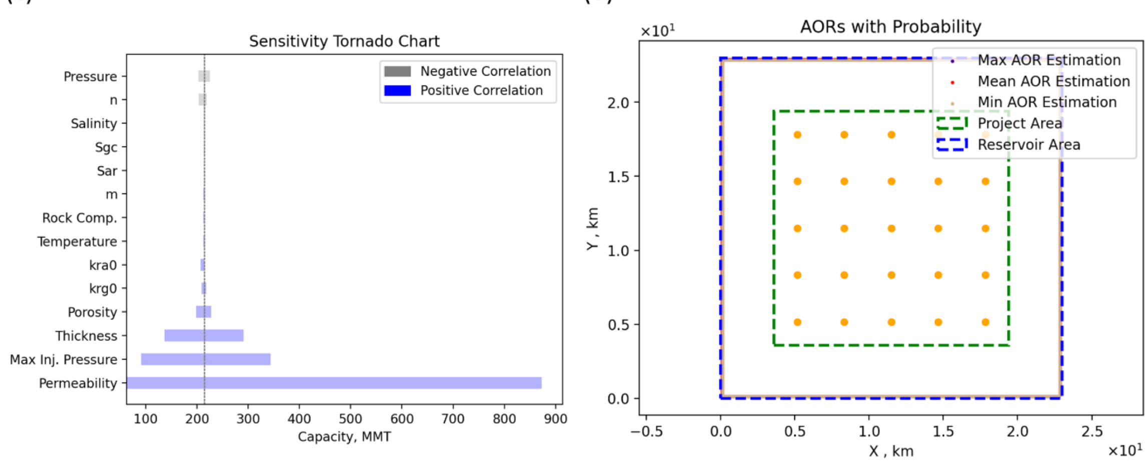

Figure A-12. EASiTool simulation outputs for the reservoir in Zone 3 at Site WK under open-boundary conditions:
(a) capacity vs. number of injection wells; (b) Monte Carlo simulation for sensitivity analysis; (c) sensitivity tornado chart; (d) AORs with probability.

A.3 SITE KK

A.3.1 Simulation Input

EASiTool inputs	Site KK								
Reservoir area (square kilometer)	280.63								
depth of USDW base (m)	1862.66 (at the base of Jasper Aquifer)								
	Zone 1			Zone 2			Zone 3		
Representative Depth (m)	2278.34			2677.67			3156.20		
Critical pressure increase (MPa)	0.04			0.17			0.40		
	min	base	max	min	base	max	min	base	max
Initial Pressure (MPa)	23.48	23.96	24.44	27.60	28.16	28.72	32.48	33.14	33.80
Net sand thickness (m)	133.31	152.75	172.18	143.37	166.73	190.08	119.17	150.26	181.36
Porosity	0.21	0.24	0.28	0.21	0.24	0.28	0.15	0.21	0.26
Permeability (md)	5.55	21.66	84.58	5.55	21.66	84.58	9.46	57.22	345.83
Temperature (C)	66	67.35	68.70	80.62	82.27	83.92	98.15	100.15	102.15
Salinity (mol/kg)	1.37	1.40	1.43	1.45	1.48	1.50	2.19	2.23	2.28
Maximum allowable injection pressure (MPa)	27.25	32.06	36.87	32.58	38.33	44.08	37.90	44.59	51.28

Table A-3 Simulation input parameters for Site KK

A.3.2 Output Figures

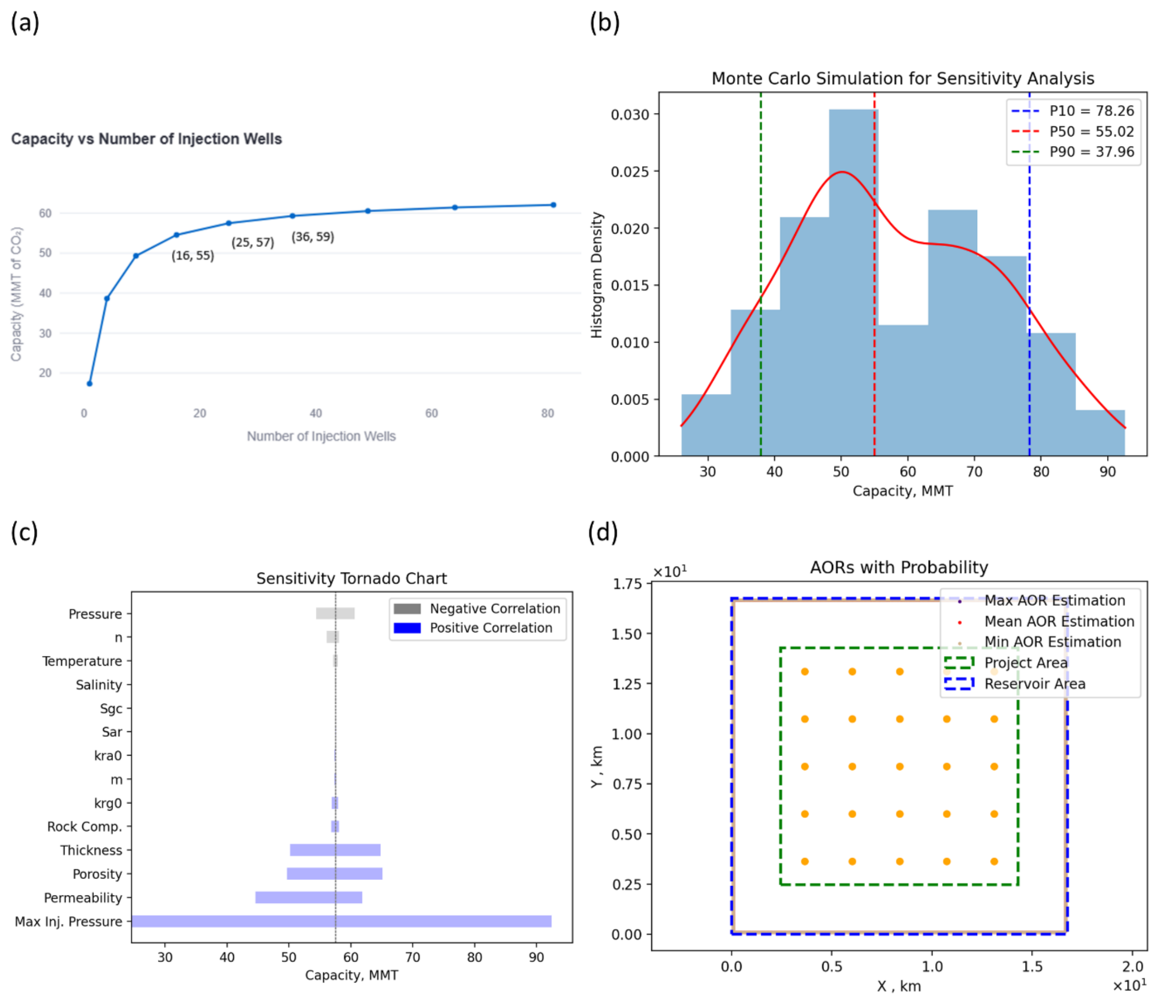

Figure A-13. EASiTool simulation outputs for the reservoir in Zone 1 at Site KK under closed-boundary conditions:
(a) capacity vs. number of injection wells; (b) Monte Carlo simulation for sensitivity analysis; (c) sensitivity tornado chart; (d) AORs with probability.

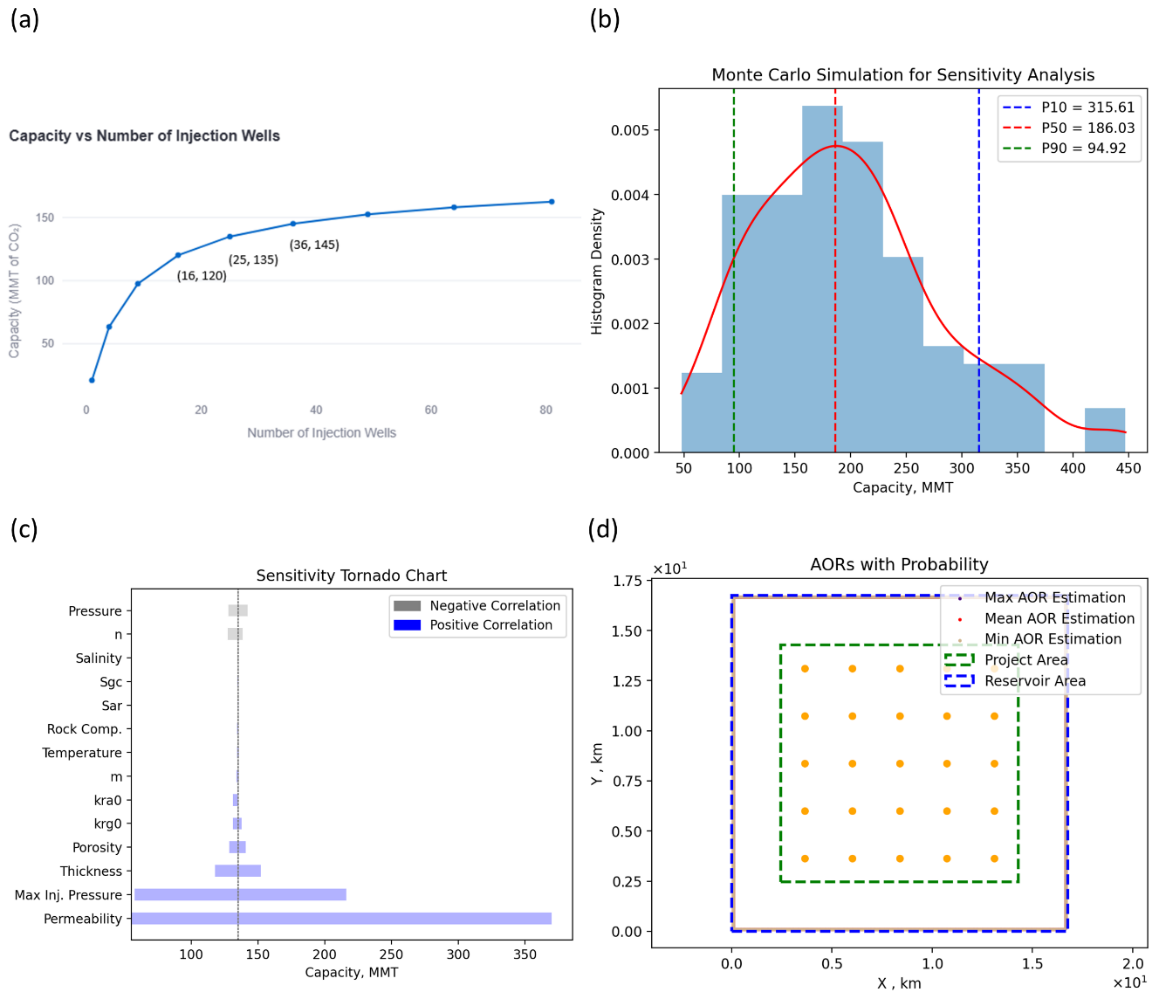

Figure A-14. EASiTool simulation outputs for the reservoir in Zone 1 at Site KK under open-boundary conditions:
(a) capacity vs. number of injection wells; (b) Monte Carlo simulation for sensitivity analysis; (c) sensitivity tornado chart; (d) AORs with probability.

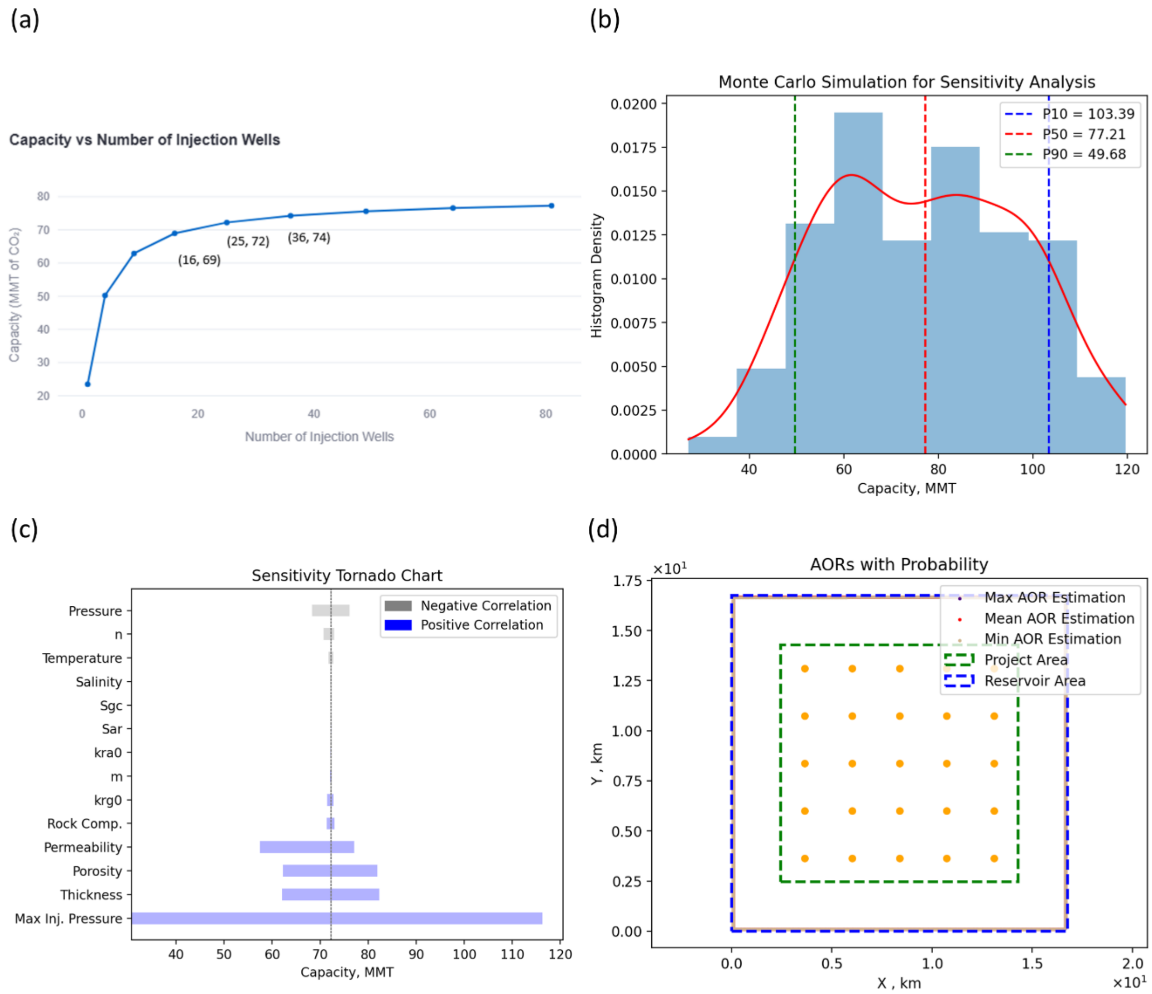

Figure A-15. EASiTool simulation outputs for the reservoir in Zone 2 at Site KK under closed-boundary conditions:
(a) capacity vs. number of injection wells; (b) Monte Carlo simulation for sensitivity analysis; (c) sensitivity tornado chart; (d) AORs with probability.

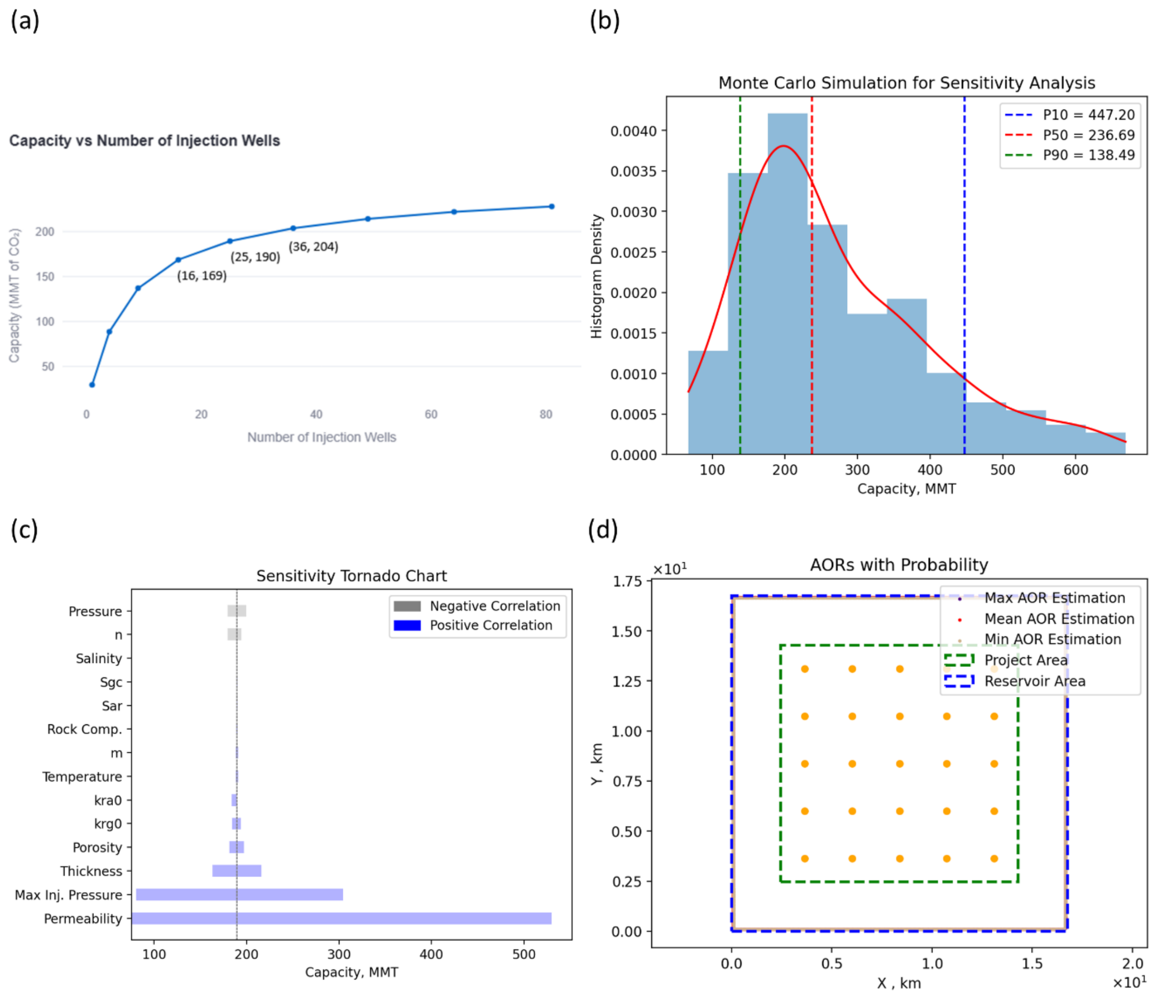

Figure A-16. EASiTool simulation outputs for the reservoir in Zone 2 at Site KK under open-boundary conditions:
(a) capacity vs. number of injection wells; (b) Monte Carlo simulation for sensitivity analysis; (c) sensitivity tornado chart; (d) AORs with probability.

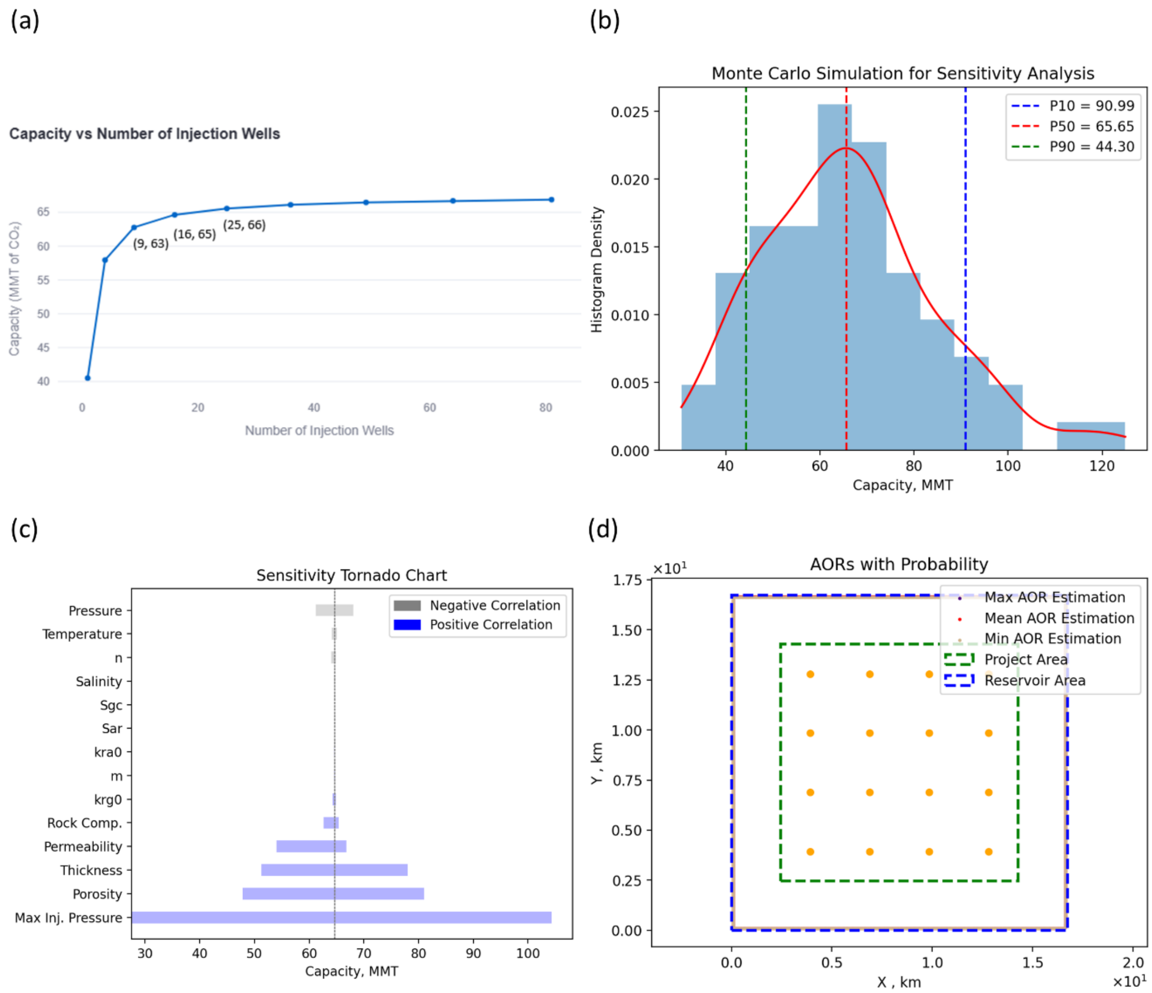

Figure A-17. EASiTool simulation outputs for the reservoir in Zone 3 at Site KK under closed-boundary conditions:
(a) capacity vs. number of injection wells; (b) Monte Carlo simulation for sensitivity analysis; (c) sensitivity tornado chart; (d) AORs with probability.

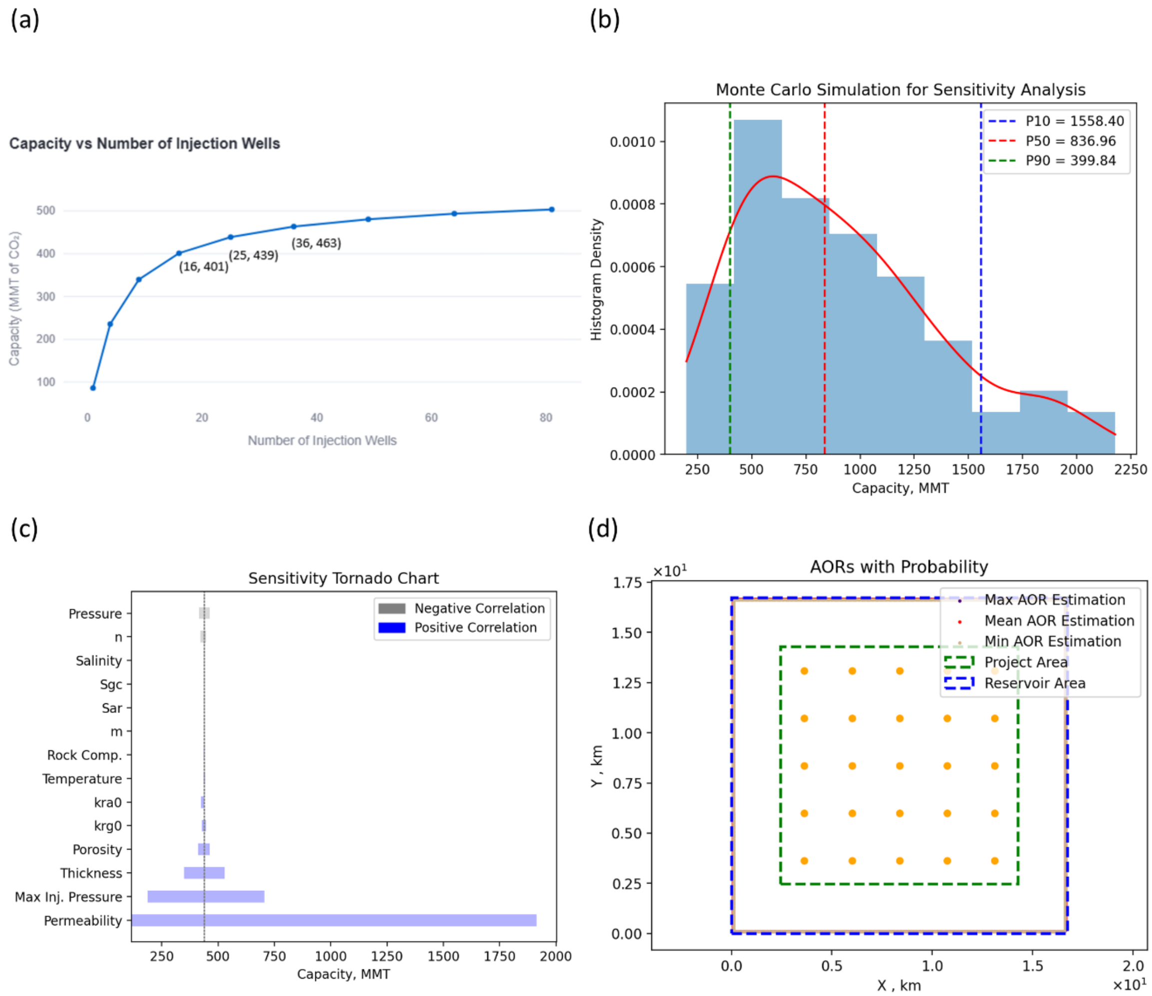

Figure A-18. EASiTool simulation outputs for the reservoir in Zone 3 at Site KK under open-boundary conditions:
(a) capacity vs. number of injection wells; (b) Monte Carlo simulation for sensitivity analysis; (c) sensitivity tornado chart; (d) AORs with probability.

A.4 Site KND

A.4.1 Simulation Input

EASiTool inputs	Site KND								
Reservoir area (square kilometer)	657								
depth of USDW base (m)	1219.20 (at the base of Evangeline Aquifer)								
	Zone 1			Zone 2			Zone 3		
Representative Depth (m)	2543.71			2917.09			3341.37		
Critical pressure increase (MPa)	0.22			0.38			0.88		
	min	base	max	min	base	max	min	base	max
Initial Pressure (MPa)	26.22	26.76	27.29	30.07	30.68	31.29	34.45	35.15	35.85
Net sand thickness (m)	123.12	147.22	171.30	143.56	180.44	217.32	237.13	237.13	258.47
Porosity	0.18	0.21	0.23	0.19	0.20	0.22	0.19	0.20	0.22
Permeability (md)	5.54	14.14	36.08	6.43	12.03	22.53	6.43	12.03	22.53
Temperature (C)	75.72	77.27	78.81	89.40	91.22	93.04	104.86	107.00	109.14
Salinity (mol/kg)	1.37	1.40	1.43	1.72	1.76	1.80	2.82	2.88	2.94
Maximum allowable injection pressure (MPa)	31.24	36.76	42.27	35.83	42.15	48.47	40.80	48.00	55.20

Table A-4 Simulation input parameters for Site KND

A.4.2 Output Figures

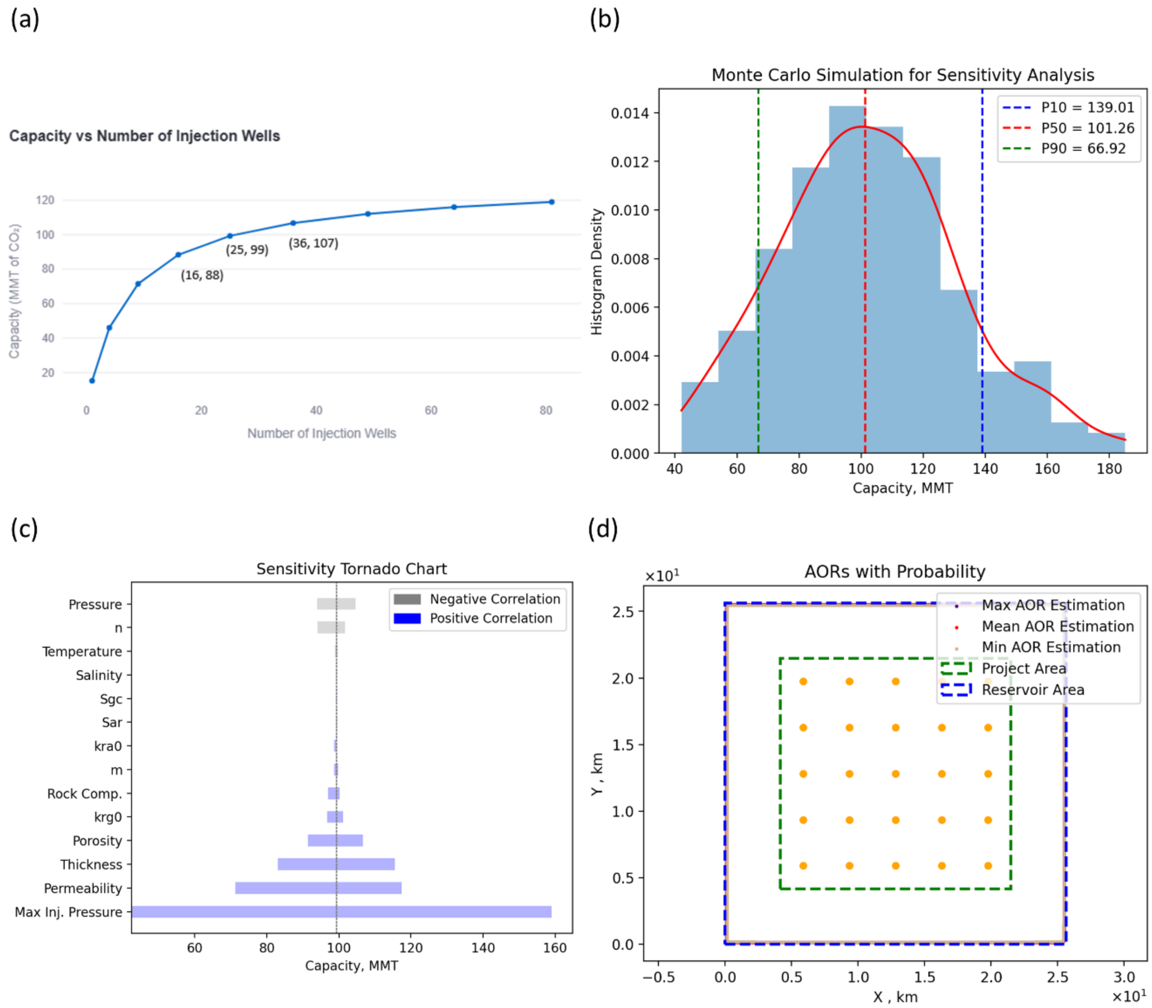

Figure A-19. EASiTool simulation outputs for the reservoir in Zone 1 at Site KND under closed-boundary conditions:
(a) capacity vs. number of injection wells; (b) Monte Carlo simulation for sensitivity analysis; (c) sensitivity tornado chart; (d) AORs with probability.

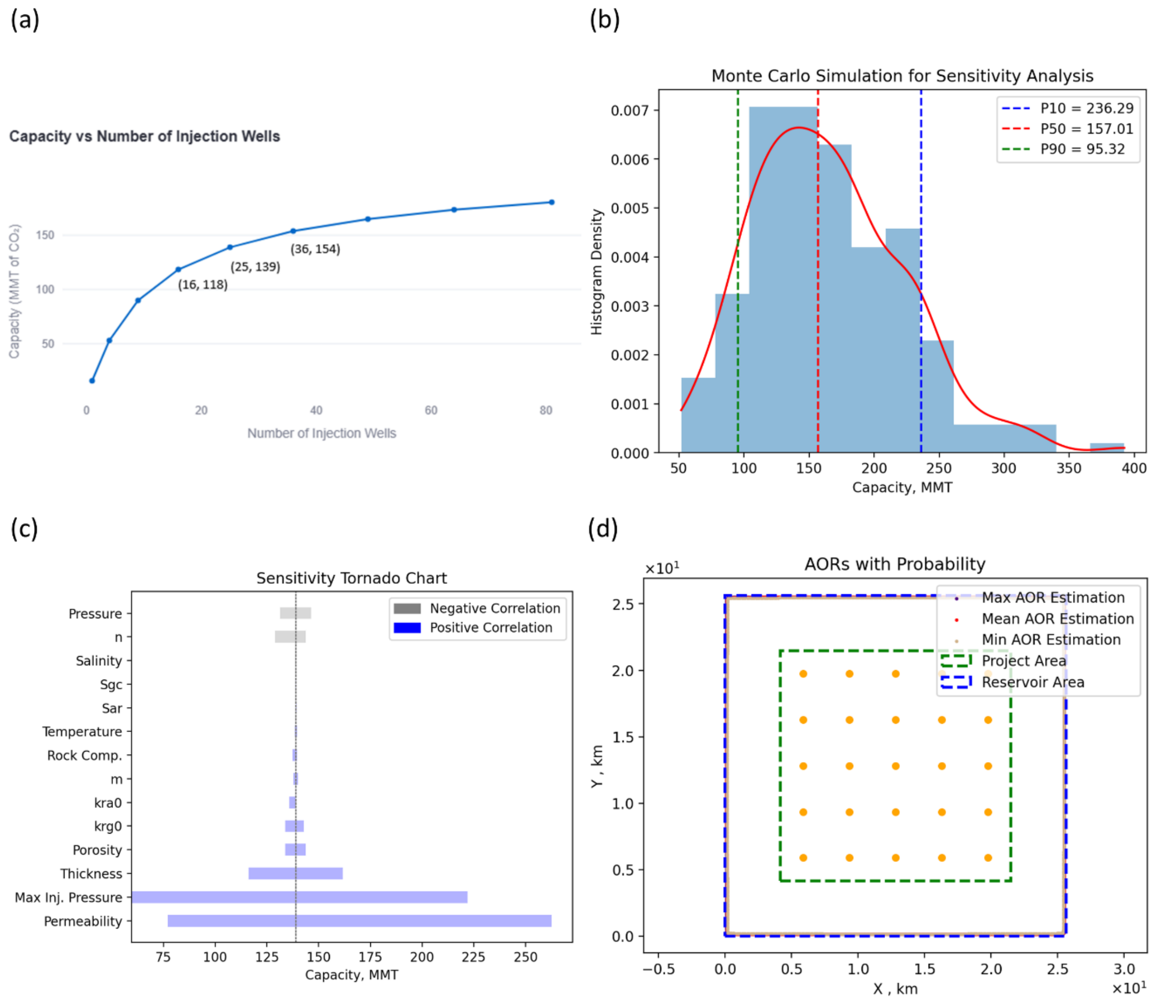

Figure A-20. EASiTool simulation outputs for the reservoir in Zone 1 at Site KND under open-boundary conditions:
(a) capacity vs. number of injection wells; (b) Monte Carlo simulation for sensitivity analysis; (c) sensitivity tornado chart; (d) AORs with probability.

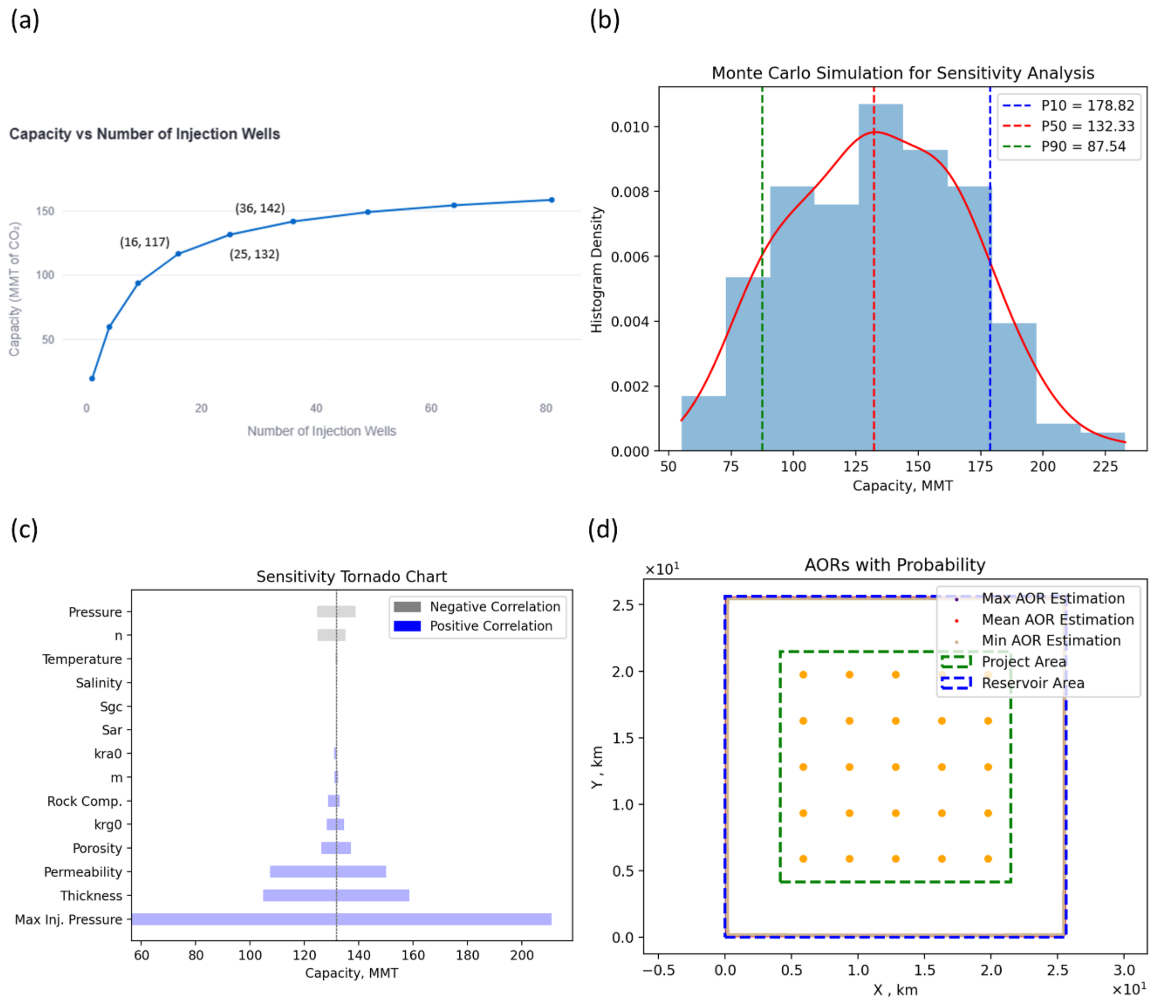

Figure A-21. EASiTool simulation outputs for the reservoir in Zone 2 at Site KND under closed-boundary conditions:
(a) capacity vs. number of injection wells; (b) Monte Carlo simulation for sensitivity analysis; (c) sensitivity tornado chart; (d) AORs with probability.

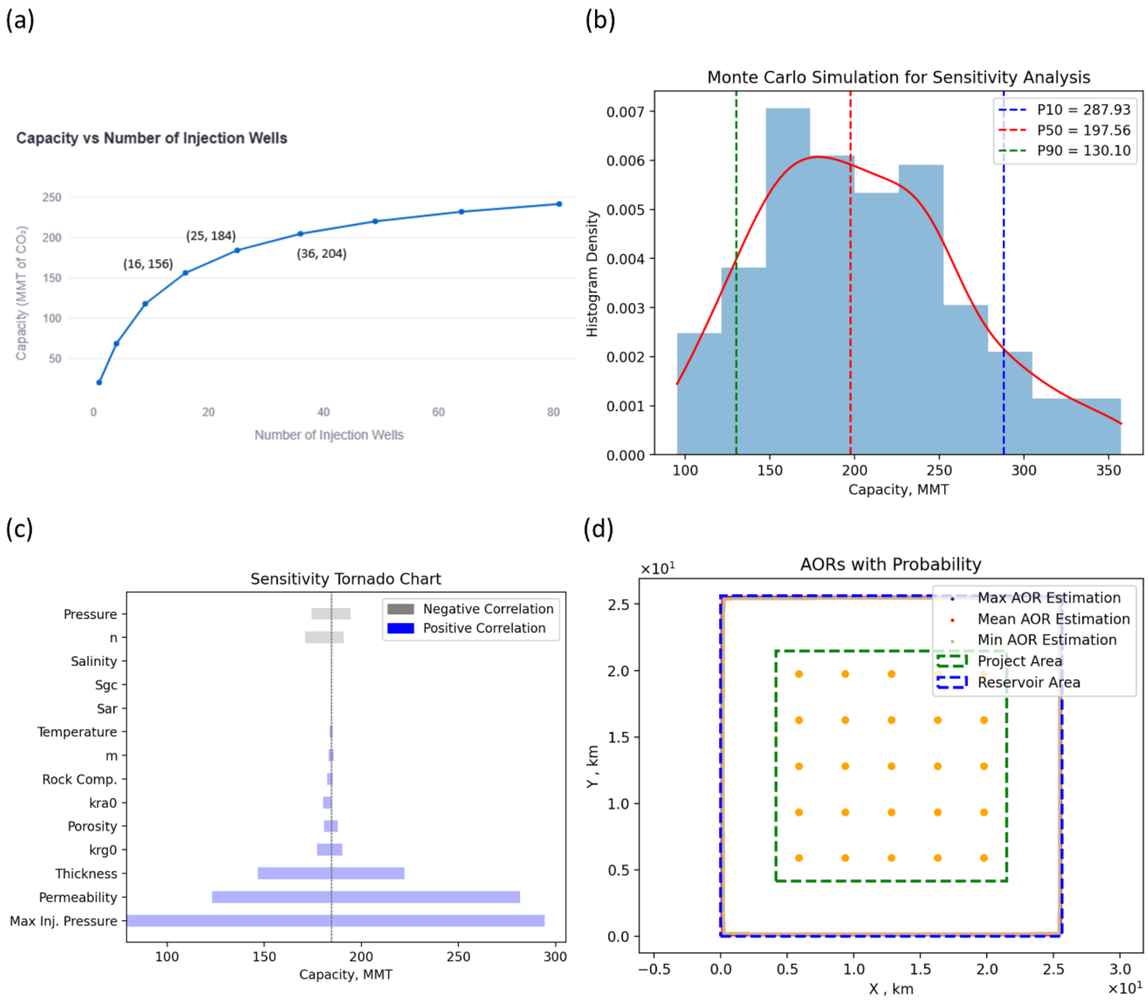

Figure A-22. EASiTool simulation outputs for the reservoir in Zone 2 at Site KND under open-boundary conditions:
(a) capacity vs. number of injection wells; (b) Monte Carlo simulation for sensitivity analysis; (c) sensitivity tornado chart; (d) AORs with probability.

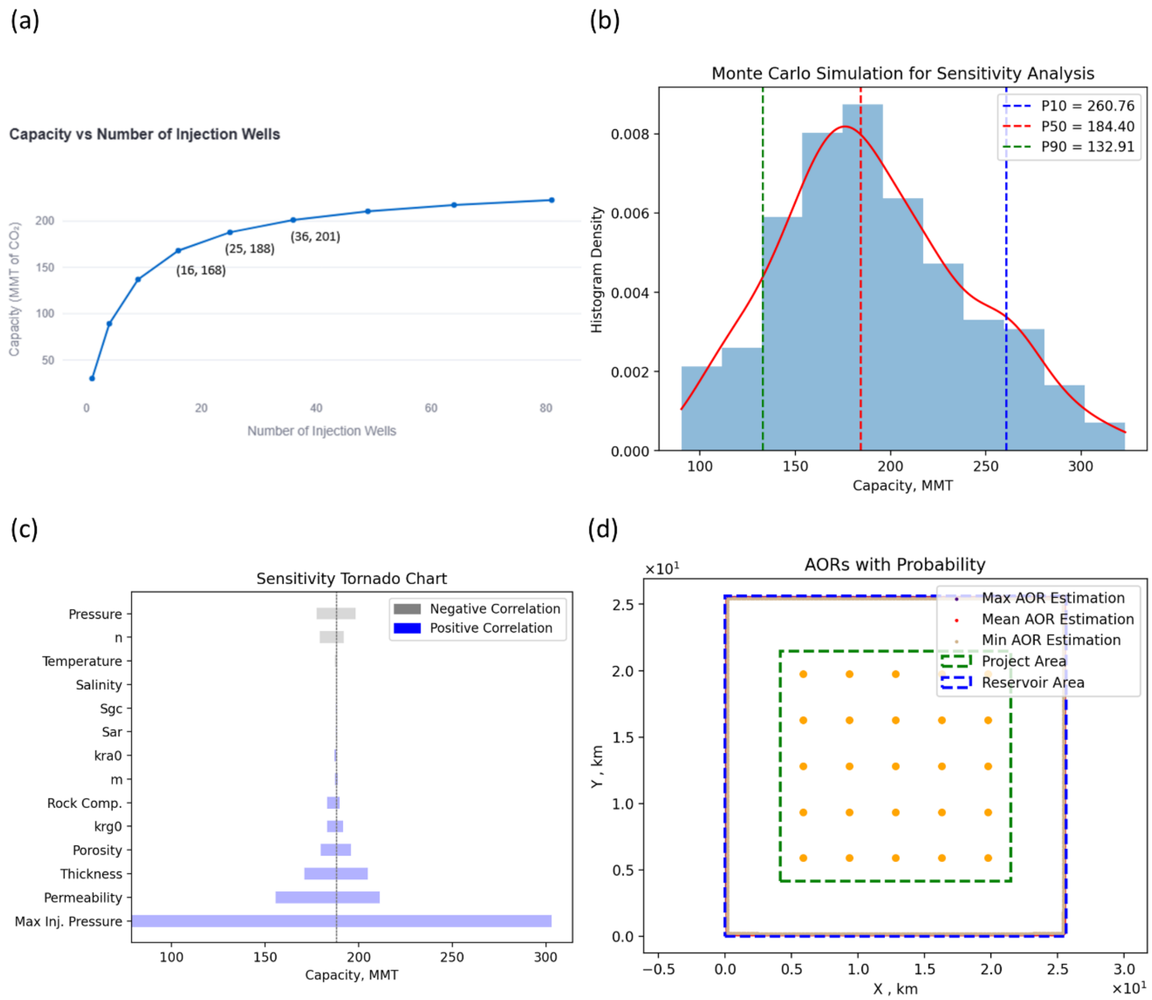

Figure A-23. EASiTool simulation outputs for the reservoir in Zone 3 at Site KND under closed-boundary conditions:
(a) capacity vs. number of injection wells; (b) Monte Carlo simulation for sensitivity analysis; (c) sensitivity tornado chart; (d) AORs with probability.

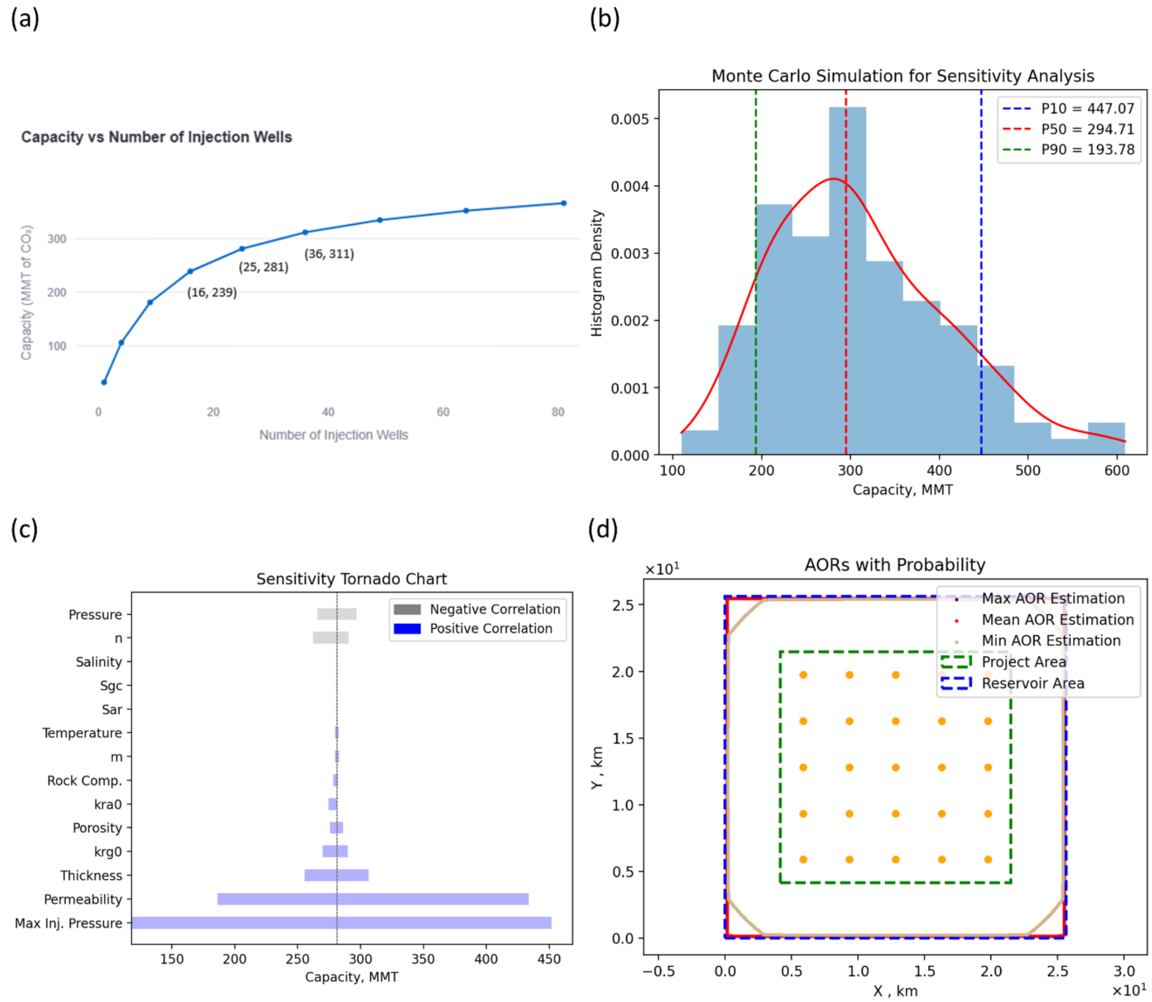

Figure A-24. EASiTool simulation outputs for the reservoir in Zone 3 at Site KND under open-boundary conditions:
(a) capacity vs. number of injection wells; (b) Monte Carlo simulation for sensitivity analysis; (c) sensitivity tornado chart; (d) AORs with probability.

A.5 Site W

A.5.1 Simulation Input

EASiTool inputs	Site W		
Reservoir area (square kilometer)	288		
depth of USDW base (m)	670.56 (at the base of Burkeville Formation)		
	Zone 3		
Representative Depth (m)	2734.82		
Critical pressure increase (MPa)	0.42		
	min	mean	max
Initial Pressure (MPa)	33.10	33.78	34.45
Net sand thickness (m)	139.25	172.00	204.76
Porosity	0.12	0.17	0.22
Permeability (md)	9.95	20.23	41.16
Temperature (C)	97.08	99.06	101.04
Salinity (mol/kg)	1.50	1.53	1.56
Maximum allowable injection pressure (MPa)	33.59	39.52	45.45

Table A-5 Simulation input parameters for Site W

A.5.2 Output Figures

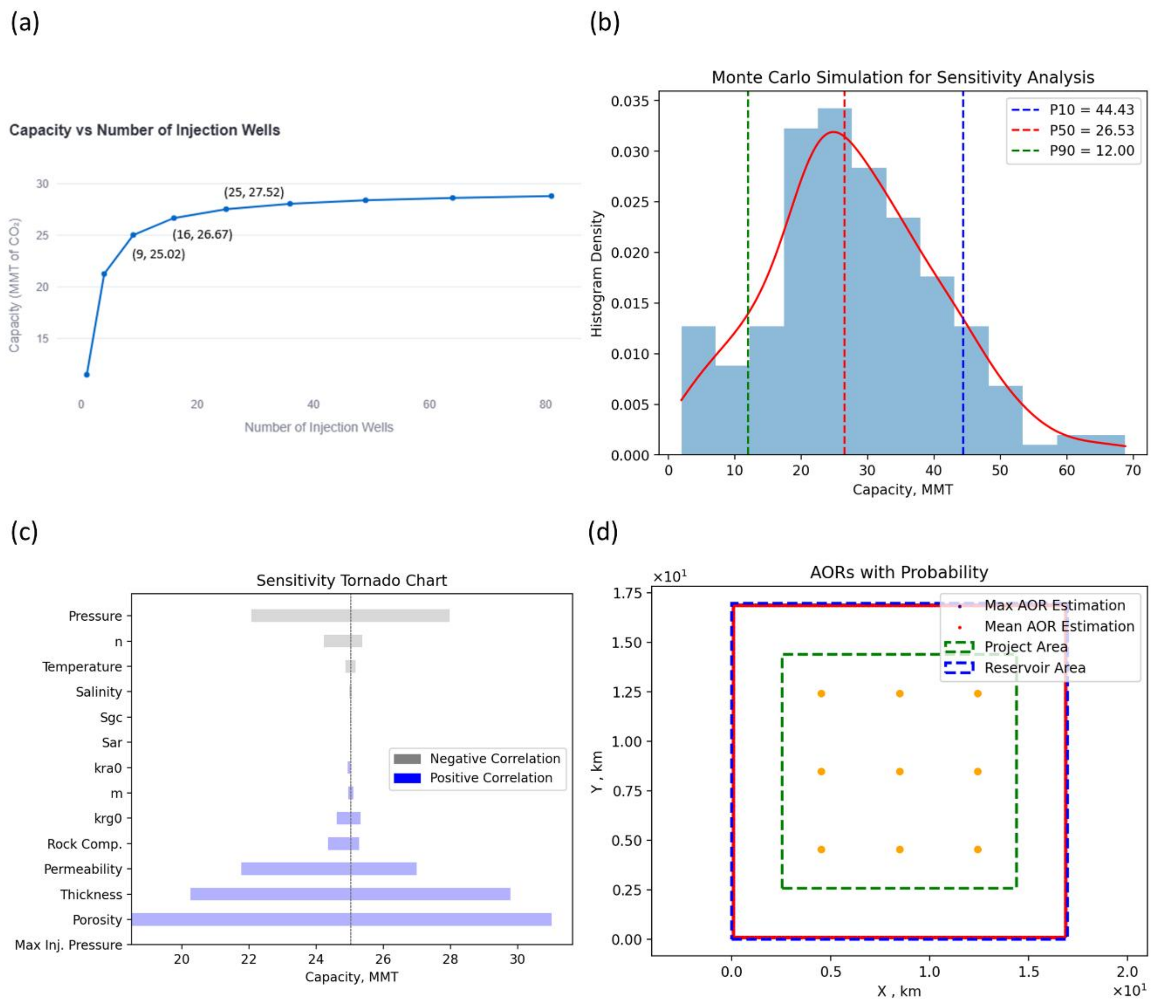

Figure A-25. EASiTool simulation outputs for the reservoir in Zone 3 at Site W under closed-boundary conditions:
(a) capacity vs. number of injection wells; (b) Monte Carlo simulation for sensitivity analysis; (c) sensitivity tornado chart; (d) AORs with probability.

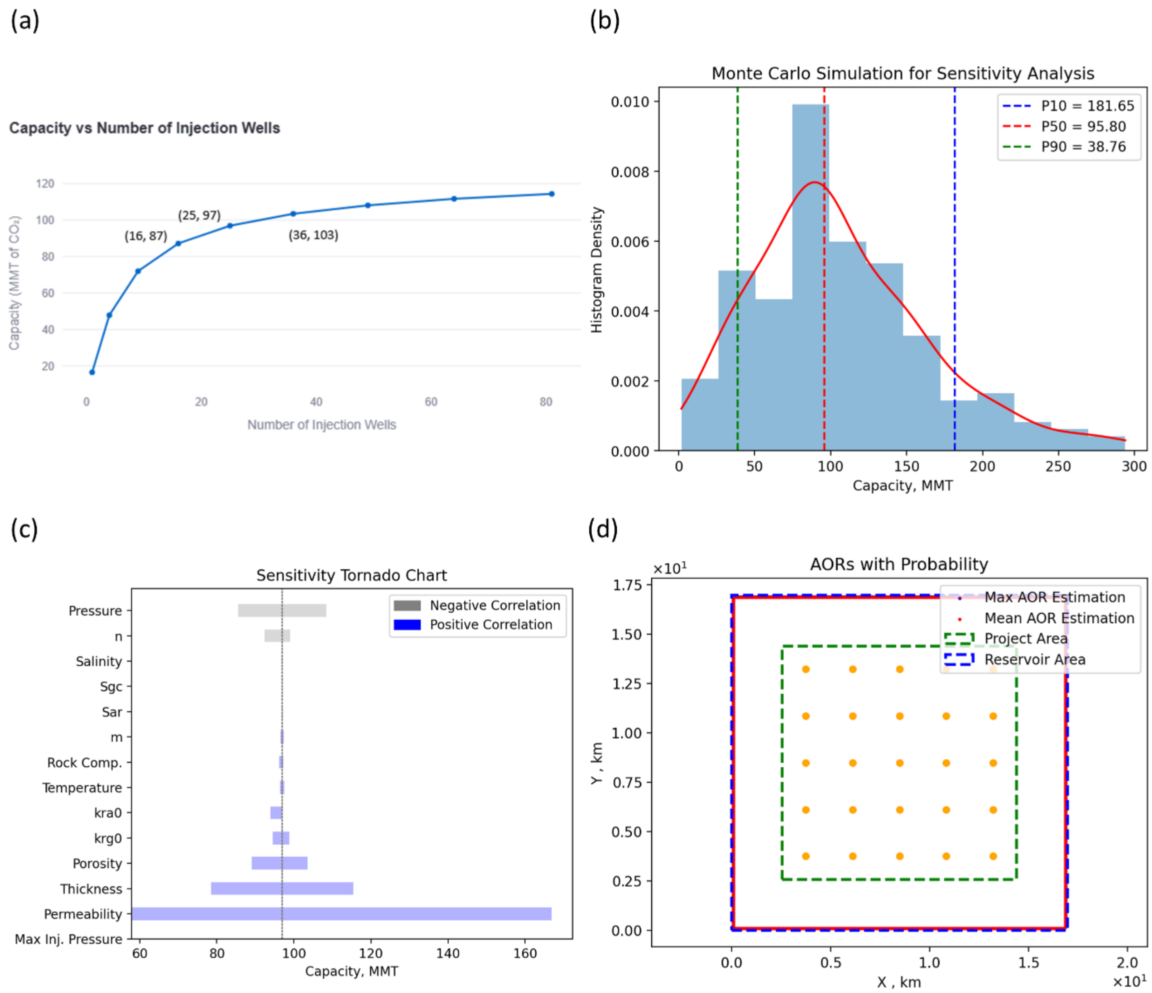

Figure A-26. EASiTool simulation outputs for the reservoir in Zone 3 at Site W under open-boundary conditions:
(a) capacity vs. number of injection wells; (b) Monte Carlo simulation for sensitivity analysis; (c) sensitivity tornado chart; (d) AORs with probability.

Bibliography

40 C.F.R. §. 144.3 (2026)

Baker, Jr., E. T., (1995). Stratigraphic nomenclature and geologic sections of the gulf coastal plain of Texas. U.S. GEOLOGICAL SURVEY Open-File Report 94-461, 34 p.

Bandilla, K. W., Kraemer, S. R., & Birkholzer, J. T. (2012). Using semi-analytic solutions to approximate the area of potential impact for carbon dioxide injection, International Journal of Greenhouse Gas Control, 8:196-204, ISSN 1750-5836, 10.1016/j.ijggc.2012.02.009.

Benson, S., Cook, P., Anderson, J., Bachu, S., Nimir, H. B., Basu, B., Bradshaw, J., Deguchi, G., Gale, J., von Goerne, G., Heidug, W., Holloway, S., Kamal, R., Keith, D., Lloyd, P., Rocha, P., Senior, B., Thomson, J., Torp, T., Wildenborg, T., Wilson, M., Zarlenga, F., & Zhou, D. (2005). Underground geological storage. In B. Metz, O. Davidson, H. de Coninck, M. Loos, & L. Meyer (Eds.), IPCC Special Report on Carbon Dioxide Capture and Storage. Cambridge University Press.

Brown, L. F., Jr., Loucks, R. G., Treviño, R. H., and Hammes, U. (2004). Understanding growth-faulted intraslope subbasins by applying sequence-stratigraphic principles: Examples from the south Texas Oligocene Frio Formation. AAPG Bulletin, v.88, no. 11 (November2004), pp. 1501–1522

Domenico, S. N. (1980) Velocity and lithology: Notes, American Association of Petroleum Geologists - Society of Exploration Geophysicists Stratigraphic Interpretation of Seismic Data School, September 23-27. American Association of Petroleum Geologists, Tulsa, Oklahoma, 62 p.

EIA (2025a). Rankings: Total Carbon Dioxide Emissions 2023, U.S. Energy Information Administration. (https://www.eia.gov/state/rankings/?sid=US#/series/226

EIA (2025b). Texas used twice as much energy as California and three times as much as Florida in 2023. https://www.eia.gov/todayinenergy/detail.php?id=66224#

EIA (2025c). We expect rapid electricity demand growth in Texas and the mid-Atlantic. https://www.eia.gov/todayinenergy/detail.php?id=65844

EPA (2013a). Geologic Sequestration of Carbon Dioxide: Underground Injection Control (UIC) Program Class VI Well Area of Review Evaluation and Corrective Action Guidance.

EPA (2013b). Geologic Sequestration of Carbon Dioxide: Underground Injection Control (UIC) Program Class VI Well Site Characterization Guidance

EPA (2026a). Facility Level Information on Green House gases Tool (FLIGHT). https://ghgdata.epa.gov/flight/?viewType=map

EPA (2026b). GHGRP State and Tribal Fact Sheet https://www.epa.gov/ghgreporting/ghgrp-state-and-tribal-fact-sheet

EPA (2026c). Class VI - Wells used for Geologic Sequestration of Carbon Dioxide. https://www.epa.gov/uic/class-vi-wells-used-geologic-sequestration-carbon-dioxide

EPA (2026d). General Information About Injection Wells. https://www.epa.gov/uic/general-information-about-injection-wells#:~:text=An%20underground%20source%20of%20drinking,as%20a%20drinking%20water%20source.

Ewing, T.E., Budnik, R.T., Ames, J.T., Ridner, D.M., Dillon, R.L. (1990) Tectonic map of Texas. University of Texas at Austin, Bureau of Economic Geology.

Ewing, T.E. (1991) The Tectonic Framework of Texas: Text to accompany "The tectonic Map of Texas". University of Texas at Austin, Bureau of Economic Geology.

Galloway, W.E (1977). Catahoula Formation of the Texas Coastal Plain: depositional systems. composition, structural development. ground-water flow history, and uranium distribution: The University of Texas at Austin, Bureau of Economic Geology Report of Investigations No. 87, 59 p.

Galloway, W. E., Hobday, D. K., and Magara, K. (1982a). Frio Formation of Texas Gulf Coastal Plain: Depositional Systems, Structural Framework, and Hydrocarbon Distribution, The American Association of Petroleum Geologists Bulletin V, 66, No. 5 (June 1982), P. 649-688,

Galloway, W. E., Hobday, D. K., and Magara, K. (1982b). FRIO FORMATION OF THE TEXAS GULF COAST BASIN Depositional Systems, Structural Framework, and Hydrocarbon Origin; Migration, Distribution, and Exploration Potential. Report of Investigations No. 122, BUREAU OF ECONOMIC GEOLOGY

Ganjdanesh, R.; Hosseini, S. A. (2017) Geologic Carbon Storage Capacity Estimation Using Enhanced Analytical Simulation Tool (EASiTool). Energy Procedia 2017, 114, 4690–4696. https://doi.org/10.1016/j.egypro.2017.03.1601.

Hammes, U., Loucks, R. G., Brown, L. F., Jr., Treviño, R. H., Montoya, P., and Remington, R. L. (2007). Reservoir Geology, Structural Architecture, and Sequence Stratigraphy of a Growth-Faulted Subbasin: Oligocene Lower Frio Formation, Red Fish Bay Area, South Texas Gulf Coast. Report of Investigations No. 272, BUREAU OF ECONOMIC GEOLOGY

Hoffman, N., Carman, G., Bagheri, M., & Goebel, T. (2015). Site characterisation for carbon sequestration in the nearshore Gippsland Basin. In P. McCabe & S. Mackie (Eds.), Proceedings of the International Conference and Exhibition (ICE

2015), Melbourne, Australia, 13–16 September 2015 (p. 265). ASME. https://doi.org/10.1190/ice2015-2209980

Langford, R. P., and Combes, J. M. (1994). Depositional Environments of Unstable Shelf-Margin Deltas of the Oligocene Vicksburg Formation, McAllen Ranch Field, South Texas: The University of Texas at Austin, Bureau of Economic Geology, Report of Investigations 219, 60 p.

Loucks, R. G., Dodge, M. M., and Galloway, W. E. (1984). Regional Controls on Diagenesis and Reservoir Quality in Lower Tertiary Sandstones along the Texas Gulf Coast: AAPG Memoir, V. 37, p. 15-45.

Loucks, R. G., Dodge, M. M., and Galloway, W. E. (1986). Controls on Porosity and Permeability of Hydrocarbon Reservoirs in Lower Tertiary Sandstones along the Texas Gulf Coast. Report of Investigations No.149, BUREAU OF ECONOMIC GEOLOGY

Nicot, J. P., Oldenburg, C. M., Bryant, S. L., & Hovorka, S. D. (2008). Pressure perturbation from geologic carbon sequestration: Area-of-review boundaries and borehole leakage driving forces. Energy Procedia.

NextDecade (2026). Rio Grande LNG. https://www.next-decade.com/our-business/rio-grande-lng/

Morton, R. A., Garrett, Jr, C. M., Posey, J. S., Han, J. H., & Jirik, L. A. (1981). Salinity variations and chemical compositions of waters in the Frio Formation, Texas Gulf Coast. Annual report.

Rogers, H. H., III and Ambrose, W. A. (2024). Facies Variability in Paleogeographic Trends from Core Data in the Lower and Middle Frio Formation in South Texas. GCAGS Journal, v. 13 (2024), p. 15–33.

Shi, J., Boghici, R., Anaya, R. (2022). Conceptual Model Report: Central and Southern Portions of Gulf Coast Aquifer System in Texas.

SLB (2025). Energy Glossary website. https://glossary.slb.com/terms/o/overpressure#:~:text=Subsurface%20pressure%20that%20is%20abnormally,%2C%20and%20incorrectly%2C%20used%20synonymously.

Snedden, J.W., and Galloway, W.E., (2019). The Gulf of Mexico Sedimentary Basin Depositional Evolution and Petroleum Applications. Chapter 6 Cenozoic Depositional History 2

Texas LNG Brownsville LLC (2026). Texas LNG, Project overview. https://www.texaslng.com/theproject/project-overview.html

Tiab, D., & Donaldson, E. C. (2016). Fluid-rock interactions. In D. Tiab & E. C. Donaldson (Eds.), Petrophysics (4th ed., pp. 641–717). Gulf Professional Publishing. https://doi.org/10.1016/B978-0-12-803188-9.00011-5

United Nation (2015). Paris Agreement. https://www.un.org/en/climatechange/paris-agreement

United Nation (2025). For a livable climate: Net-zero commitments must be backed by credible action https://www.un.org/en/climatechange/net-zero-coalition

Valluri, M., Mishra, S. and Ravi Ganesh, P. (2021), Injectivity index: a powerful tool for characterizing CO_2 storage reservoirs—a technical note. Greenhouse Gas Sci Technol, 11: 251-265. https://doi.org/10.1002/ghg.2046

Zhang, Jon & Yin, Shang-Xian. (2017). Fracture gradient prediction: an overview and an improved method. Petroleum Science. 14. 10.1007/s12182-017-0182-1.

1PointFive, LLC, (2026) 1PointFive: Carbon Removal and Sequestration. https://www.1pointfive.com/projects/south-texas-dacCampbell, W. G. 1990. Form and Style in Thesis Writing, a Manual of Style. Chicago: The University of Chicago Press.

Turabian, K. L. 1987. A Manual for Writers of Term Papers, Theses, and Dissertations. 5th ed. Chicago: The University of Chicago Press.]